

6760

NATIONAL LIBRARY
OTTAWA



BIBLIOTHÈQUE NATIONALE
OTTAWA

NAME OF AUTHOR..... D. SIMPSON

TITLE OF THESIS... LIGHT REFLECTION FROM
SUCK WAVES

UNIVERSITY OF... ALBERTA

DEGREE FOR WHICH THESIS WAS PRESENTED..... Ph.D.

YEAR THIS DEGREE GRANTED..... 1970

Permission is hereby granted to THE NATIONAL LIBRARY
 OF CANADA to microfilm this thesis and to lend or sell copies
 of the film.

The author reserves other publication rights, and
 neither the thesis nor extensive extracts from it may be
 printed or otherwise reproduced without the author's
 written permission.

(Signed)..... D. Simpson

PERMANENT ADDRESS:

ELECTRICITY COUNCIL RESEARCH CENTRE
CAPENHURST
CHESTER CH1-6ES

DATED..... September 17 1970

ENGLAND

THE UNIVERSITY OF ALBERTA
LIGHT REFLECTION FROM SHOCK WAVES

by



D. Simpson

A THESIS
SUBMITTED TO THE FACULTY OF GRADUATE STUDIES
IN PARTIAL FULFILMENT OF THE REQUIREMENTS FOR THE DEGREE
OF DOCTOR OF PHILOSOPHY

DEPARTMENT OF ELECTRICAL ENGINEERING

EDMONTON, ALBERTA

FALL 1970

UNIVERSITY OF ALBERTA
FACULTY OF GRADUATE STUDIES

The undersigned certify that they have read,
and recommend to the Faculty of Graduate Studies for
acceptance, a thesis entitled "Light Reflection from
Shock Waves" submitted by D. Simpson in partial
fulfilment of the requirements for the degree of Doctor
of Philosophy.

Peter R. Smy
.....
Supervisor
A. Hoffenberg
.....
J. Karlin
.....
A. Lequin
.....

J. L. Curzon
.....
External Examiner

Date. *September 11/70*

.....

LIGHT REFLECTION FROM SHOCK WAVESABSTRACT

The process by which light is reflected by a moving shock front is examined in some detail, and techniques are described by which the shock velocity, reflectivity, curvature and tilt can be measured simultaneously or separately without perturbing the shock wave in any way. The techniques developed are shown to be particularly applicable to the complex experimental situations encountered in plasma physics and give a considerable improvement over previous measurements in accuracy and information retrieval capability. To check the validity of the measurements at high pressures, a new form of shock tube has been developed to generate hypersonic shock waves in air at one atmosphere.

Acknowledgements

As always, the research reported here is the result of the cooperative efforts of a large number of people, but I would particularly like to thank Dr. P.R. Smy for his excellent supervision and encouragement, Dr. G.J. Pert for many helpful suggestions and Mr. C. Davies whose advice and assistance on technical matters were invaluable through the whole course of the project.

My thanks are also due to Mr. E. Buck and his staff for the construction of the shock tubes, particularly Mr. G. Fij, and to Mr. G.M. Seeds for assistance in obtaining the experimental results.

Finally, I am grateful to the University of Alberta and the National Research Council of Canada for their financial assistance throughout the project.

LIGHT REFLECTION FROM SHOCK WAVESTABLE OF CONTENTS

ABSTRACT	II
TABLE OF CONTENTS	IV
LIST OF FIGURES	VII
NOTATION	IX
I INTRODUCTION	1
1.1 Purpose and Scope of the Thesis	1
1.2 Previous Experiments	2
II EXPERIMENTAL CONDITIONS	5
2.1 Light Source	5
2.2 Detector	5
2.3 Theoretical Calculation of Photodetector Noise and Bandwidth	6
III THEORY	13
3.1 Summary of Shock Tube Theory	13
3.1.1 Introduction	13
3.1.2 Compressible Gas Flow	13
3.1.3 Formation of Shock Waves	14
3.1.4 Shock Relations for an Ideal Gas	15
3.1.5 Shock Tube Theory	17
3.1.6 Production of Strong Shock Waves	21
3.1.7 Strong Shock Equations	23

3.2	Theory of Light Reflection from a Density Discontinuity	24
3.2.1	First Order Theory	24
3.2.2	Second Order Theory	25
3.2.3	Calculation of Reflection Coefficient	30
IV	SIMPLE MEASUREMENT OF SHOCK VELOCITY AND REFLECTION COEFFICIENT	35
4.1	Introduction	35
4.2	Shock Tube	37
4.3	Optical System	38
4.3.1	Method of Measuring Shock Velocity	41
4.3.2	Effect of Shock Tilt	41
4.3.3	Effect of Shock Curvature	43
V	MEASUREMENT OF SHOCK VELOCITY, REFLECTIVITY AND CURVATURE USING	
A	DIFFERENTIAL INTERFEROMETER	46
5.1	Magnitude of Doppler Shift	46
5.2	Observation of Doppler Shift	47
5.3	The Differential Doppler Interferometer	48
5.4	Modulation Depth	51
5.5	Measurement of Shock Velocity	52
5.6	Measurement of Shock Front Curvature	54
5.7	Measurement of Shock Reflectivity	56
5.7.1	Rejection of Stray and Scattered Light	56
5.7.2	Spatial Resolution	57
5.8	Effect of Shock Front Tilt	58
5.8.1	Effect on Shock Velocity Measurement	58
5.8.2	Effect on Shock Curvature Measurement	58

5.8.3	Effect on Shock Reflectivity Measurement	59
5.9	Experimental Results	60
VI	ALTERNATIVE MEASUREMENT OF SHOCK CURVATURE AND TILT	70
6.1	Introduction	70
6.2	Experimental Arrangement	70
6.3	Determination of Curvature	72
6.4	Determination of Shock Tilt	75
VII	THE HIGH INTENSITY SHOCK SYSTEM	79
7.1	Purpose	79
7.2	Production of Strong Shock Waves	79
7.3	Theory of the Electrothermal Shock Tube	80
7.4	Design of the Shock System	84
7.5	Operation and Performance of the Shock Tube	88
VIII	MEASUREMENT OF REFLECTIVITY AND CURVATURE OF HYPERSONIC SHOCKS	93
8.1	Reflection Coefficient	93
8.1.1	Choice of Method of Measurement	93
8.1.2	Experimental Results	95
8.2	Measurement of Shock Curvature	97
IX	CONCLUSION AND SUGGESTIONS FOR FURTHER WORK	103
9.1	Conclusion	103
9.2	Suggestions for Further Work	103
	REFERENCES	106
	BIBLIOGRAPHY	109
	ACKNOWLEDGEMENTS	110
	APPENDIX	

Theory of Reflection from a Beam Splitter

LIGHT REFLECTION FROM SHOCK WAVESLIST OF FIGURES

<u>Figure</u>	<u>Title</u>	
1.1	General Arrangement: Shock Tube and Optical System	4
2.1	Photomultiplier Circuit	7
2.2	Bandwidth vs Light Signal	11
3.1	Shock Strength vs Driving Pressure Ratio	19
3.2	Mach Number vs Shock Strength	20
3.3	Driving Pressure Ratio vs Mach Number	22
3.4	Reflection Coefficient vs Angle	29
3.5	Reflection Coefficient vs Mach Number	33
3.6	Reflection Coefficient vs Angle	34
4.1	Reflectivity Measurement	36
4.2	Method of measuring Shock Velocity from Duration of Reflected Pulse	39
4.3	Effect of Shock Tilt	40
4.4	Effect of Shock Curvature	42
4.5	Intensity Reflection Coefficient vs Angle	45
5.1	Differential Doppler Interferometer	49
5.2	Traces obtained with Differential Interferometer	61
5.3	Variation of Beat Frequency with Shock Velocity	63
5.4	Variation of Beat Frequency with Angular Beam Separation	64
5.5	Signals Observed with curved reflectors	66

<u>Figure</u>	<u>Title</u>	
5.6	Shock Front Radius vs Pressure	67
5.7	Intensity Reflection Coefficient vs Angle	69
6.1	Curvature Measurement	73
6.2	Tilt Measurement	76
7.1	Driver Chamber Temperature and Pressure vs Shock Strength and Mach Number	83
7.2	Longitudinal Section of High Intensity Shock Tube	86
7.3	Velocity Measurement with Ionization Probes	90
7.4	Mach Number vs Capacitor Bank Voltage	91
8.1	Reflection Coefficient vs Mach Number	96
8.2	Shock Radius of Curvature vs Mach Number	98
8.3	Shock Curvature vs Mach Number	99

LIGHT REFLECTION FROM SHOCK WAVESNOTATIONRoman Capital Letters

A	Shock Tube Cross Sectional Area	(m ²)
C	Photomultiplier Circuit Capacitance	(F)
<u>E</u>	Electromagnetic Wave Electric Field Vector	(V.m. ⁻¹)
E ₀	Amplitude of Incident Electric Field Vector	(V.m. ⁻¹)
E ₁	Amplitude of Refracted Electric Field Vector	(V.m. ⁻¹)
E _r	Amplitude of Reflected Electric Field Vector	(V.m. ⁻¹)
F	Focal Length of Detecting System Collimating Lens	(m.)
I _p	Photodetector Noise Current	(A)
I _s	Photomultiplier Output Signal Current	(A)
I _{max}	Maximum Reflected Light Intensity	(W)
I _{min}	Minimum Reflected Light Intensity	(W)
K	Gladstone-Dale Constant	(m. ³ .Kg ⁻¹)
M	Mach Number of Shock Wave	(dimensionless)
N	Total Number of Beats in Reflected Pulse	(dimensionless)
R	Shock Front Reflection Coefficient	(dimensionless)
R ₀	Universal Gas Constant (=287 joule. Kg ⁻¹ °K ⁻¹)	
R ₁	Upper Limit of R	(dimensionless)
R ₂	Lower Limit of R	(dimensionless)
R _L	Photomultiplier Load Resistance	(Ω)
S	Photomultiplier Sensitivity	(A.W ⁻¹)

T	Absolute Temperature	(°K)
T _R	Absolute Temperature of Load Resistor	(°K)
U	Internal Energy of Gas	(J.m ⁻³)
V _m	Photomultiplier Measuring Circuit Noise Voltage	(V.)
V _P	Photodetector Noise Voltage	(V)
V _R	Photomultiplier Load Resistor Noise Voltage	(V.)
V _S	Photomultiplier Output Signal Voltage	(V.)
V ₃	Shock Tube Driver Chamber Volume	(m ³)
W	Photomultiplier Input Light Intensity	(W.)

Roman Lower Case Letters

c	Velocity of Light in Free Space (=2.998 x 10 ⁸ m.sec. ⁻¹)	
c ₀	Velocity of Sound in Downstream Gas	(m.sec. ⁻¹)
c ₃	Velocity of Sound in Driver Gas	(m.sec. ⁻¹)
c ₃₀	Velocity of Sound in Driver Gas at Room Temperature	(m.sec. ⁻¹)
d	Incident Light Beam Width	(m.)
e	Electronic Charge (=1.602 x 10 ⁻¹⁹ c.)	
f	Frequency of Photomultiplier Output Signal	(Hz)
i	Angle of Incidence	(rad.)
j	√-1	(dimensionless)
k	Boltzmann's Constant (=1.38 x 10 ⁻²³ J.°K ⁻¹)	
l	Length of Reflection Region	(m.)
l _φ	Length of Reflection Region for a Tilted Shock	(m.)
n	Refractive Index	(dimensionless)

p	Gas Pressure	$(N.m.^{-2})$
p_o	Downstream Gas Pressure	$(N.m.^{-2})$
p_3	Driver Gas Pressure	$(N.m.^{-2})$
p_{30}	Driver Gas Pressure at Room Temperature	$(N.m.^{-2})$
r	Angle of Refraction	$(rad.)$
r_s	Shock Front Radius of Curvature	$(m.)$
r_t	Shock Tube Internal Radius	$(m.)$
r_3	Gas Constant for Unit Mass of Driver Gas	$(m.^2 \text{ } ^\circ K.^{-1} \text{ sec.}^{-1})$
t	Generalized Time	$(sec.)$
t_D	Interaction Duration	$(sec.)$
t_ϕ	Interaction Duration for a Tilted Shock	$(sec.)$
u	Gas Velocity	$(m.sec^{-1})$
u_p	Pressure Pulse Velocity	$(m.sec^{-1})$
v	Generalized Velocity	$(m.sec^{-1})$
v_s	Shock velocity	$(m.sec^{-1})$
x	Spatial Coordinate Parallel to Shock Tube Axis	$(m.)$
x_m	Axial Extent of Shock Front	$(m.)$
y	Shock Strength $(\equiv p/p_o)$	$(dimensionless)$

Greek Capital Letters

Δ	Optical Path Length	$(m.)$
$\Delta\nu$	Doppler Shift of Frequency ν	$(Hz.)$
$\Delta\nu$	Doppler Shift of Frequency ν_i	$(Hz.)$
$\Delta\nu_{i+\delta_i}$	Doppler Shift of Frequency $\nu_{i+\delta_i}$	$(Hz.)$

Greek Lower Case Letters

α	Shock Front Curvature Parameter ($\cong r_c/r_s$)	(dimensionless)
γ	Ratio of Specific Heats of a Gas	(dimensionless)
γ_0	Ratio of Specific Heats of Downstream Gas	(dimensionless)
γ_3	Ratio of Specific Heats of Driver Gas	(dimensionless)
δE	Change in Magnitude of Electric Field Vector	(V.m. ⁻¹)
δf	Bandwidth of Photomultiplier System	(Hz.)
δi	Difference in Angles of Incidence	(rad.)
δn	Change in Refractive Index Across a Shock Front	(dimensionless)
δt	Time Shift of Reflected Pulse 'Dip'	(sec.)
δx	Shock Front Thickness	(m.)
$\delta \theta$	Difference in Grazing Angles of Incidence ($\cong \delta i$)	(rad.)
ϵ	Shock Tube Thermal Efficiency	(dimensionless)
η	Shock Compression ($\cong \rho/\rho_0$)	(dimensionless)
θ	Nominal Grazing Angle of Incidence	(rad.)
θ_0	Actual Grazing Angle of Incidence ($\cong \pi/2-i$)	(rad.)
θ_1	Grazing Angle of Refraction ($\cong \pi/2-r$)	(rad.)
λ	Wavelength of Light	(m.)
μ	$\cong \frac{\gamma-1}{\gamma+1}$	(dimensionless)
ν	Frequency of Light	(Hz.)
ν_D	Differential Beat Frequency	(Hz.)
ν_i	Frequency of Light Reflected at Angle i	(Hz.)
$\nu_{i+\delta i}$	Frequency of Light reflected at Angle $i+\delta i$	(Hz.)
π	Ratio of Circumference to Diameter of a Circle ($\cong 3.142$)	(dimensionless)

ρ	Gas Density	(Kg.m. ⁻³)
ρ_0	Density of Downstream Gas	(Kg.m. ⁻³)
τ	Photomultiplier System Risetime	(sec.)
ϕ	Angle of Shock Front Tilt	(rad.)

Subscripts

0	Downstream Gas; Incident Light Beam
1	Shocked Gas; Refracted Light Beam
2	Driver Gas, after Rarefaction
3	Driver Gas, Initial Conditions
r	Reflected Light Beam
s	Shock Wave
p	Pressure Wave

I Introduction

1.1 Purpose and Scope of the Thesis

The use of measurements of the scattering of a laser beam is now a well-established diagnostic technique in Plasma Physics⁽¹⁾. In the majority of cases, using quiescent plasmas, valid results have been obtained, but a number of workers^(2,3,4) have reported results of situations where the plasma is either moving bodily, or expanding rapidly. In these cases pressure gradients are present in the plasma, and can cause refraction effects which may be confused with the scattering produced by the plasma. In the extreme case, the plasma boundary moves so rapidly that a shock wave is set up ahead of the plasma and a relatively strong reflection of the diagnostic light beam can occur at the resulting discontinuity in gas or plasma density. An example of this type of plasma is that produced by focusing a ruby laser in a high pressure gas, and anomalous results have been reported for the scattering of light by such plasmas^(5,6).

An investigation of the range of "scattering angles" and mach numbers in which light-reflection by shock waves is significant is thus clearly of considerable importance in the field of plasma diagnostics, and the exact mechanism of reflection is also of interest in its own right, as well as for the information on shock-structure which can be obtained. The primary purpose of this thesis

is thus to determine under what conditions light reflection can be expected to occur from the shock wave associated with a rapidly moving or expanding plasma, and how this light can be distinguished from that scattered by the plasma producing the shock front. Some new information on the structure of shock fronts has also been obtained, and a powerful tool for the investigation of the general behaviour of shock waves has been developed.

1.2 Previous Experiments

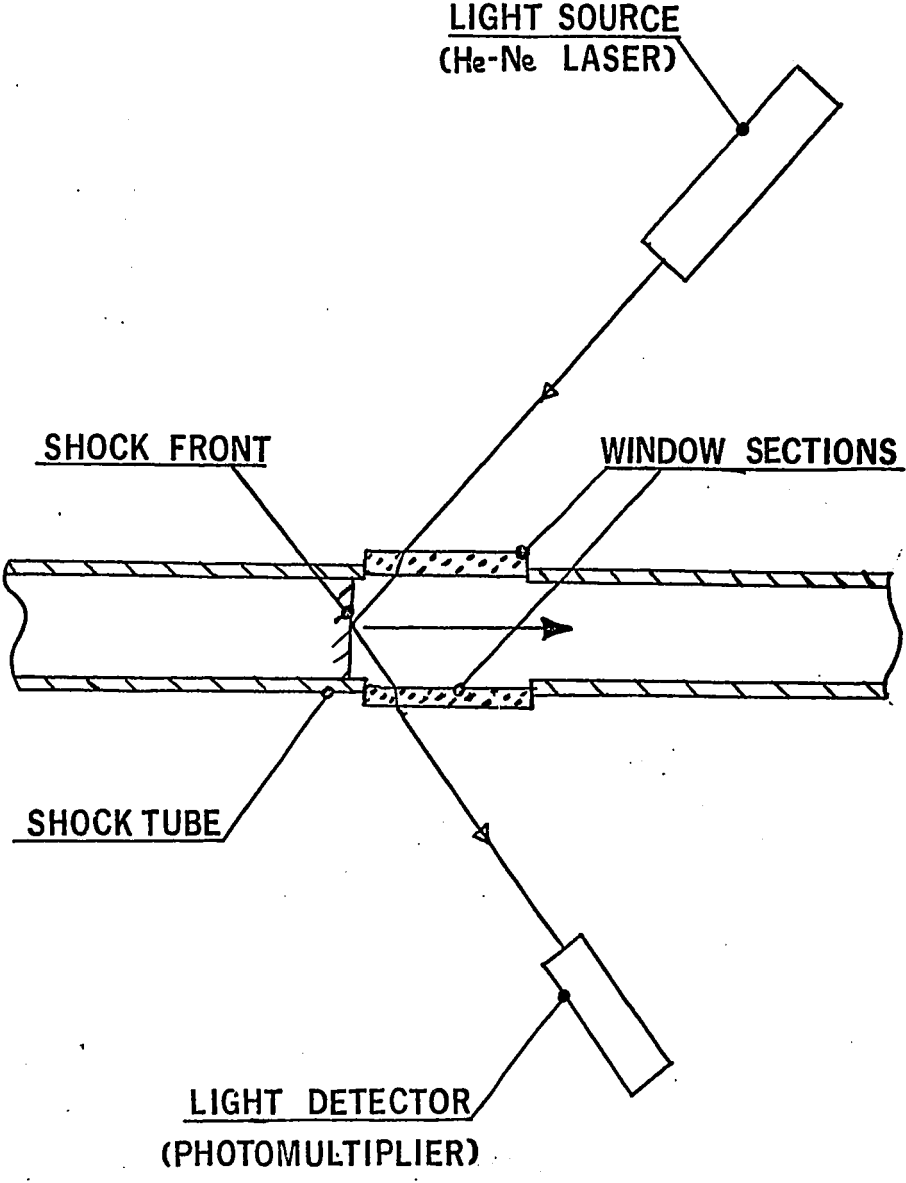
The interaction of electromagnetic radiation with a shock wave has been investigated by several workers. Hey et al.⁽⁷⁾ working at microwave frequencies have used the Doppler Shift of the frequency of the reflected radiation to determine the shock velocity. The use of microwave radiation, however, is restricted to the case of high mach number shock waves, which produce appreciable ionization behind the shock front.

An extensive investigation of the reflection of light by a low mach number shock wave has been carried out by Hornig and his co-workers^(8,9,10,11) over a number of years, and some useful information on shock structure has been obtained. A number of anomalies in the values of reflection coefficient derived from these, and the similar experiments of Court & Mallory⁽¹²⁾ were observed however, and variously attributed to scattering of light by dust^(9,10) or water vapour⁽¹²⁾ in the shocked gas, or to shock wave curvature⁽¹¹⁾.

The problems encountered in these experiments are thus similar to those present in laser-plasma scattering experiments (which frequently involve highly non-planar shock waves⁽⁵⁾) in that both require a distinction to be made between scattered and reflected light, although different parts of the total light-signal are required to extract the required information in each field.

The experiments carried out in the course of this investigation follow the general lines of those of Hornig et al.^(8,9,10,11) with the exception that a gas laser has been used as the light source instead of the intense, broadband thermal light source of Hornig et al. The coherence, narrow wavelength spread and low divergence inherent in the laser, apart from simplifying the optical arrangements necessary in the direct measurement of reflection coefficient, have made possible a number of new measurement techniques not previously available at such short wavelength (632.8 nm). A general outline of the experimental arrangement using a shock tube to produce the shock wave is given in fig 1.1.

FIG. 1:1 GENERAL ARRANGEMENT-SHOCK TUBE AND OPTICAL SYSTEM



II Experimental Conditions

2.1 Light Source

The most frequently-used light source for plasma scattering experiments is the pulsed ruby laser⁽¹⁾, but it is more convenient for most experiments to use a continuous-wave laser. In the experiments described here a Helium-Neon laser was used, operating at a wavelength of 632.8 nm, and a power of 1 mW. The wavelength is thus very close to that of the commonly-used ruby laser (694.3 nm) but the power density is considerably less, and consequently there is much less possibility of the diagnostic laser beam perturbing the shock front in any way.

2.2 Detector

The choice of a low-power light source imposes fairly stringent requirements on the detector used, since the coefficients of reflection involved are of the order of 10^{-3} to 10^{-5} , so that the detector must be capable of distinguishing a signal of 10^{-6} to 10^{-8} w, from the background noise, stray light etc. In addition, the response of the detector must be fast enough to observe the reflected light signal during the necessarily short time for which the shock wave and light beam interact. Typical shock wave-laser beam interactions will have durations of only a few microseconds, so a 'bandwidth' of approximately d.c to 10 MHz is required.

The only type of light detector with sufficient sensitivity for use in these reflection experiments was found to be a photomultiplier. The high gain R.C.A. type 8645 was chosen, and a preliminary investigation undertaken to determine under what operating conditions this type of photomultiplier could meet the requirements of low noise and 'bandwidth'.

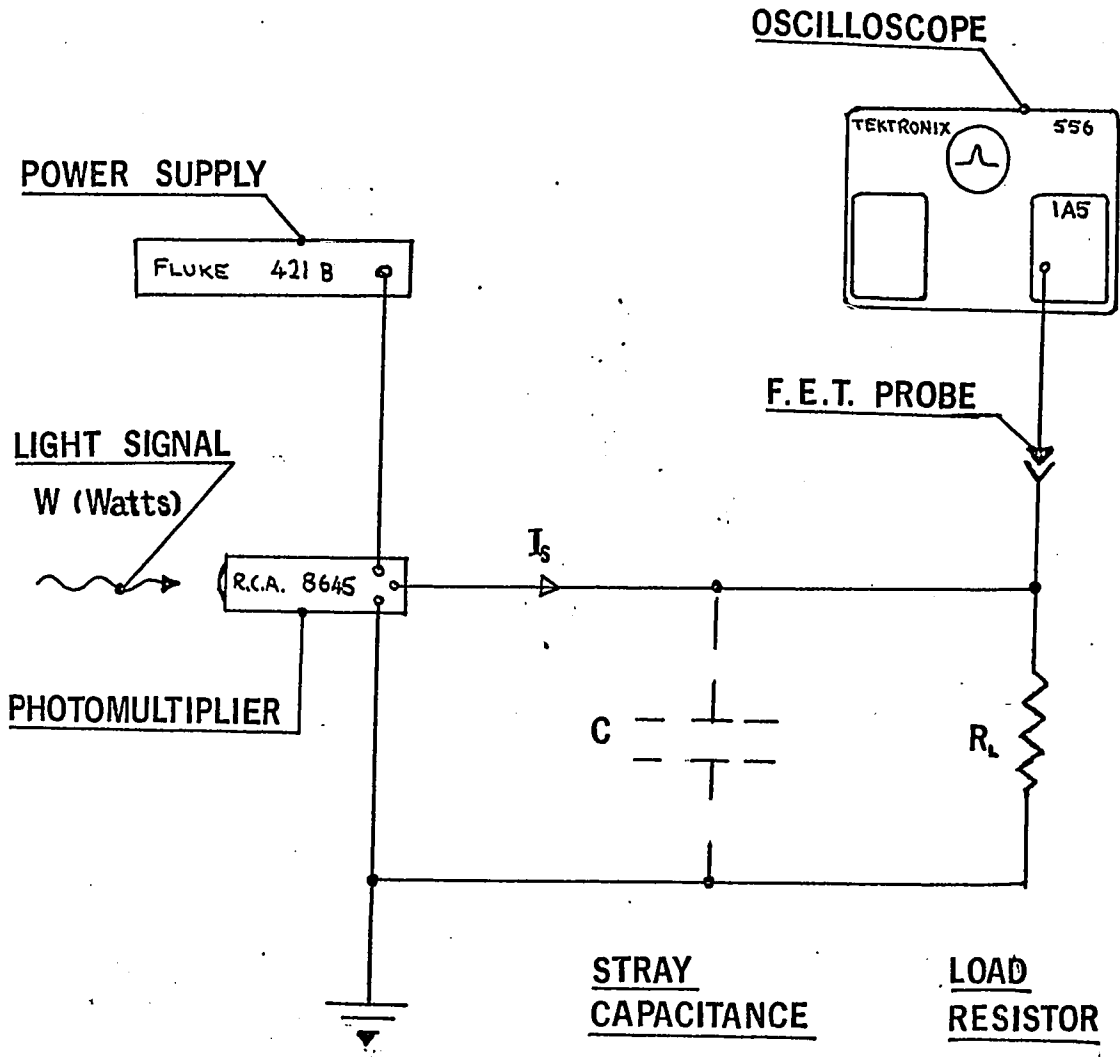
2.3 Theoretical Calculation of Photomultiplier Noise and Bandwidth

The theory of noise in photodetectors is well understood (13,14) and need not be reproduced in detail here. The use of a photomultiplier entails the introduction of additional sources of noise, however, since this type of light-detector is basically a current generator (RCA 8645 tube - maximum sensitivity, $S = 1000 \text{ A/W}$) and thus requires a load resistor in order to display a time-dependent voltage on conventional measuring equipment. Noise is introduced both by the load resistor, R_L and the measuring equipment itself. The type of measuring system used is shown in fig 2.1.

The signal voltage generated by such a system for an input light power of W (watts) is then given by:-

$$V_s = S R_L W \quad (2.1)$$

FIG. 2-1 PHOTOMULTIPLIER CIRCUIT



And this signal must be observable over a total noise voltage comprising the resistor noise:-

$$V_R = \sqrt{4kT_R R_L \delta f} \quad (2.2)$$

where δf is the bandwidth of the system

T_R is the resistor temperature

and k is Boltzmann's constant

added to the measuring system noise, V_m , which with the equipment used here, (Tektronix 556 oscilloscope, type 1A5 pre-amplifier and P6045 field-effect transistor active probe) was constant at 1 mV over the entire range of signal voltages and frequency, and also added to the photodetector noise V_p .

The Photodetector noise V_p originates as a noise current

$$I_p = \sqrt{I_s \cdot e \cdot \delta f \cdot G} \quad (2.3)$$

where G is the current gain of the photomultiplier,

I_s is the signal current

and e the electronic charge

$$\text{clearly } V_p = I_p R_L \quad (2.4)$$

$$\text{and } I_s = V_s / R_L \quad (2.5)$$

$$\text{giving } V_p = \sqrt{e V_s \cdot R_L \cdot \delta f} \quad (2.6)$$

It is apparent from equations (2.2) and (2.6) that the noise voltages present are proportional to the square root of R_L , whilst the signal voltage is directly proportional to R_L , so that it should be possible to obtain any desired signal-to-noise ratio by simply increasing the load resistance, R_L .

Unfortunately, however, the photomultiplier possesses a small but finite output capacitance C (in which can be included any stray capacitance in the load resistor circuit, and the measuring probe) which couples with the load resistance to give a minimum system risetime:-

$$\tau = R_L C \quad (2.7)$$

so that the maximum frequency, f , which can be observed is:-

$$f = \frac{1}{2\pi\tau} = \frac{1}{2\pi R_L C} \quad (2.8)$$

and this frequency is also equal to the maximum bandwidth of the system, δf , since the system must be capable of observing d.c signals.

$$\text{i.e.} \quad \delta f = \frac{1}{2\pi R_L C} \quad (2.9)$$

So the quantity $R_L \delta f$ which appears in both noise voltages is in fact fixed at

$$R_L \delta f = \frac{1}{2\pi C} \quad (2.10)$$

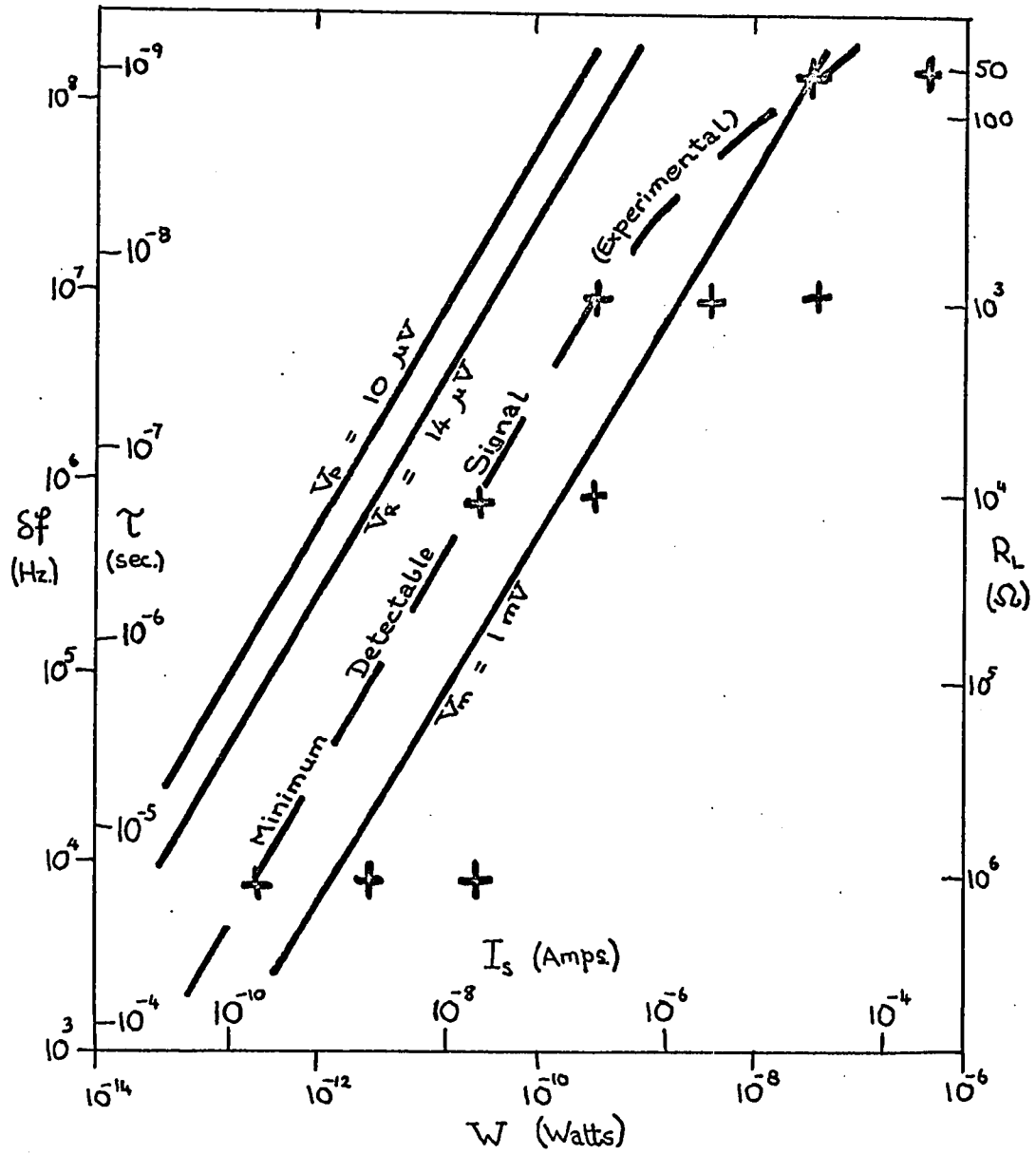
and the value of R_L used to obtain the signal voltage V_s (eq. 2.1) is

determined from eq.(2.9) by the maximum bandwidth required.

To obtain the maximum photomultiplier-measuring system gain and bandwidth it is thus primarily necessary to reduce the capacitance, C , as much as possible. By using connectors between the photomultiplier and load resistor which are as short as possible, and by using a low-capacitance voltage measuring probe it was found possible to reduce C to a total of 20 pF, comprised of 8 pF intrinsic photo-tube capacitance, 4 pF probe capacitance and 8 pF stray capacitance to ground. Different load resistors can then be employed to obtain a high sensitivity or a large bandwidth system, as required. The effect variation of R_L on the minimum observable signal power is shown in fig 2.2 which is a plot of δf against W for a typical photomultiplier voltage (1200V; giving $S = 600$ A/W) for equations (2.2) and (2.6), and also for the measuring system noise voltage of 1 mV. Only signals which lie to the right of one of the solid lines on the graph can be distinguished from the appropriate noise signal, (signal to noise ratio of one). In practice, of course, slightly smaller signals can be observed, as shown by the experimental points on the graph, which were obtained by using neutral density filters to vary the laser input power to the phototube with a number of different load resistors, R_L . The minimum observable power is found to correspond to a ratio of signal to total noise of about one to ten.

FIG. 2-2 BANDWIDTH VS. LIGHT SIGNAL

† • Experimental Verification Points.



The graph shows that the system is capable of reducing the resistor and photomultiplier noise components to negligible levels, leaving the noise in the measuring system. Even with this relatively high noise level, however, system bandwidths of 10 MHz are attainable even for input powers as low as 10^{-6} - 10^{-7} watts, so that using such a measuring system, reflection coefficients of 10^{-3} to 10^{-4} should be measureable, using a 1 mW laser as the light source.

III Theory

3.1 Summary of Shock Tube Theory

3.1.1 Introduction

The production of shock waves, and the operation of the conventional shock tube is now well-understood, and is discussed in some detail by Wright⁽¹⁵⁾. Only a brief outline of the theory will be given here.

3.1.2 Compressible gas flow

Three equations can be conveniently set up to describe the motion of a compressible gas in one dimension relative to the laboratory frame of reference.

a) The equation of conservation of mass

$$A \frac{\partial \rho}{\partial t} + \frac{\partial}{\partial x} (\rho u A) = 0 \quad (3.1)$$

where ρ is the gas density
 u is the gas velocity

and A is the cross-sectional area of the mass of gas considered.

b) The equation of conservation of momentum

$$\frac{\partial u}{\partial t} + u \frac{\partial u}{\partial x} = - \frac{1}{\rho} \frac{\partial p}{\partial x} \quad (3.2)$$

where p is the gas pressure

c) The equation of state of the gas

$$p = R_0 \rho T \quad (3.3)$$

where T is the gas temperature

and R_0 is the universal gas constant

Assuming that we have an ideal gas.

If we further assume that the gas is contained in a tube of constant cross-section, A , and that the propagation of the pressure-disturbance is adiabatic, equations (3.1), (3.2) and (3.3) can be combined with the relationship

$$p \rho^{-\gamma} = \text{constant} \quad (3.4)$$

to give the propagation velocity of a pressure-pulse through a gas as

$$u_p = C_0 \left[\frac{\gamma+1}{\gamma-1} \left(\frac{p}{p_0} \right)^{\frac{\gamma-1}{2\gamma}} - \frac{2}{\gamma-1} \right] \quad (3.5)$$

where C_0 is the velocity of sound

and p_0 the pressure in the undisturbed gas

3.1.3 Formation of Shock Waves

It follows from eq.(3.5) that for a weak pressure pulse ($p=p_0$), U_p tends towards C_0 , the sound speed in the undisturbed gas, but that for large overpressures, p , the disturbance may be propagated considerably faster than the velocity of sound. Furthermore, it is

evident from eq.(3.5) that the velocity, u_p increases as the pressure, p , increases, so that the higher pressure region of any pulse will tend to propagate faster than the preceding lower pressure regions, causing the pulse to 'steepen up' as it propagates, and ultimately to form a pressure discontinuity - termed a 'shock wave'.

3.1.4 Shock Relations for an Ideal Gas

The equations derived in section 3.1.2 for a simple pressure pulse no longer hold once the shock wave has developed, since the assumption of adiabatic (more exactly - isentropic) behaviour at the pressure discontinuity is no longer valid.

We consider a frame of reference moving at the shock velocity v_s . Distinguishing quantities in the undisturbed and shocked gases by the subscripts 0 and 1 respectively, we define for convenience, three new quantities:-

$$\text{Shock Mach Number} \quad M = v_s / C_0 \quad (3.6)$$

$$\text{Shock Strength} \quad y = p_1 / p_0 \quad (3.7)$$

$$\text{Shock Compression} \quad \eta = \rho_1 / \rho_0 \quad (3.8)$$

The law of Conservation of Matter then gives:-

$$\rho_0 v_s = \rho_1 (v_s - u_1) = \dot{m} \quad (3.9)$$

where \dot{m} = the mass of gas "swept-up" by the shock front in unit time

and u_1 = gas flow velocity behind the shock

Newton's 3rd Law of Motion gives:-

$$\rho u_1 = p_1 - p_0 \quad (3.10)$$

The Law of Conservation of Energy gives:-

$$p_0 v_s + \rho U_0 + \frac{1}{2} \rho v_s^2 = p_1 (v_s - u_1) + \rho U_1 + \frac{1}{2} \rho (v_s - u_1)^2 \quad (3.11)$$

where U is the internal energy of the gas.

Eqs. (3.9), (3.10) and (3.11) are known as the Rankine-Hugoniot Equations

For an ideal gas:-

$$U = C_v T \quad (3.12)$$

$$p = R_0 \rho T \quad (3.13)$$

$$C_p = \gamma C_v \quad (3.14)$$

$$\text{and } C_p - C_v = R_0 \quad (3.15)$$

$$\text{so that } U = \frac{p}{(\gamma-1)\rho} \quad (3.16)$$

We can now solve the Rankine-Hugoniot Equations, to give:-

$$M \equiv \frac{v_s}{C_0} = \sqrt{\frac{\gamma + \mu}{1 + \mu}} \quad (3.17)$$

$$\text{and } \eta \equiv \frac{\rho_1}{\rho_0} = \frac{\mu + \gamma}{1 + \mu \gamma} \quad (3.18)$$

$$\text{where } \mu \equiv \frac{\gamma - 1}{\gamma + 1} \quad (3.18)$$

giving the Mach Number and Shock Compression as a function of shock strength (γ).

3.1.5 Shock Tube Theory

The typical shock tube consists of two sections, separated initially by a gas-tight diaphragm - a driver section, at a high pressure, p_3 , and an expansion chamber, at a lower pressure, p_0 .

When the diaphragm is ruptured, a shock wave is formed, and propagates down the expansion chamber, whilst an expansion wave propagates back through the driver section. In order to avoid discontinuities forming in gas density and pressure behind the shock front, it is clear that the gas flow velocities behind the shock and the rarefaction waves must be identical. Since it is possible to have different gases, initially in the drive and expansion sections, we denote quantities referring to the region behind the shock front, as far as the 'contact surface' which separates the two gases, by the subscript 1, and quantities referring to the driver gas between the contact surface and the rarefaction wave by the subscript 2. The subscripts 0 and 3 refer to the undisturbed expansion chamber and driver section gases respectively.

From eqs.(3.1), (3.2) and (3.3) we can derive the gas flow velocity behind the rarefaction wave as

$$u_2 = - \frac{2c_3}{\gamma_3 - 1} \left[\frac{p_2}{p_3} \frac{\gamma_3 - 1}{2\gamma_3} - 1 \right] \quad (3.20)$$

whilst the Rankine-Hugoniot equations can be solved in terms of the gas flow velocity behind the shock wave, to give

$$u_1 = \frac{C_o (1-\mu_o) (p_1/p_o - 1)}{\sqrt{(1+\mu_o) (p_1/p_o + \mu_o)}} \quad (3.21)$$

And, to avoid discontinuities at the contact surface, we must have:-

$$p_1 = p_2 \quad (3.22)$$

$$u_1 = u_2 \quad (3.23)$$

$$\text{and we define } y \equiv p_1/p_3 \quad (=p_2/p_3) \quad (3.24)$$

so we have:-

$$\frac{C_o}{C_3} \frac{(1-\mu_o)(y-1)}{\sqrt{(1+\mu_o)(y+\mu_o)}} = \frac{2}{\gamma_3 - 1} \left[1 - \left(\frac{p_o}{p_3} \cdot y \right)^{\frac{\gamma_3 - 1}{2\gamma_3}} \right] \quad (3.25)$$

which defines the shock strength, y , in terms of the initial pressure ratio p_o/p_3 , and the quantities μ_o , γ_3 , C_o , C_3 , which are characteristic of the gases used.

We can thus determine the shock strength, y , for any given experimental conditions, and then use eq.(3.17) to predict the Mach number of the shock wave produced. Fig. 3.1 is a typical plot of y vs p_3/p_o ; whilst fig. 3.2 shows M as a function of y .

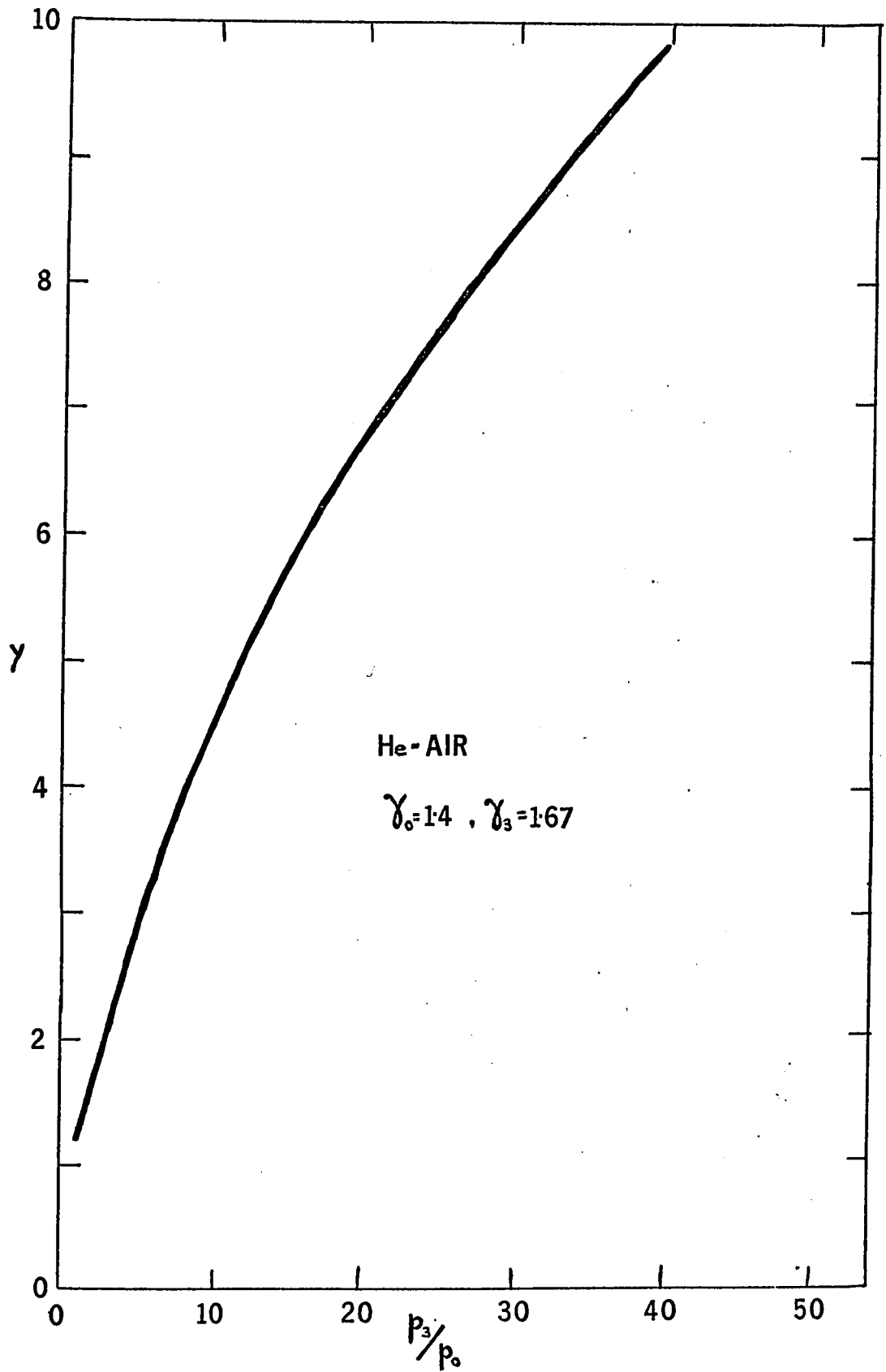
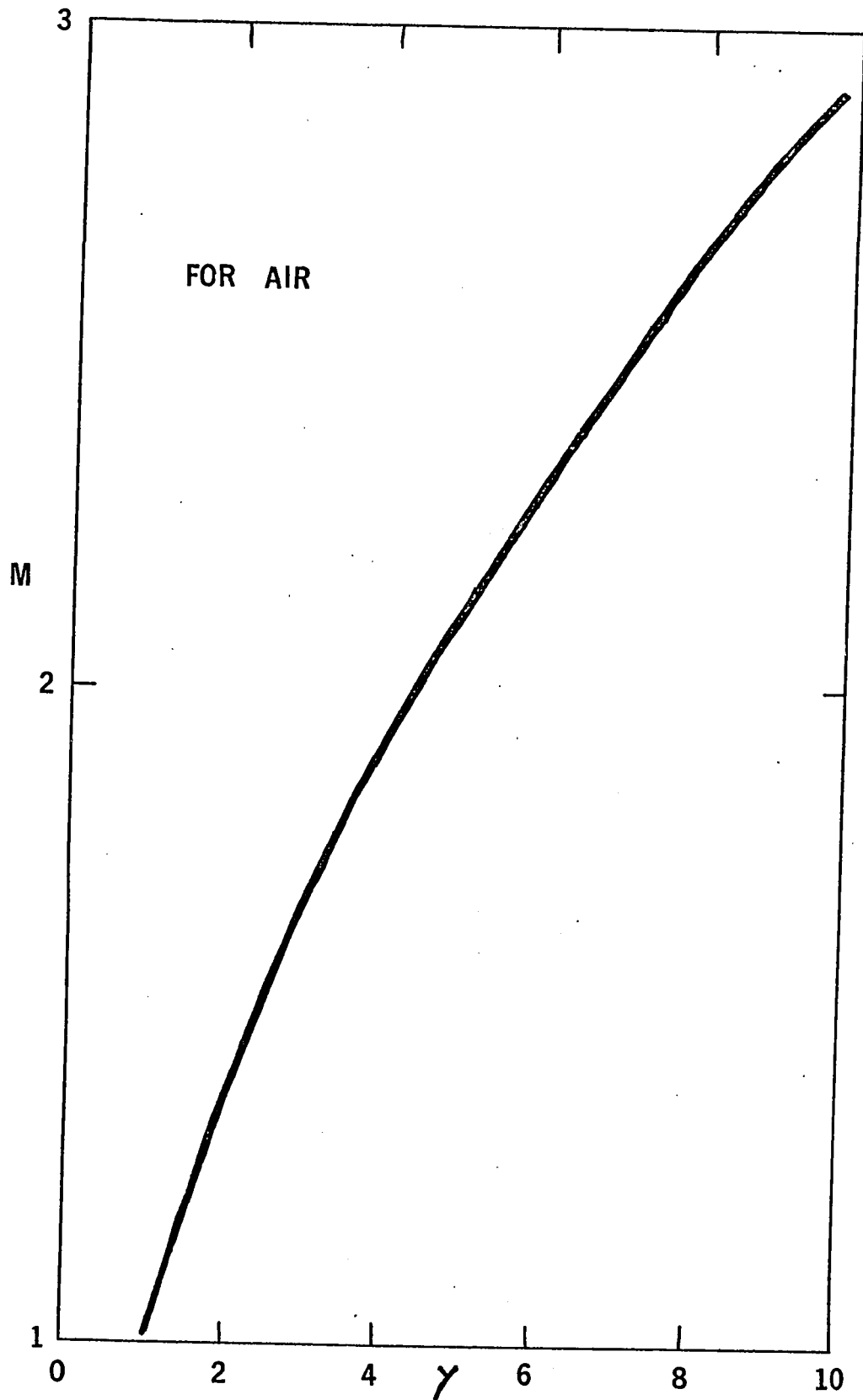
FIG. 3-1 SHOCK STRENGTH VS. DRIVING PRESSURE RATIO

FIG. 3-2 MACH NUMBER VS. SHOCK STRENGTH

3.1.6 Production of Strong Shock Waves

It is apparent from eq.(3.17) that a high mach number shock requires a large value of y , the shock strength. Consideration of eq.(3.25) shows that the largest values of y are obtained if the pressure ratio p_3/p_0 is made very large. The right-hand side of eq.(3.25) then simplifies giving:-

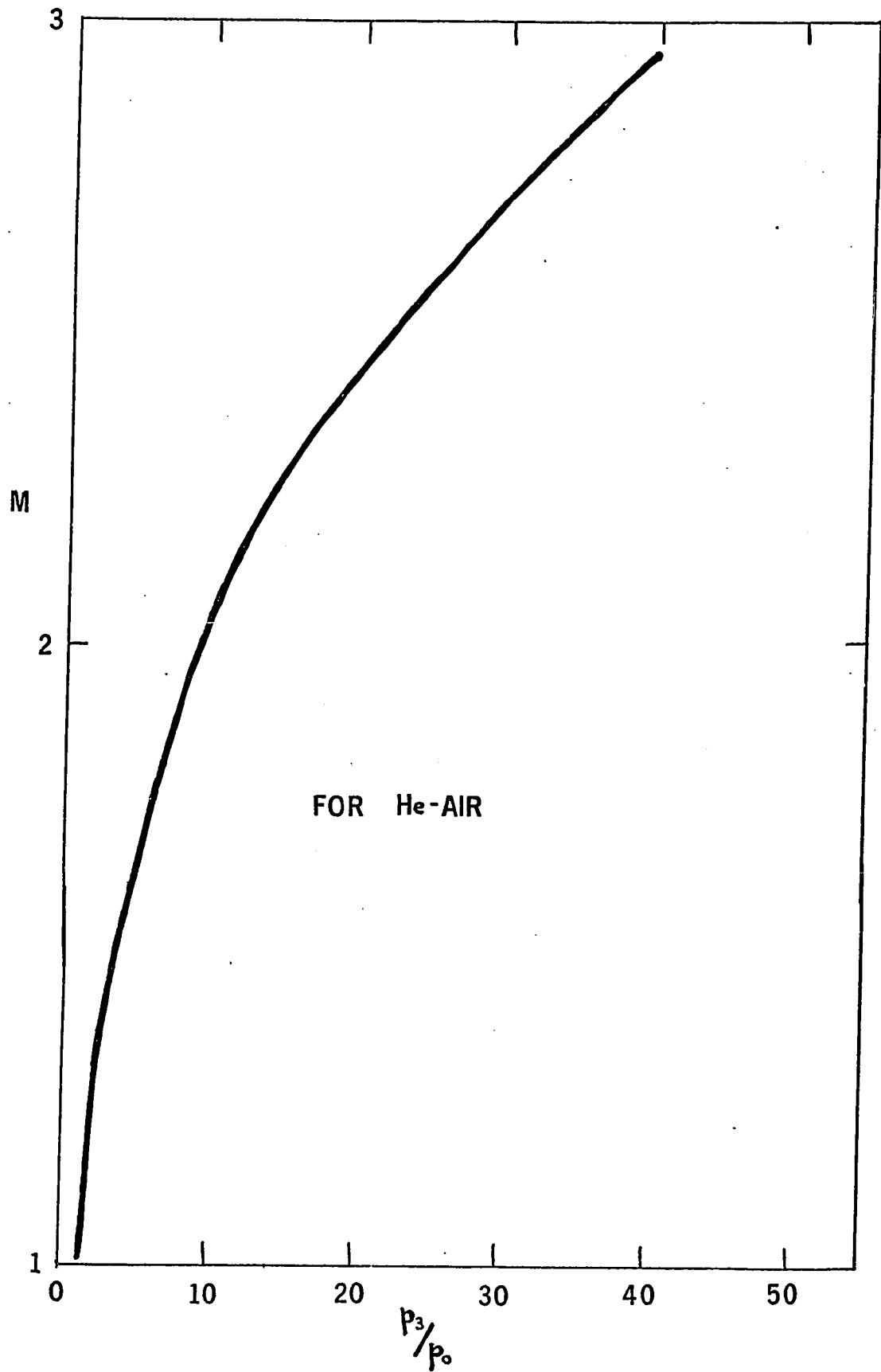
$$\frac{C_o (1-\mu_o)(y-1)}{C_3 \sqrt{(1+\mu_o)(y+\mu_o)}} = \frac{2}{(\gamma_3-1)} \quad (3.26)$$

or

$$y = \frac{2\gamma_o(\gamma_o+1)(C_3)^2}{(\gamma_3-1)^2 (C_o)^2} \quad (3.27)$$

if $y \gg 1$

It is thus essential, once p_3/p_0 has been made as large as possible, to choose the gases so as to give as large a sound-speed ratio (C_3/C_o) as possible. For this reason, Helium is commonly used as the driver gas, and air as the expansion chamber gas ($C_3/C_o = 2.91$). Fig. 3.1 shows the variation of y with initial pressure ratio p_3/p_0 for a Helium-Air shock tube. Fig. 3.2 is a plot of eq.(3.17) for air, whilst fig. 3.3 is derived from 3.1 and 3.2, and shows the Shock Mach number as a function of p_3/p_0 . It is evident from fig. 3.3 that for shock waves moving into air at 1 atmosphere, the driver section pressure becomes prohibitively high for shock waves beyond about Mach 3.5, and the simple pressure-driven shock tube described here cannot be used to produce strong shock waves in atmosphere pressure air.

FIG. 3-3 MACH NUMBER VS. DRIVING PRESSURE RATIO

3.1.7 Strong Shock Equations

In addition to the simple relation for y (eq.3.27) the following approximation can be made, for the case where y is large (strong shock waves).

$$u_1 = u_2 = \frac{2C_3}{\gamma_3 - 1} \quad (\text{from eq.3.20}) \quad (3.28)$$

and from eq.(3.17)

$$M = \sqrt{\frac{y}{1 + \mu_0}} \quad (3.29)$$

giving
$$M = \sqrt{(\gamma_0 + 1) \frac{y}{2\gamma_0}} \quad (3.30)$$

so using eq.(3.26) we find

$$M = \left(\frac{\gamma_0 + 1}{\gamma_3 - 1} \right) \left(\frac{C_3}{C_0} \right) \quad (3.31)$$

for strong shock waves.

i.e. once the initial pressure ratio p_3/p_0 is large enough to produce a strong shock wave ($y \gg 1$), the mach number becomes independent of the pressure ratio, and can only be further increased by increasing the sound speed ratio, C_3/C_0 .

It should be noted here that the value of M given by eq.(3.31) is an absolute maximum, and can never be achieved in practice. Eq.(3.31) would give $M = 10.5$ for Helium-Air for instance, at which value the shocked gas would be heated sufficiently so as to become ionized, so that γ_0 would no longer be a constant, and the equations

must thus be modified to account for the non-ideal gas behaviour of a strongly shocked gas. In addition the shock wave will only achieve its full theoretical strength if the driver gas can escape from the driver section fast enough. The maximum speed of the driver gas is, of course u_1 , and is given by eq.(3.42) for the strong shock case. The value of a high C_3 is again immediately apparent. This effect can be mitigated somewhat by the use of a non-uniform driver tube cross section (converging conically towards the diaphragm) to increase the gas efflux velocity. An increase of 10% in M has been obtained by Alpher & White⁽¹⁶⁾ by this method.

High values of C_3 are attained in practice by heating the driver gas, either by combustion⁽¹⁷⁾ or, more recently, by means of an electrical discharge^(18,19). In chapter 7 a form of shock tube which combines a coned driver section, helium filled, with intense heating by means of an electrical discharge to achieve Mach numbers greater than ten into air at one atmosphere is described.

3.2 Theory of Light Reflection from a density discontinuity

3.2.1 First order theory

Cowan & Hornig⁽⁷⁾ have shown that to first order, the reflectivity of a shock front is given by:-

$$R = \left| \frac{1 + \tan^4 \theta_0}{4} \right| \left| \int_0^\infty \frac{1}{n} \frac{dn}{dx} \exp(-4\pi x j \frac{\cos \theta_0}{\lambda}) dx \right|^2 \quad (3.32)$$

where $n(x)$ is the refractive index profile through the shock front, x being the spatial coordinate parallel to the axis of the shock tube.

λ is the wavelength of light used.

$\theta_0 \equiv \pi/2 - i$ is the grazing angle of incidence.

and $j \equiv \sqrt{-1}$

Equation (3.31) has been found to give values for R larger than are found in practice⁽¹⁰⁾, and it is apparent that the simple first-order theory used is not adequate, at grazing incidence.

3.2.2. Second order Effects

At grazing incidence refraction, attenuation and multiple reflection effects may become important. Pert & Smy⁽²⁰⁾ have analyzed these effects in some detail, but for these experiments a more approximate analysis proves to be sufficient.

It is clear that the second-order effects all tend to reduce the value of the coefficient of reflection. For the case where the optical path length of the reflected beam is small compared to the wavelength of the radiation used, the shock front will behave as a planar refractive index discontinuity. From classical optical theory⁽²¹⁾ the intensity reflection coefficient is given by the Fresnel relations, which reduce, at grazing incidence to:-

$$R_1 = \left(\frac{\theta_1 - \theta_0}{\theta_1 + \theta_0} \right)^2 \quad (3.33)$$

where $\theta_1 \equiv \pi/2 - r$ (3.34)

$\theta_o = \pi/2 - i$ (3.35)

being the grazing angles of refraction and incidence, respectively. Eq.(3.33) which ignores second-order effects thus defines an upper limit, R_1 , to the true value of R .

In general, however, the optical path length, Δ , is not sufficiently small to give zero phase difference between successive multiply-reflected beams, i.e.,

$$\Delta = 2d \cos \theta_o \approx \frac{\lambda}{2\pi} \quad (3.36)$$

where $d =$ incident beam width

The multiply reflected beams can thus destructively interfere, as the angle θ_o is reduced, (at larger path lengths) and in the limit, complete interference occurs, and the contribution of the multiply reflected beams can be neglected, in determining a lower limit to the reflection coefficient. Absorption of light is also negligible in most experimental situations, so the only contribution to be included is that due to refraction in the shock front.

The effect of refraction may be determined by summing the contributions to the electric field vector, \underline{E} , from elements of

thickness, δx , of the shock front. The decrease in the electric vector is thus given by:-

$$E_r \equiv E_o - E_1 = E_o - \delta E \quad (3.37)$$

since the phase difference between the elemental components will be small, at grazing incidence, and the fields can be added scalarly.

Applying the Fresnel relation (3.33) to the element, δx , of the shock front then yields a deflection in beam direction given by:-

$$\delta E = - \frac{E}{2\theta} \delta\theta \quad (3.38)$$

so that
$$\ln \frac{E_1}{E_o} = - \frac{1}{2} \ln \frac{\theta_1}{\theta_o} \quad (3.39)$$

since the incident wave has electric vector strength E_o and angle θ_o and the transmitted wave has strength E_1 , at angle θ_1 . Eqs.(3.37) and (3.39) then give the reflected field intensity as:-

$$\frac{E_r}{E_o} = \frac{(\theta_1^{1/2} - \theta_o^{1/2})}{\theta_1^{1/2}} \quad (3.40)$$

so the intensity reflection coefficient will now be:-

$$R_2 = \frac{(\theta_1^{1/2} - \theta_o^{1/2})^2}{\theta_1} \quad (3.41)$$

defining a lower limit to the value of R.

$$R_2 < R < R_1 \quad (3.42)$$

The more careful and detailed analysis of Pert & Smy⁽²⁰⁾ gives an identical expression for R_2 , and also a general relationship for R , which is complex and cannot be evaluated analytically. Fig. 3.4 shows, however, that R_1 and R_2 do not differ significantly in these experiments, and either relationship (3.33) or (3.41) can be used in practice.

The angle θ_1 in (3.33) and (3.41) is determined from Snell's law:

$$n \cos \theta_0 = (n + \delta n) \cos \theta_1 \quad (3.43)$$

where δn is the refractive index change across the shock front. For small angles, θ_0 , θ_1 , (3.43) can be expressed as

$$\theta_1^2 - \theta_0^2 = \frac{2\delta n}{n} \quad (3.44)$$

and substitution of (3.44) in (3.33) or (3.41) gives,

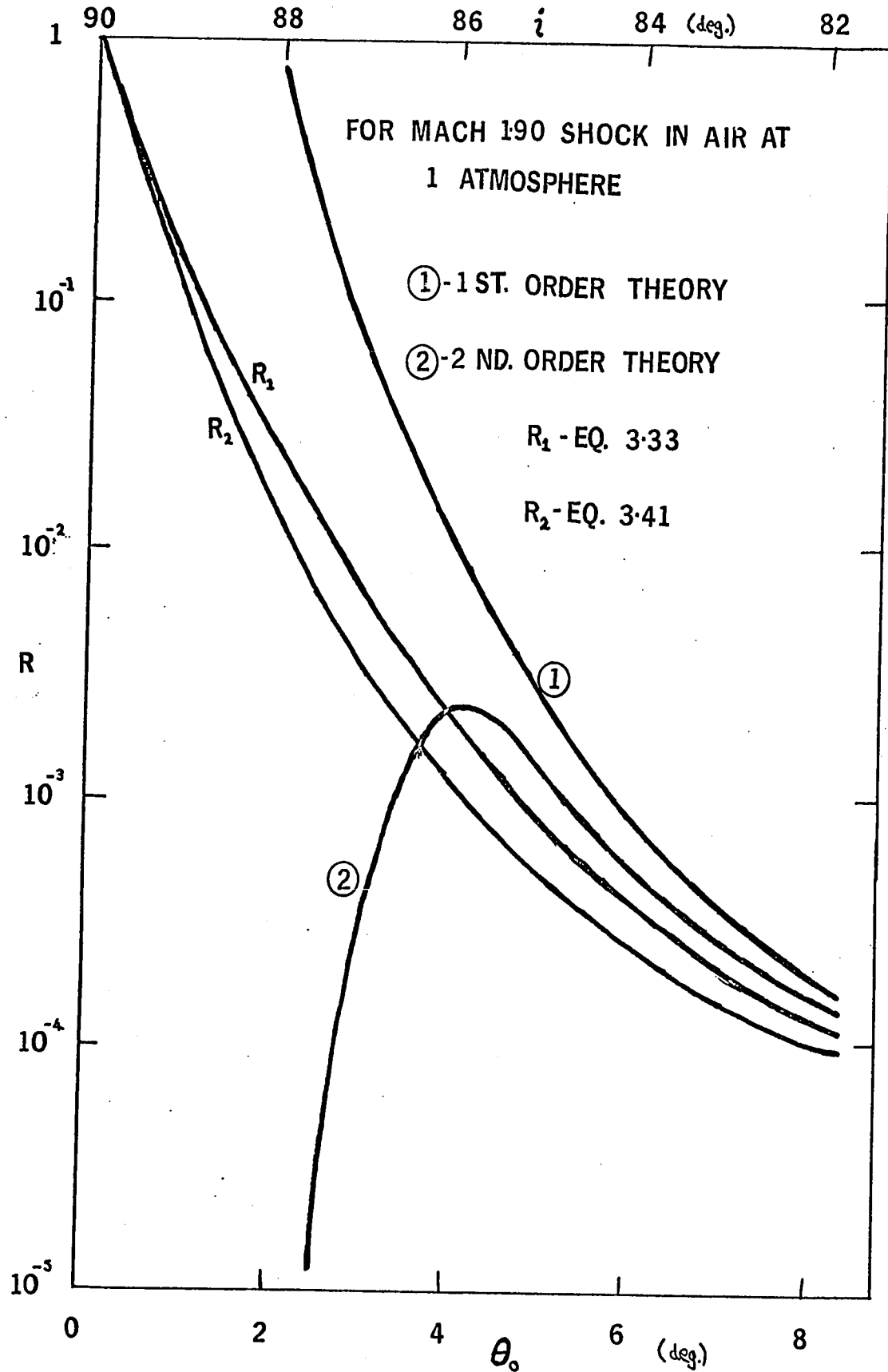
$$R = \frac{1}{4\theta_0^4} \left(\frac{\delta n}{n}\right)^2 \left[1 - \frac{1}{2} \left(\frac{\delta n}{n}\right)\right] \quad (3.45)$$

which reduces to:

$$R \approx \frac{1}{4\theta_0^4} \left(\frac{\delta n}{n}\right)^2 \quad (3.46)$$

as found by Cowan and Hornig⁽⁸⁾ and shown in Fig. 3.4 ('first order theory').

FIG. 3-4 REFLECTION COEFFICIENT VS. ANGLE (THEORY)



It is thus seen that R varies as $1/\theta_o^4$, near grazing incidence, and any change in inclination of the shock front to the tube axis, due to curvature or tilt of the front will have a large effect on the measurement of R .

3.2.3 Calculation of Reflection Coefficient R

Any quantitative calculation of R requires a knowledge of the refractive index change, δn , across the shock front. For a gas, at any given wavelength, the refractive index is given by⁽¹⁵⁾:-

$$n = 1 + K\rho \quad (3.47)$$

where K is a constant, known as the Gladstone-Dale constant. The value of K for air, at visible wavelengths is 0.226 ⁽¹⁵⁾.

For the gas in front of, and behind the shock front we then have:-

$$n_o = 1 + K\rho_o \quad (3.48)$$

$$n_1 = 1 + K\rho_1 \quad (3.49)$$

so that $n_1 - n_o = \delta n = K(\rho_1 - \rho_o)$

or $\delta n = K\rho_o(\eta - 1) \quad (3.50)$

since η the shock compression is defined by

$$\eta \equiv \frac{\rho_1}{\rho_o} \quad (3.8)$$

we then have $\frac{\delta n}{n_o} = \frac{k\rho_o}{n_o} (\eta-1)$ (3.51)

or $\frac{\delta n}{n_o} = \frac{(n_o-1)}{n_o} (\eta-1)$ (3.52)

(using (3.48))

η is given by eq.(3.18):-

$$\eta = \frac{\mu_o + y}{1 + \mu_o y} \quad (3.53)$$

where $\mu_o \equiv \frac{\gamma_o - 1}{\gamma_o + 1}$ ((3.19))

and y is related to the Mach number by eq.(3.17) which gives:

$$y = (1 + \mu)M^2 - \mu \quad (3.54)$$

so that by using eqs.(3.52), (3.53) and (3.54) the quantity

$\frac{\delta n}{n_o}$ can be determined in terms of the experimental variable (M),

and the constants of the shocked gas ($n_o; \mu_o$), giving:-

$$\frac{\delta n}{n_o} = \left(\frac{n_o - 1}{n_o} \right) \frac{(1 - \mu_o^2)(M^2 - 1)}{1 - \mu_o^2 + \mu_o(1 + \mu_o)M^2} \quad (3.55)$$

From eq.(3.43) we have

$$\cos \theta_1 = \frac{\cos \theta_o}{\left(1 + \frac{\delta n_o}{n_o}\right)} \quad (3.56)$$

so that θ_1 can now be determined (θ_0 is an experimental variable), and hence R_1 or R_2 can be calculated from eqs. (3.33) and (3.41) respectively. The first and second order approximations [eqs. (3.46) and (3.45)] can be calculated directly from the value of $\frac{\delta n}{n_0}$.

The theoretical variation of R_1 with mach number and angle is shown in Figs. 3.5 and 3.6. The value of R_2 is experimentally indistinguishable from R_1 , (fig 3.4) and the approximations to R are of little interest in themselves, and are therefore not shown.

FIG. 3-5 REFLECTION COEFFICIENT VS. MACH NUMBER (THEORY)

FOR A SHOCK WAVE MOVING INTO AIR AT 1 ATM.

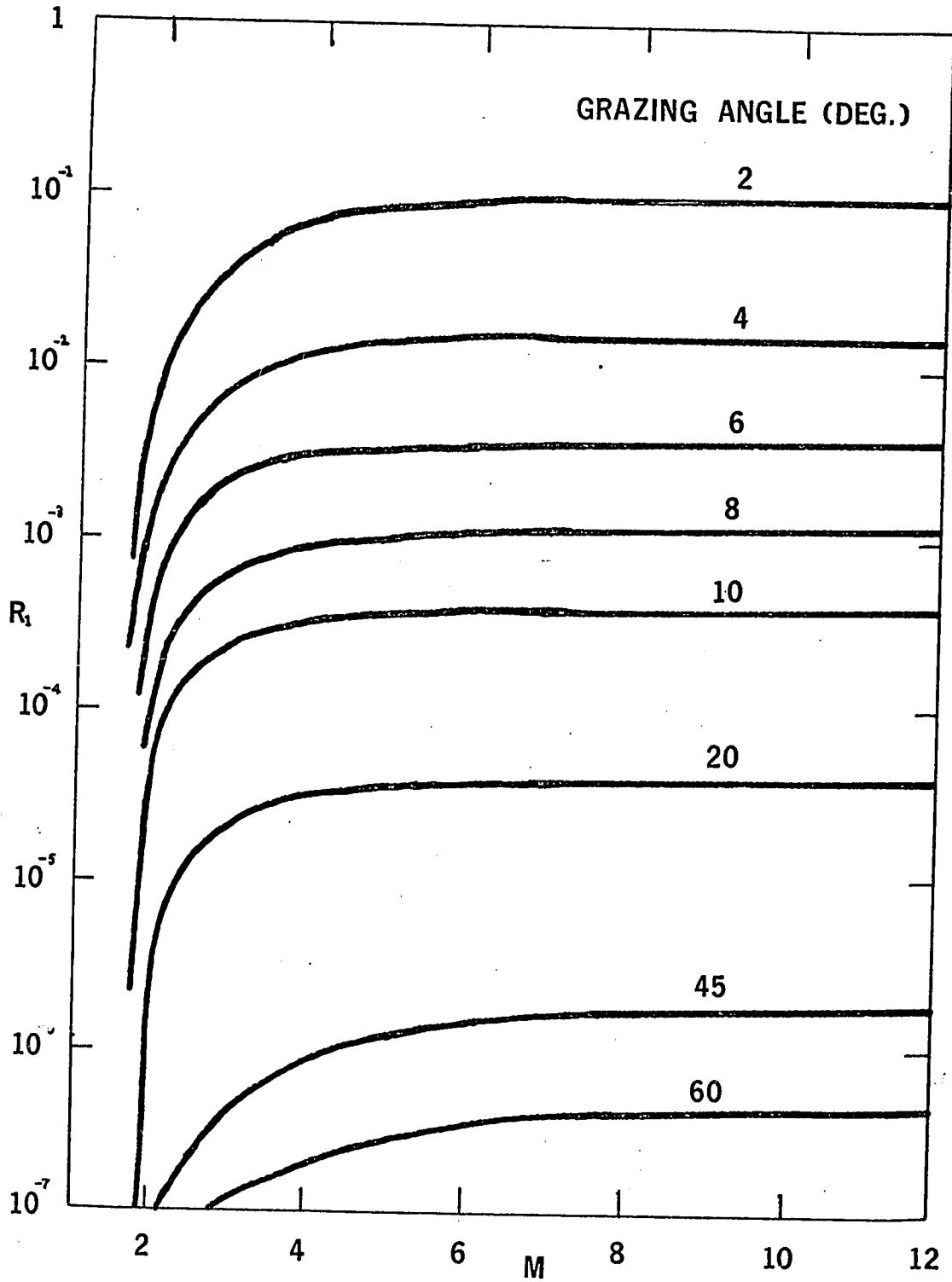
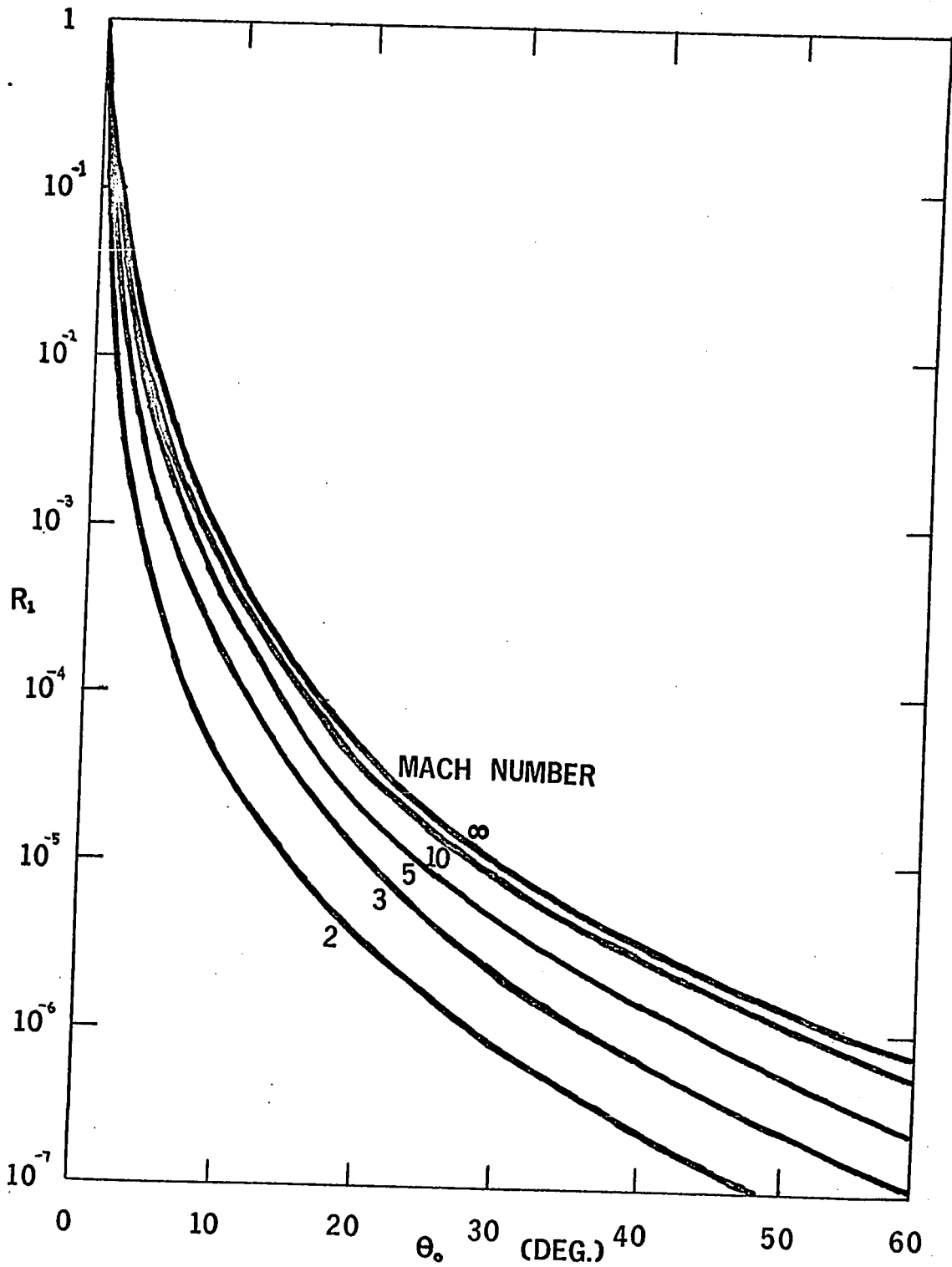


FIG. 3-6 REFLECTION COEFFICIENT VS. GRAZING ANGLE (THEORY)

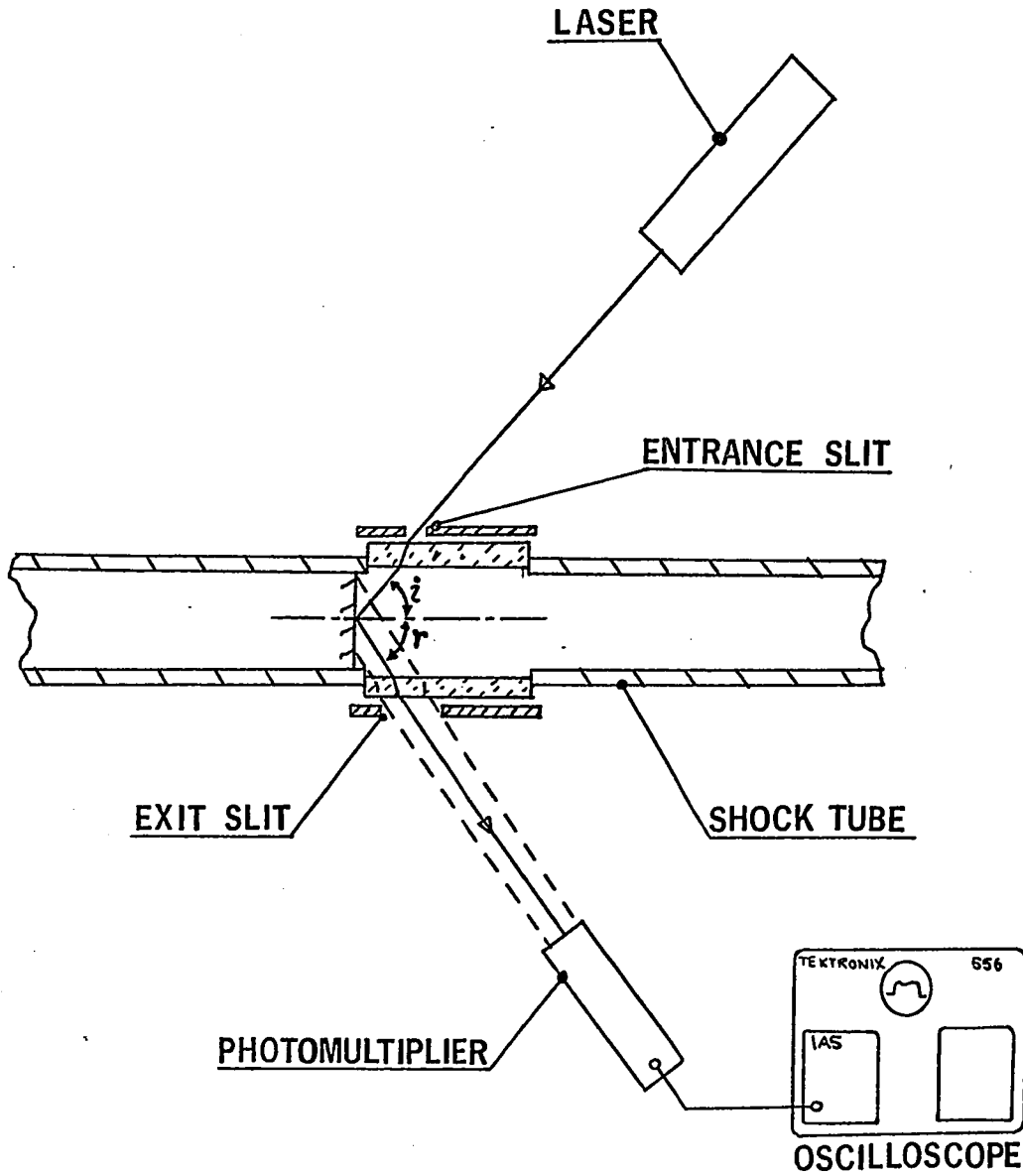
FOR A SHOCK WAVE MOVING INTO AIR AT 1 ATM.



IV Simple Measurement of Shock Velocity and Reflection Coefficient

4.1 Introduction

This initial experiment followed directly the method of Cowan & Hornig⁽⁸⁾ except that the laser-photomultiplier system described in chapter two was used in place of the white-light system and complicated optical arrangement of previous workers. The experimental arrangement is shown in general outline in figure 1.1 and in more detail in figure 4.1:-

FIG. 4-1 REFLECTION MEASUREMENT

4.2 Shock Tube

The shock tube used in these experiments was a low mach-number pressure-driven tube 51 mm in internal diameter and 6000 mm long. The shock wave was generated by rupturing a 0.13 mm thick 'mylar' diaphragm by overpressuring a 930 mm long 'driver section' at the upstream end of the tube. Typical rupturing pressures were $2 \times 10^5 \text{ N/m}^2$ (5 atmospheres). The theory of operation of shock tubes of this type is well-understood (see chapter 3). In these experiments Helium was used as the 'driver' gas, with air at one atmosphere as the 'shocked' gas. Under these conditions shock waves having Mach numbers of up to approximately 3.5 can be obtained (chapter 3). Approximately 1000 mm of tube length were allowed downstream of the diaphragm for the shock wave to develop and stabilize, and all measurements were made in the following 1000 mm of the tube, the overall distance of 1700 mm from the diaphragm being sufficiently short at Mach numbers above about 1.4 to avoid interference between the shock wave and the rarefaction which propagates back from the ruptured diaphragm, to reflect off the back of the driver section, and thence down the shock tube, at approximately the speed of sound in the driver gas. 'Mylar' was used as a diaphragm material since its mode of rupture is a simple splitting across a single diameter, so that no fragments of diaphragm material are introduced into the shock tube.

The velocity of the shock wave was measured by observing the

output from a number of piezo-electric transducers ('pressure probes') mounted flush with the shock tube wall at various points along the length of the tube, on either side of the test region. The pressure probes had a risetime of about 10 μ sec and an output of approximately one volt under the experimental conditions giving a sufficiently accurate velocity determination over separation of 1000 mm as used. The average velocity derived from 14 measurements taken over 1000 mm lengths of the shock tube on either side of the test region, simultaneously with the reflection measurements was (680 ± 80) m/sec; or Mach (1.8 ± 0.2) at room temperature.

4.3 Optical System

Light was introduced to the shock tube, and the resulting reflection observed by means of a window section having two 200 mm by 10 mm flat plate glass windows 10 mm thick, mounted in the shock tube wall parallel to the axis of the tube, and diametrically opposite each other. The windows were recessed by 2 mm at their centre-line, and 5 mm of the edges, so care was taken always to work as close as possible to the upstream end of the windows so as to minimize the effect of any disturbance to the shock wave introduced on traversing the wall-discontinuity introduced by the windows. The laser beam passed through entrance and exit slits at the windows to define the angle of incidence, i , of the beam as shown in figure 4.1. The method used to calculate the shock velocity, and the effect upon the measurements of any tilt or curvature of the shock wave are shown in

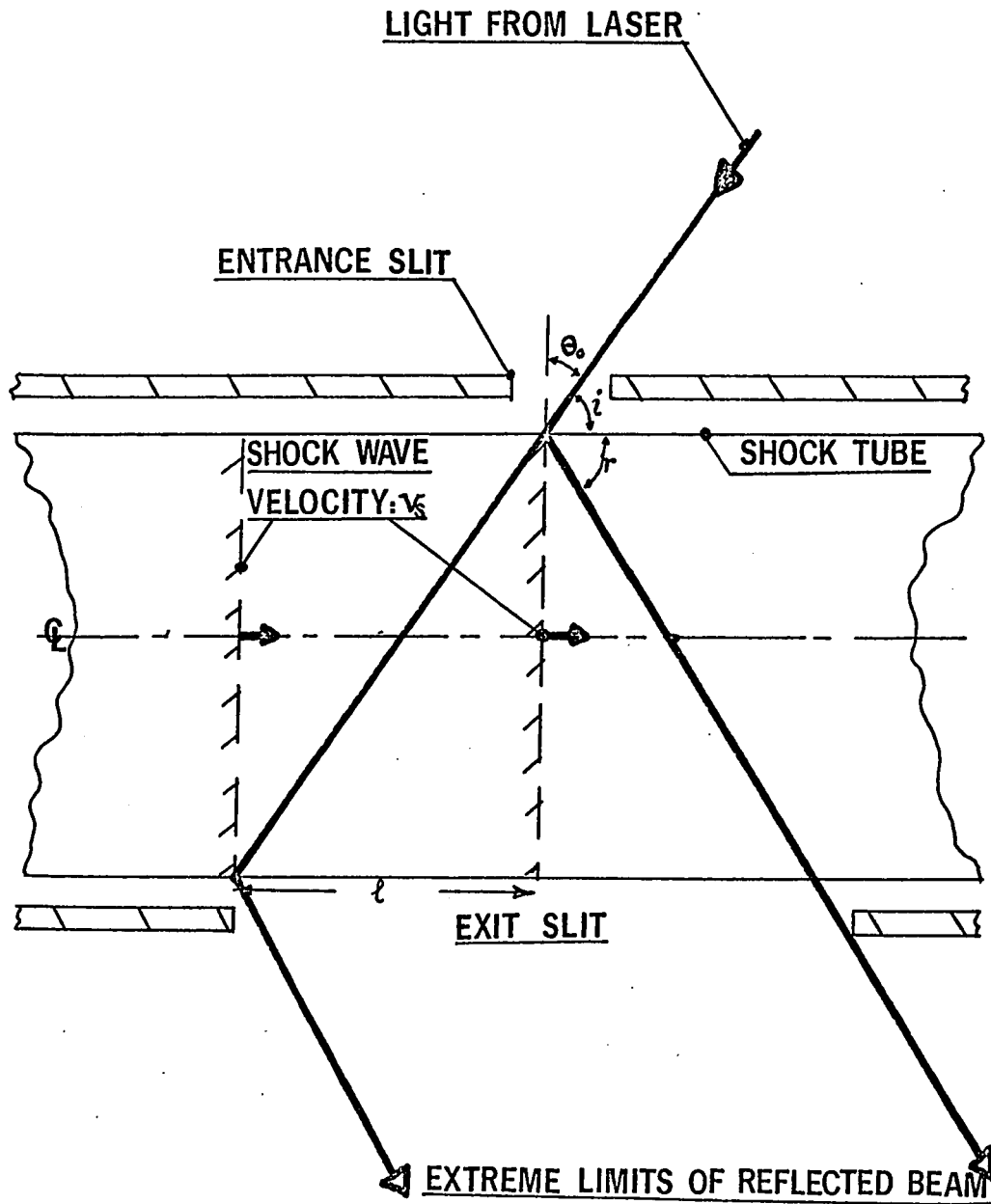
FIG. 4.2 SHOCK VELOCITY MEASUREMENT FROM PULSE DURATION

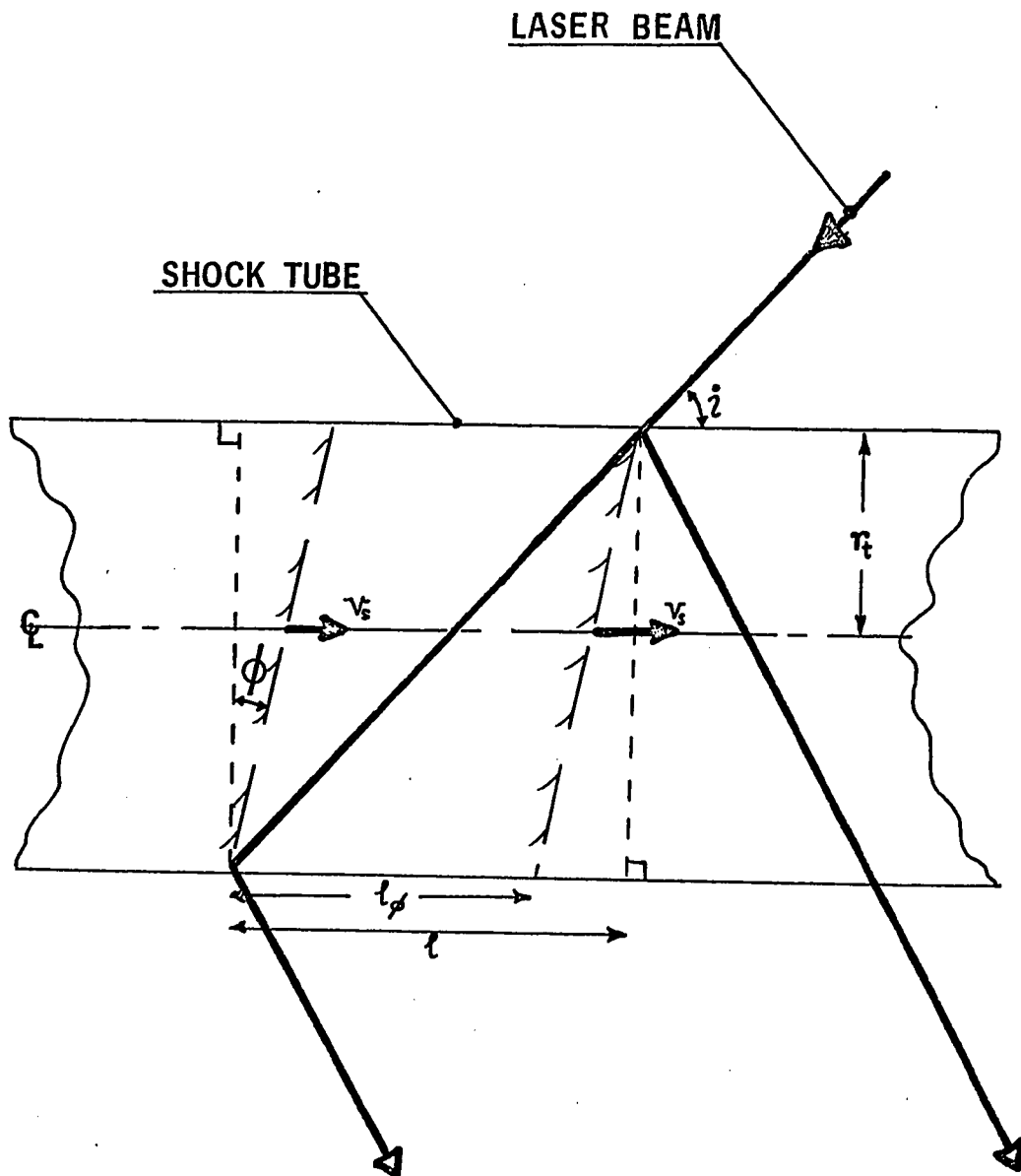
FIG. 43 **EFFECT OF SHOCK TILT**

figure 4.2

4.3.1 Method of Measuring Shock Velocity from Duration of Reflected Pulse

The 'interaction distance', l , for which a reflected pulse can be observed is given by:

$$l = 2r_t \cot i \quad (4.1)$$

so the duration t_D of the reflected pulse is

$$t_D = \frac{2r_t}{v_s} \cot i \quad (4.2)$$

where r_t = shock tube radius

v_s = shock velocity

i = angle of incidence

4.3.2 Effect of Shock Tilt (fig 4.3)

For a shock tilt of ϕ (fig 4.3) the interaction distance l is reduced by an amount $2r_t \tan \phi$, giving

$$l_\phi = 2r_t (\cot i - \tan \phi) \quad (4.3)$$

and

$$t_\phi = 2 \frac{r_t}{v_s} (\cot i - \tan \phi) \quad (4.4)$$

4.3.3. Effect of Shock Curvature

The effect here is not to shorten or lengthen the duration of the reflected pulse, provided that all the reflected light is collected by the photomultiplier, but to alter the angle through which the incident beam is deviated by an extreme amount of $2 \sin^{-1} \left(\frac{r_t}{r_s} \right)$ where r_s is the radius of curvature of the shock front. The system used here is not sensitive to such changes in angle.

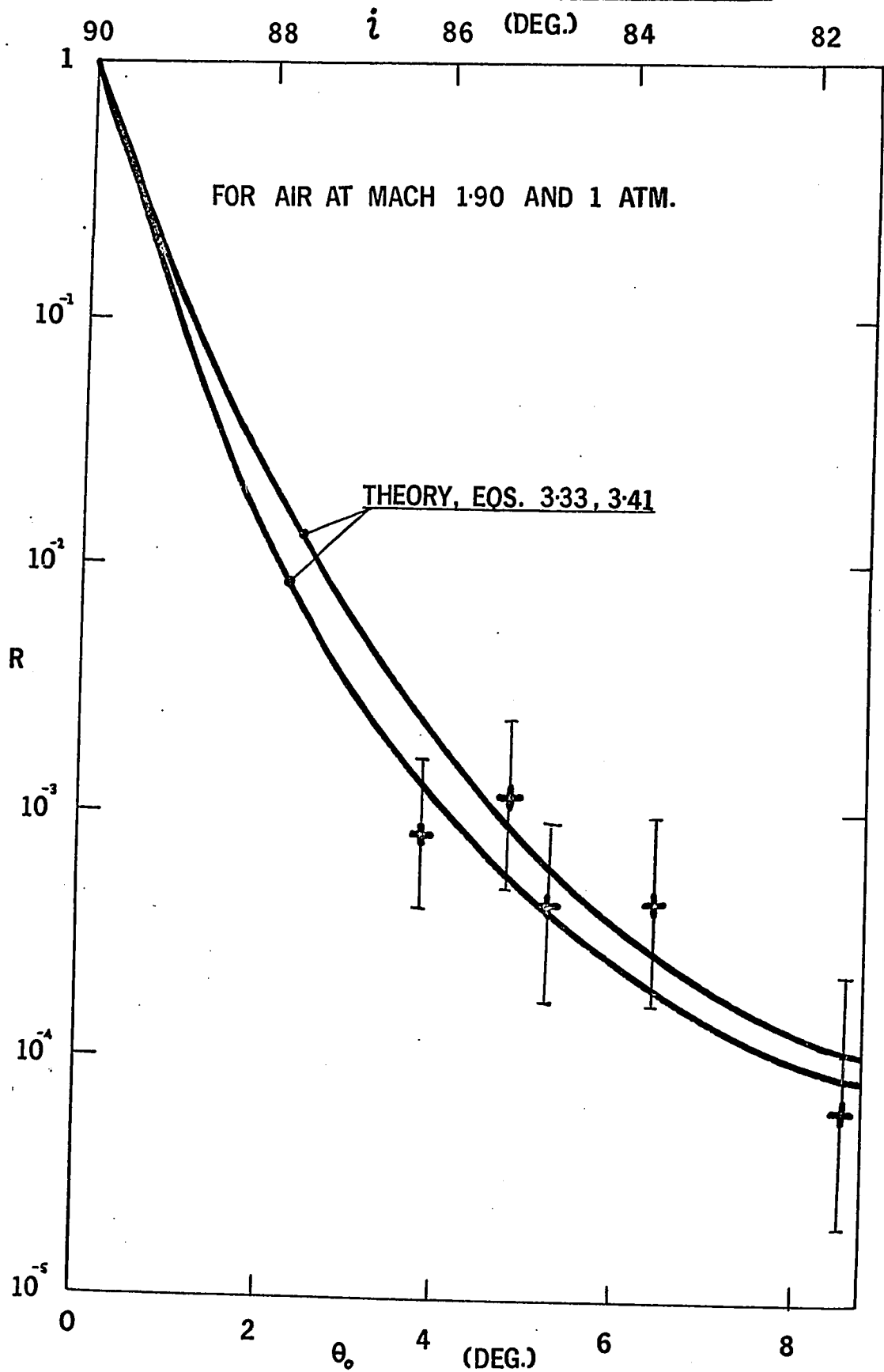
The shock velocity determined from the pulse length, averaged over 10 results at each of seven different angles of incidence was found to be (800 ± 200) m/sec, independent of the angle of incidence - in good agreement with the value obtained from the pressure probes, but of considerably less accuracy. The relatively large variation in the velocities determined from the pulse lengths was probably due to a random variation in shock tilt.

Theory (chapter 3) indicates that the reflection coefficient should vary approximately as the fourth power of the grazing angle of incidence, θ_0 . Fig 4.5 shows the measured intensity reflection coefficient as a function of angle of incidence, together with the theoretical curves derived from eqs. (3.33) and (3.41).

Although the experimental error was fairly large for these preliminary measurements, fairly good agreement with theory is

obtained, particularly at the smaller angles. The results thus indicate that the general procedure used gives valid results, and that the measuring system performs sufficiently well. A more accurate and sophisticated investigation of shock reflectivity was therefore undertaken, following the same general lines.

FIG. 4.5 REFLECTION COEFFICIENT VS. ANGLE (EXPERIMENT)



V Measurement of Shock Velocity, Curvature & Reflectivity using a Differential Interferometer

5.1 Magnitude of Doppler Shift

Microwave measurements⁽⁷⁾ have established the validity of using the Doppler Shift in the frequency of electromagnetic waves reflected from a shock front to determine the velocity of the shock wave. The use of long wavelength radiation gives poor spatial resolution, however, and optical wavelengths appear very attractive from this point of view. Their use has only become practicable in recent years, however, with the advent of the gas laser, with its narrow bandwidth and long coherence length.

The Doppler Shift, $\Delta\nu$, is given by:-

$$\frac{\Delta\nu}{\nu} = \frac{2v}{c} \cos i \quad (5.1)$$

or
$$\Delta\nu = \frac{2\nu}{\lambda} \cos i \quad (5.2)$$

where ν is the frequency

and λ is the wavelength of the electromagnetic wave

Thus for a shock wave at Mach 2 (in air) using a H_e-N_e laser,

$$\Delta\nu = \frac{2 \times 664}{633 \times 10^{-9}} \cos i \quad (5.3)$$

$$\text{or } \Delta\nu = 2.10 \times 10^9 \cos i \quad (5.4)$$

so that even for grazing angles of 10^{-3} or so, frequency shifts of the region of 1 MHz are expected. However, earlier results (chapter 4) indicated that a shock front tilt of 1° or more might be expected and that difficulties with stray light reaching the photodetector are experienced at angles less than about 2° . These considerations limited the maximum grazing angle of incidence to 3.5×10^{-2} radians giving a minimum Doppler shift of 37 MHz.

5.2 Observation of Doppler Shift

Any small frequency shift in a beam of electromagnetic waves relative to some beam of standard frequency is most conveniently measured by observing the heterodyne frequency produced when the frequency-shifted beam is mixed with a part of the reference beam, the heterodyne frequency being equal to the frequency difference between the two beams. Only part of the reference beam can be used, since it is necessary to operate the photomultiplier near saturation.

This technique suffers from two major drawbacks, under the present circumstances:-

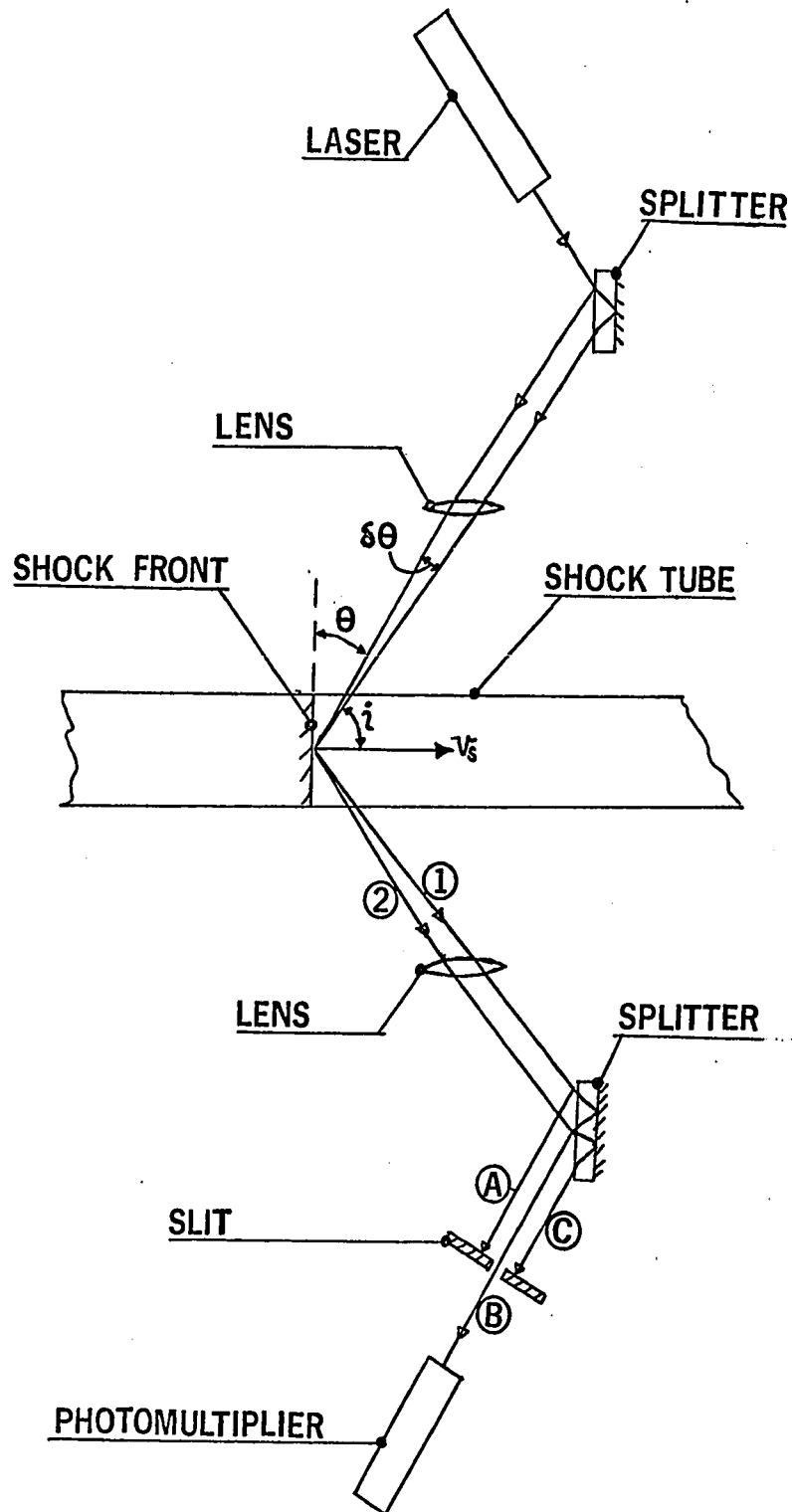
(a) The incident, (reference) beam is three to six orders of magnitude more intense than the beam reflected off the shock front so to get efficient mixing to produce a clearly defined heterodyne frequency, for which beams of similar order of intensity, are required, a variable, but extremely dense calibrated filter would be required. Such filters are unobtainable commercially and

and can only be roughly approximated to by the use of absorbing liquid solution (e.g. CuSO_4) of variable concentrations.

(b) The reflected beam is not fixed in point of origin so that the beam moves bodily to one side as the shock wave traverses the interaction region. This lateral movement can be transformed into an angular one, by means of a suitable lens system, but the process of mixing the incident and reflected beam to produce the heterodyne signal then occurs with a continuously varying angle between the beams, with a resulting variation in beat frequency. To overcome both these problems, the Differential Doppler Interferometer described below was developed.

5.3 The Differential Doppler Interferometer

The general arrangement of the interferometer is shown in fig. 5.1.

FIG. 5-1 DIFFERENTIAL DOPPLER INTERFEROMETER

The optical arrangement is symmetrical about the centre-line of the shock tube. The light beam from the laser is first directed onto a beam splitter, having a 50% reflecting front surface, and a 100% reflecting back surface, and a thickness of approximately 8 mm. Two beams of approximately equal intensity are reflected from the splitter, one for each surface, and by varying the angle of the splitter relative to the incident beam, the lateral separation of these two beams can be varied. The two beams are brought to a common focus at the point within the shock tube where the shock velocity is to be measured, using a lens of about 200 mm focal length. As the angle of the splitter relative to the beam from the laser is changed, the angle, $\delta\theta$, between the two beams incident on the shock front alters, typical values being in the range $0.5 - 1.5$ degrees ($10^{-2} - 3 \times 10^{-2}$ radians). The common angle of incidence, 2° (or beam-shock wave angle θ) may also be altered, by adjusting the position of the splitters relative to the lenses. To obtain easily measureable reflected signals angles of incidence in the range $80^\circ - 87^\circ$ were used.

The reflected beams from the shock wave are brought parallel again by means of an identical lens to that on the input side, and recombined at the front surface of a second "beam splitter". Both beams are Doppler-shifted in frequency, on account of their reflection from the moving shock front, but by differing amounts, due to the difference, $\delta\theta$, between the angles of incidence. A

small frequency difference thus exists between the two reflected beams, and is observed as a heterodyne or 'beat' frequency in the recombined light reflected off the second splitter.

Because of the very small inter-beam angle, this frequency can be made very much less than the conventional Doppler frequency (section 5.1). In addition, the intensities of the two reflected beams are very nearly equal, since the angles of incidence are only very slightly different, so that a large depth of modulation of the output beam can be obtained, and both reflected beams undergo the same lateral movement as the shock wave traverses the interaction region. Both the major difficulties inherent in the conventional Doppler shift measurement are thus eliminated by the use of the Differential Interferometer. It is also apparent that any tilt or curvature of the shock front, up to angles comparable with the grazing angle, θ , will still result in an output being observed, albeit from a slightly different point on the axis of the shock tube.

5.4 Modulation Depth

In general, three distinguishable beams are reflected from the second splitter, for front surface reflectivities of 40 to 60%, as shown in fig. 5.1 at A,B and C. It is immediately apparent that beam A has no component originating from reflected beam (2) (that furthest from the downstream shock tube axis) and will thus be unmodulated. Beam C is produced by multiple

reflections at the second splitter, and is thus of considerably lower intensity than the beams A and B. Further beams, produced by still higher-order reflections also exist, but, are generally of negligible amplitude.

An elementary consideration of the means by which the two splitters produce the various beams A,B,C....., shows that a common splitter front surface intensity reflectivity of 38% will produce equal intensity components in beam B, from the two reflected beams 1 and 2, resulting in 100% modulation of this beam. Under these conditions the relative intensities of the beams A,B, and C will be 3:6:4, with the higher-order beam intensities negligible; and some 30% modulation can be expected in beam C. To obtain maximum depth of modulation in the reflected signal, a stop may be inserted in front of the photodetector, so as to admit beam B only. This aperture limitation severely restricts the time for which the reflected signal is received, however, and in practice all the light from the second splitter was allowed to fall on the photodetector surface. It can easily be shown that a maximum modulation of 65% (which should be readily detectable), can be expected, under these conditions, approximately 35% of the light from the laser being lost in the two splitters, for a reflectivity of 38%.

5.5 Measurement of Shock Velocity

Equation (5.2) gives the frequency shift in a single beam

reflected at an angle of incidence, i , from a moving shock front, of velocity v_s as

$$\Delta v = 2 \frac{v_s}{\lambda} \cos i \quad (5.5)$$

So the differential beat frequency generated by mixing two beams differing in angle of incidence by an amount δi will be

$$v_D = \Delta v_i - \Delta v_{i+\delta i} \quad (5.6)$$

$$= 2 \frac{v_s}{\lambda} [\cos i - \cos(i+\delta i)] \quad (5.7)$$

$$\approx 4 \frac{v_s}{\lambda} \sin i \times \frac{\delta i}{2} \quad (5.8)$$

$$\text{or } v_D \approx 2 \frac{v_s}{\lambda} \delta i \sin i \quad (5.9)$$

assuming $\delta i \ll i$, and is so small that $\sin \delta i \approx \delta i$

Because of noise considerations, adequate signal strengths for measurement are only obtained at very large ($\approx \pi/2$) angles of incidence, so it can also be assumed that $\sin i \approx 1$ giving

$$v_D = 2 \frac{v_s}{\lambda} \delta i \quad (5.10)$$

so the shock velocity can be readily obtained, since λ is known, and δi is fixed by the geometry of the system. Equation (5.10) may also be written as

$$N = 2 \frac{l}{\lambda} \delta i \quad (5.11)$$

where $N (= t_D \cdot v_D)$ is the total number of beats observed and

$l (= v_s \cdot t_D)$ is the length of the region in which the shock wave - light beam interaction occurs.

The variation (if any) of shock velocity across the shock front during its transit of the interaction region can clearly be determined by measuring the duration of each cycle of the observed waveform, since successive time-segments of the waveform represent reflection from successive lengths (of ~ 3 mm) of the diameter of the shock front which lies in the plane of the optical system.

5.6 Measurement of Shock front curvature

The initial alignment of the differential interferometer is such that the two beams are focused on the axis of the shock tube, so that in general, as the shock front traverses the interaction region, the two incident beams are not reflected from the same point in the shock front. Any curvature of the shock front will then mean that the angles at which the reflected beams emerge will differ from their respective angles of incidence, except when the reflection occurs from a point on the axis of the shock tube. The two beams will thus be displaced relative to each

other at the second splitter, and there will be a degradation of the mixing process, with a consequent reduction in the depth of modulation of the signal detected by the photomultiplier.

From equation (5.11) and the geometry of the optical system it can be shown that the shock front radius of curvature, r_s , in the plane of the interferometer is given by:-

$$r_s \approx \frac{Nd}{2(\theta_o + \delta\theta)\theta_o} \quad (5.12)$$

where N is the number of beats observed

d is the diameter of the unfocused laser beam

$$\theta_o = \pi_2^{-1}$$

and $\delta\theta \equiv \delta i$

In practice, d is not a well defined quantity, since the laser beam has a circular cross-section, not allowed for in the two-dimensional analysis used in deriving (5.12), and furthermore, has a non-uniform intensity distribution across that cross-section. An effective value of d can be obtained, however, by calibrating the system with a reflector of known radius of curvature, and thus curvature of the shock front can be calculated from a count of the number of beats observed in the output pulse. If beats are observed for the entire duration of the observed pulse, only a lower limit on the value of the radius of curvature can be determined, since there is always the

possibility that a system with a longer measuring time would have given a finite number of beats.

5.7 Measurement of Shock Reflectivity

5.7.1 Rejection of Stray and Scattered Light

If the interferometer is set up as described in sections 5.3 and 5.4, a number of 100%-modulated beats will be observed, during some part of the output pulse, provided that the only light entering the detector is the two beams reflected from the shock front. In practice, however, there is always some stray room light present, in addition to the possibility of light being scattered out of the main beams by dust or water vapour particles in the unshocked gas,^(9,10,12) or from the shock tube walls and window sections. This light, however, has no fixed phase relation to the input beams, and hence to either output beam, and therefore does not give rise to interference at the second splitter, but is collected by the photodetector, and observed as a d.c. level, with the beats due to the true reflected beams superimposed.

The amplitude of the beats observed in the total output is thus equal to the combined intensities of the two reflected beams, so that if the total intensity of the input beams is measured, or if the system is calibrated with a 100% reflector in the shock-tube, the true reflection coefficient of the shock-

front may be determined.

5.7.2 Spatial Resolution

If the output signal shows no signs of beat amplitude degradation due to curvature of the shock front, values of the reflection coefficient across the entire horizontal diameter of the shock front can be calculated from each cycle of the waveform giving a lateral spatial resolution of 2-3 mm. The measurement at any single point is made in a time during which the shock wave moves about 1 mm down the tube. The resolution of the measurement in the direction perpendicular to the plane of the interferometer and shock tube is at the worst 1 mm, and considerably less for points near the axis of the shock tube where the two beams are brought to a common focus. If the shock front is curved reliable reflection coefficient measurements can only be obtained for points on or near (within 2-3 mm) of the shock tube axis, but the same degree of spatial resolution in all three dimensions is obtained. The measurement time is in the region of 10^{-7} sec, and successive segments of the shock front are then measured at intervals of 10^{-7} sec, the whole front being scanned in $\sim 5 \times 10^{-6}$ sec. It is unlikely that the reflection coefficient varies much in this order of time interval, so the observed waveform can be used to determine a valid spatial variation of reflectivity across the front.

5.8 Effect of Shock Front Tilt.

5.8.1 Effect on Shock Velocity

If the measurement is performed at large angles of incidence, eq.(5.10) applies rather than eq.(5.9), and the beat frequency is independent of the actual angle of incidence. The effect of tilt of the shock front would be to alter the effective angle of incidence, so provided the tilt is not so large that the reflected beams are deflected entirely out of the aperture of the output lens, there is no effect on the velocity determination.

5.8.2 Effect on Shock Curvature

Eq.(5.12) shows that the value of the radius of curvature varies roughly as θ_o^{-2} and is thus strongly influenced by any tilt in the shock front, since this produces a variation in θ_o . However, the tolerance of the system to shock tilt can be reduced to such a point that only shocks with tilt angles, ϕ , much less than θ_o can be observed. For a system where the aperture of the output lens is small compared to its focal length, F , (this is generally true, since the maximum aperture required is just equal to the interaction length for a planar shock front, and this length, l , is given by $l = 2r_t \cot i$ (5.13) and is thus small for large angles of incidence, i even if apertures several times this minimum value are used, to accomodate curved shocks) it can be shown that the maximum tilt which can be accomodated is

given by

$$\phi = \frac{1}{2F} \quad (5.14)$$

$$\text{or} \quad \phi = 2r_t \frac{\cot i}{2F} \approx \frac{\theta r_t}{F} \quad (5.15)$$

So ϕ/θ can be reduced to any value required by using lenses with very long focal lengths.

In the system used,

$$r_t = 25 \text{ mm}$$

$$F = 250 \text{ mm}$$

$$\text{so} \quad \phi/\theta = 0.1$$

and a maximum error of 20% in r_s can thus be expected.

5.8.3 Effect on Reflection Coefficient

The reflection coefficient is expected to vary roughly as θ_o^{-4} (where $\theta_o \equiv \pi/2 - i$) (eq.3.45), and for the values of θ_o , used here, we have

$$(\theta_o + \phi)^{-4} \approx \theta_o^{-4} (1 - 4\phi/\theta_o) \quad (5.16)$$

so that for a value of ϕ/θ_o of 0.1 (section 5.8.2) a maximum error of 40% in the value of the reflection coefficient would arise if the shock front was tilted. This uncertainty is, of course, inherent in any

determination of reflection coefficient.

5.9 Experimental Results

Fig. 5.2 shows the beats observed experimentally with the interferometer shown in fig. 5.1. Fig. 5.2.1 shows the beats obtained with a plane mirror in the shock tube, with an aperture stop placed at the photomultiplier to give a 100% modulation, as described in section 5.4. In fact only 85% modulation is achieved, due to stray light, and the splitter reflectivity differing from the optimum 38% (36% or 41% reflectivity would reduce the modulation to 85%).

Fig. 5.2.2 shows the beats observed with a shock wave, all three of the major recombined beams being permitted to enter the photodetector, to give the widest possible system aperture. Under these conditions a maximum modulation of 60 to 70% is expected for the range of reflectivities which give 85 - 100% modulation as in fig. 5.2.1. In fact 50% modulation is observed, over the central part of the waveform, indicating the presence of some stray light, or a slight misalignment in the optical system.

The relevant parameters for fig. 5.2.2 are:-

Vertical Sensitivity: 2.6×10^{-7} w/cm (both beams)

zero lines displaced 2 cm.

Time Scales: 0.2 μ sec/cm and 10 μ sec/cm.

Shock Velocity, v: (468 ± 4) m/sec [Mach 1.4] in air at 720 Torr and 293^oK.

FIG. 5-2 BEATS OBSERVED WITH DOPPLER INTERFEROMETER

FIG. 5-2:1 BEATS OBSERVED WITH PLANE MIRROR IN TUBE

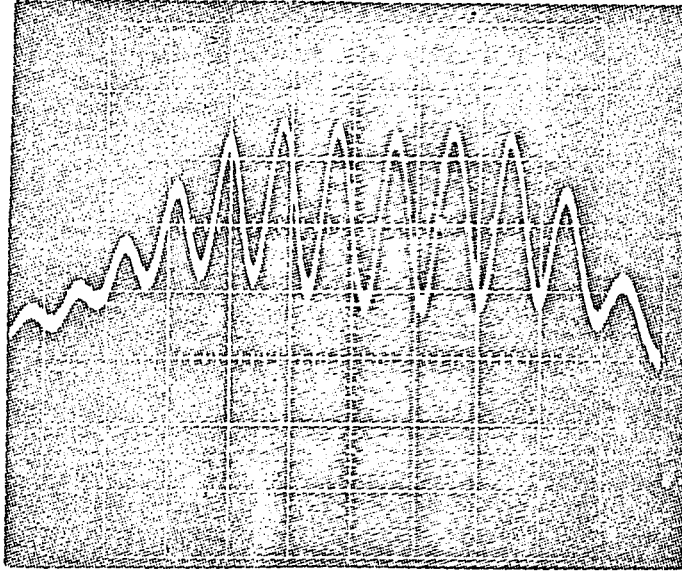
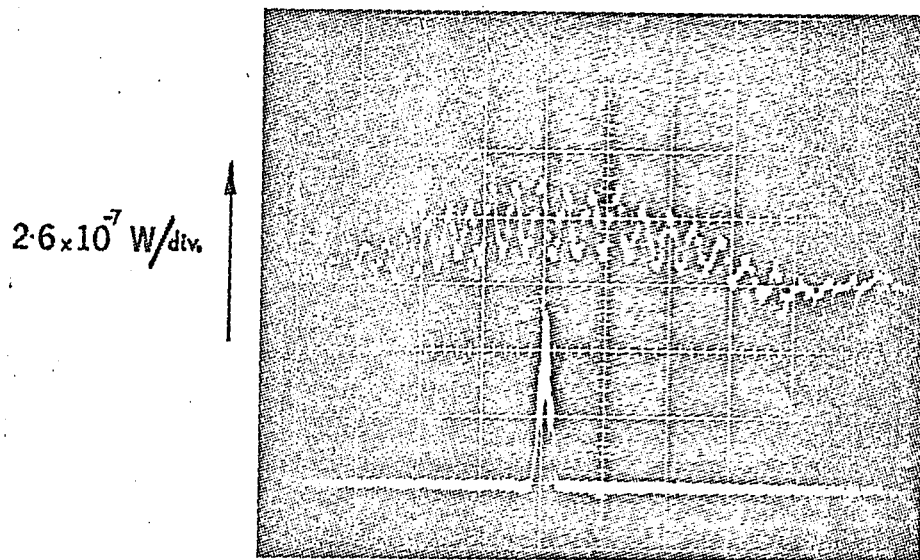


FIG. 5-2:2 BEATS OBSERVED WITH MACH 1.40 SHOCK IN AIR



0.2 $\mu\text{sec}/\text{div}$; 10 $\mu\text{sec}/\text{div}$

$\theta_0 = 2.78 \text{ DEG.}$, $\delta\theta = 0.58 \text{ DEG.}$

FIG. 5-2 BEATS OBSERVED WITH DOPPLER INTERFEROMETER

FIG. 5-2-1 BEATS OBSERVED WITH PLANE MIRROR IN TUBE

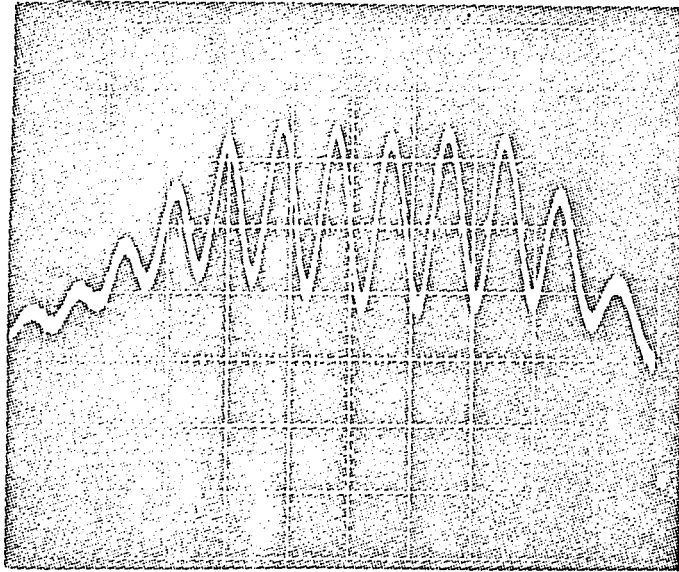
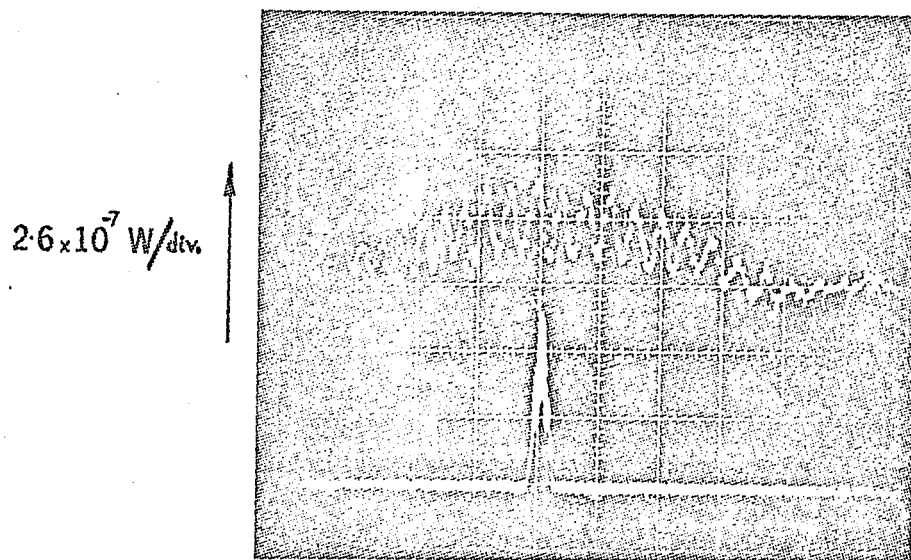


FIG. 5-2-2 BEATS OBSERVED WITH MACH 1.40 SHOCK IN AIR



$2.6 \times 10^{-7} \text{ W/div.}$

$0.2 \mu\text{sec/div.}; 10 \mu\text{sec./div.}$

$\theta_0 = 2.78 \text{ DEG.}, \quad \delta\theta = 0.58 \text{ DEG.}$

Angle of Incidence, i , = $87.82^\circ (\pm 0.02^\circ)$; $\theta = 2.78^\circ$.

Angle between Beams, $\delta i = 0.58^\circ (\pm 0.02^\circ)$.

There is some indication of shock curvature at one side of the tube since the beats die away towards one end of the pulse, but no value of the curvature could be determined in this case, since beats were present right up to the other edge of the pulse. The minimum value of R would be 300 mm.

FIG. 5-3 BEAT FREQUENCY VS. SHOCK VELOCITY

$\dot{i}=87.82$ DEG. ($\theta_s=2.18$ DEG.)

$\delta\theta=0.58$ DEG.

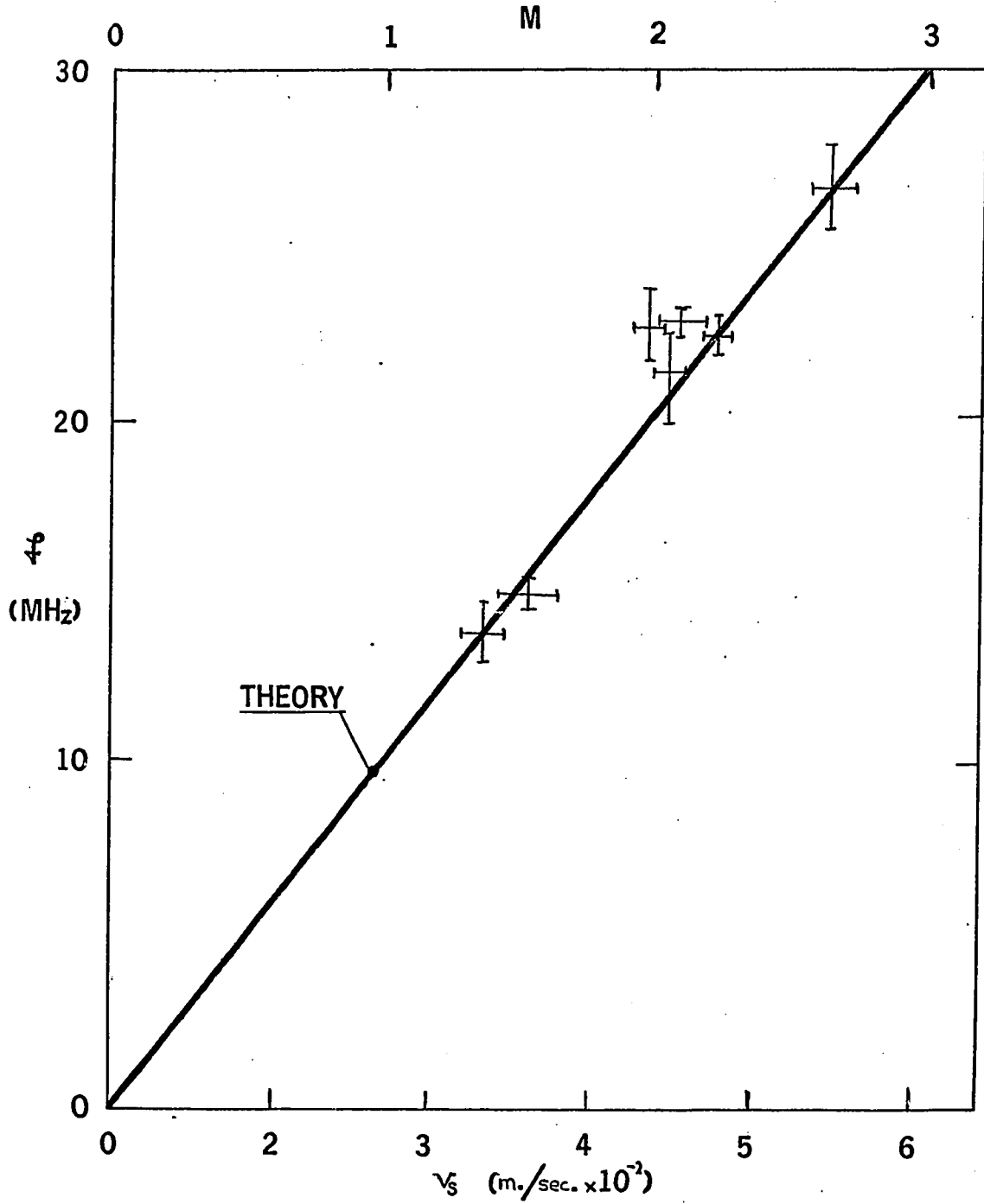
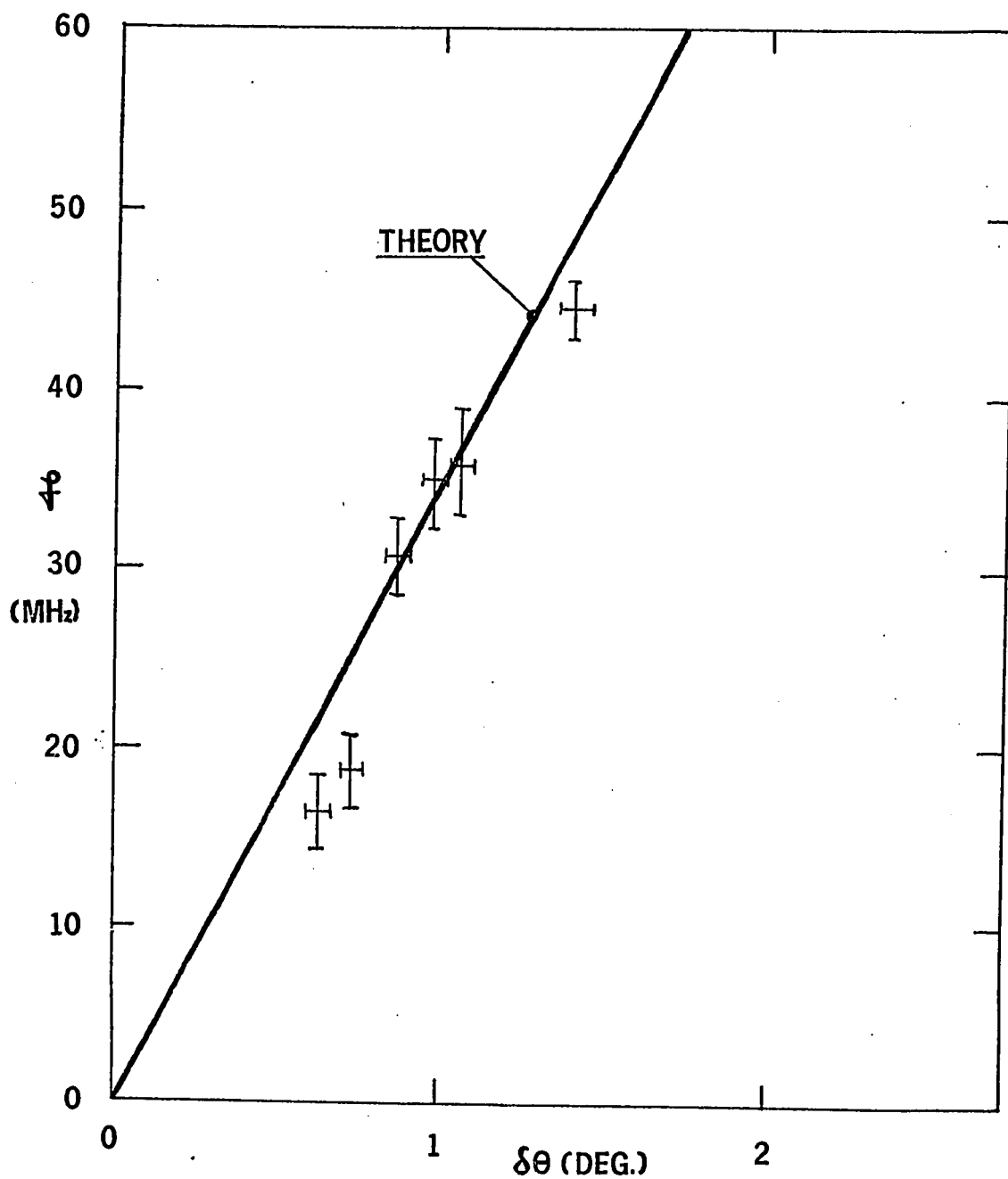


FIG. 5-4 BEAT FREQUENCY VS. BEAM SEPARATION $\dot{\lambda} = 87.82 \text{ DEG.}, \quad \theta_0 = 2.18 \text{ DEG.}$ $v_s = 652 \text{ m/sec.}, \quad M = 1.95$ 

The results of a systematic investigation of the validity of eq. (5.10) are summarized in figs. 5.3 and 5.4. Each point on the graph represents the mean of at least five determinations of each quantity, under identical experimental conditions, and the error-bars represent the experimental standard deviation. No variation in frequency with angle of incidence was found, as predicted by eq. 5.10, at the large angles used, $[80-88^\circ]$. An output pulse was observed, but with no beats present, if either one of the incident beams was obstructed.

The shock velocity was varied by using different diaphragm thicknesses and driver gases, and by varying the downstream pressure. It was found that reliable velocity measurements could be made for downstream pressures down to about 80 Torr, below which there was insufficient reflected light to give accurate measurements. At the lower pressures significant values of shock curvature became noticeable. Fig 5.5. shows the type of effect observed, the two traces shown being calibration traces taken with a plane mirror and a 140 mm radius curved reflector. Individual beats are not resolved in these measurements, since a large value of θ was used, to give a reasonable total pulse length, with the relatively small radius of the curved reflector. Fig 5.5.3 shows the effect with a shock wave as the curved reflector, giving a radius of curvature of $(6.0 \pm 0.4)\text{m}$, for a shock wave moving into air at 720 Torr at a velocity of $(635 \pm 5)\text{m/sec}$ [Mach 1.90]. Fig 5.6 is a summary of five such values determined at each of several downstream pressures, p_0 , showing also

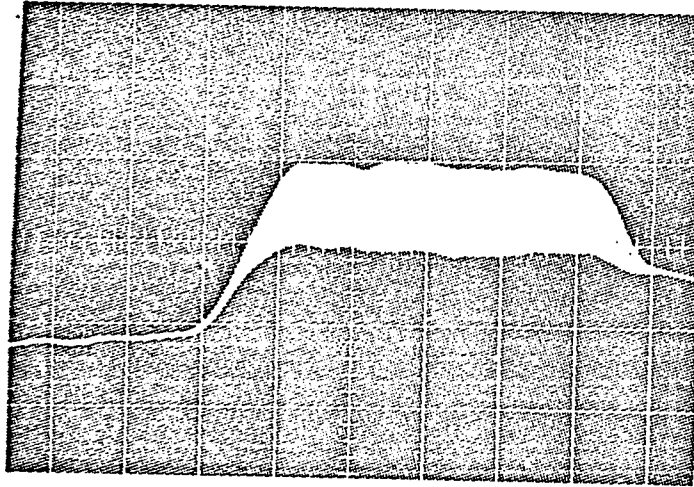
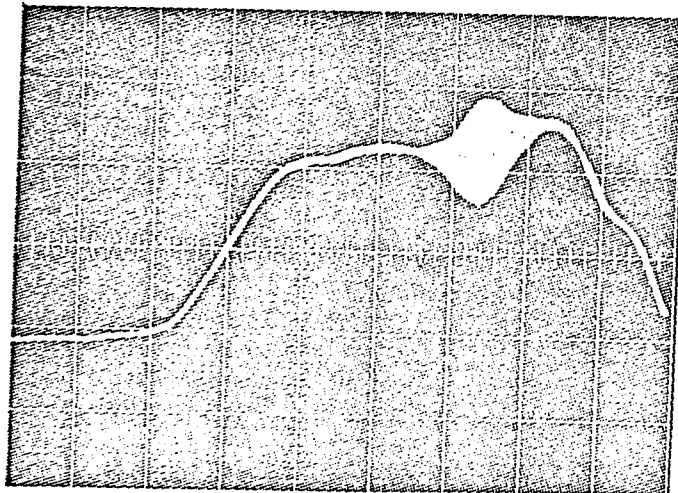
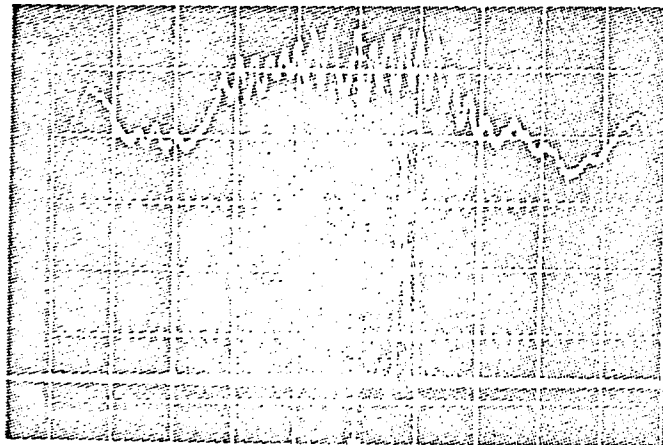
FIG. 5-5 SIGNALS OBSERVED WITH CURVED REFLECTORS**FIG. 5-5-1 PLANE MIRROR IN SHOCK TUBE****FIG. 5-5-2 140mm. RADIUS REFLECTOR IN SHOCK TUBE****FIG. 5-5-3 SHOCK REFLECTION: $r_s = 600\text{mm.}$, $M = 1.90$** 

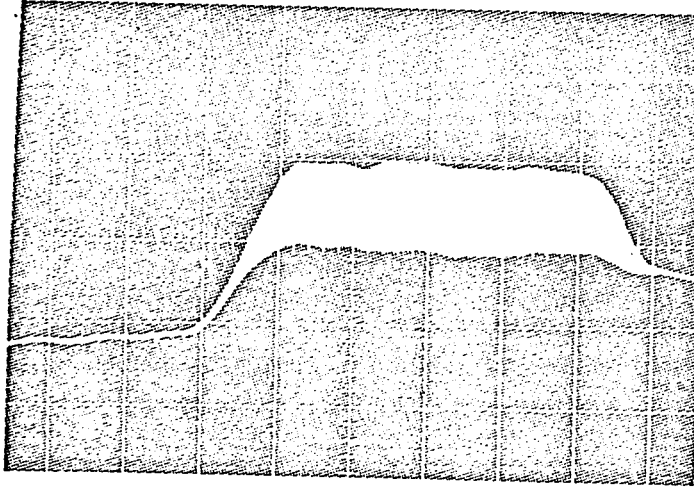
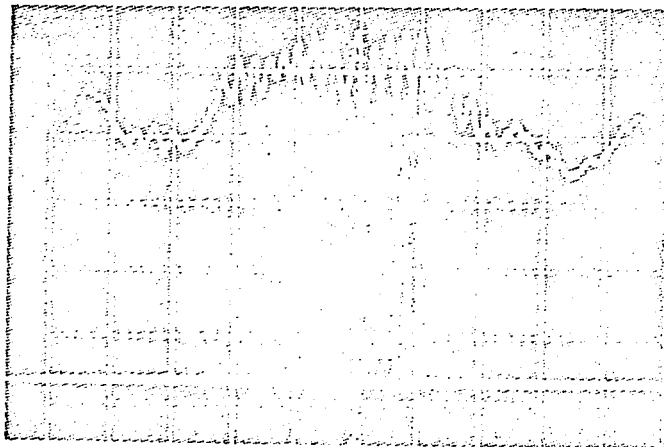
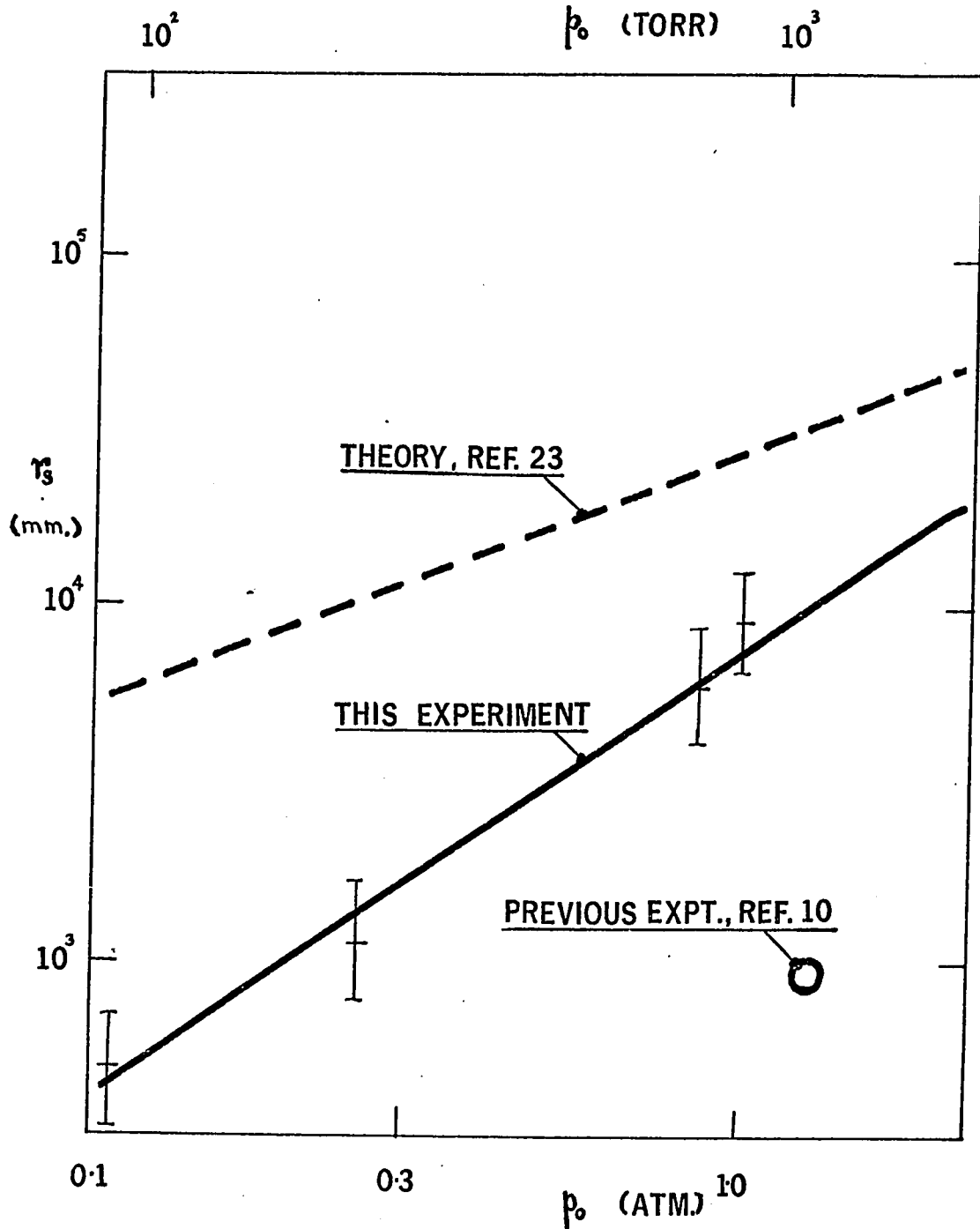
FIG. 5-5 SIGNALS OBSERVED WITH CURVED REFLECTORS**FIG. 5-5-1 PLANE MIRROR IN SHOCK TUBE****FIG. 5-5-2 140mm. RADIUS REFLECTOR IN SHOCK TUBE****FIG. 5-5-3 SHOCK REFLECTION: $r_s = 600\text{mm.}$, $M = 1.90$** 

FIG. 5-6 SHOCK FRONT RADIUS VS. PRESSURE

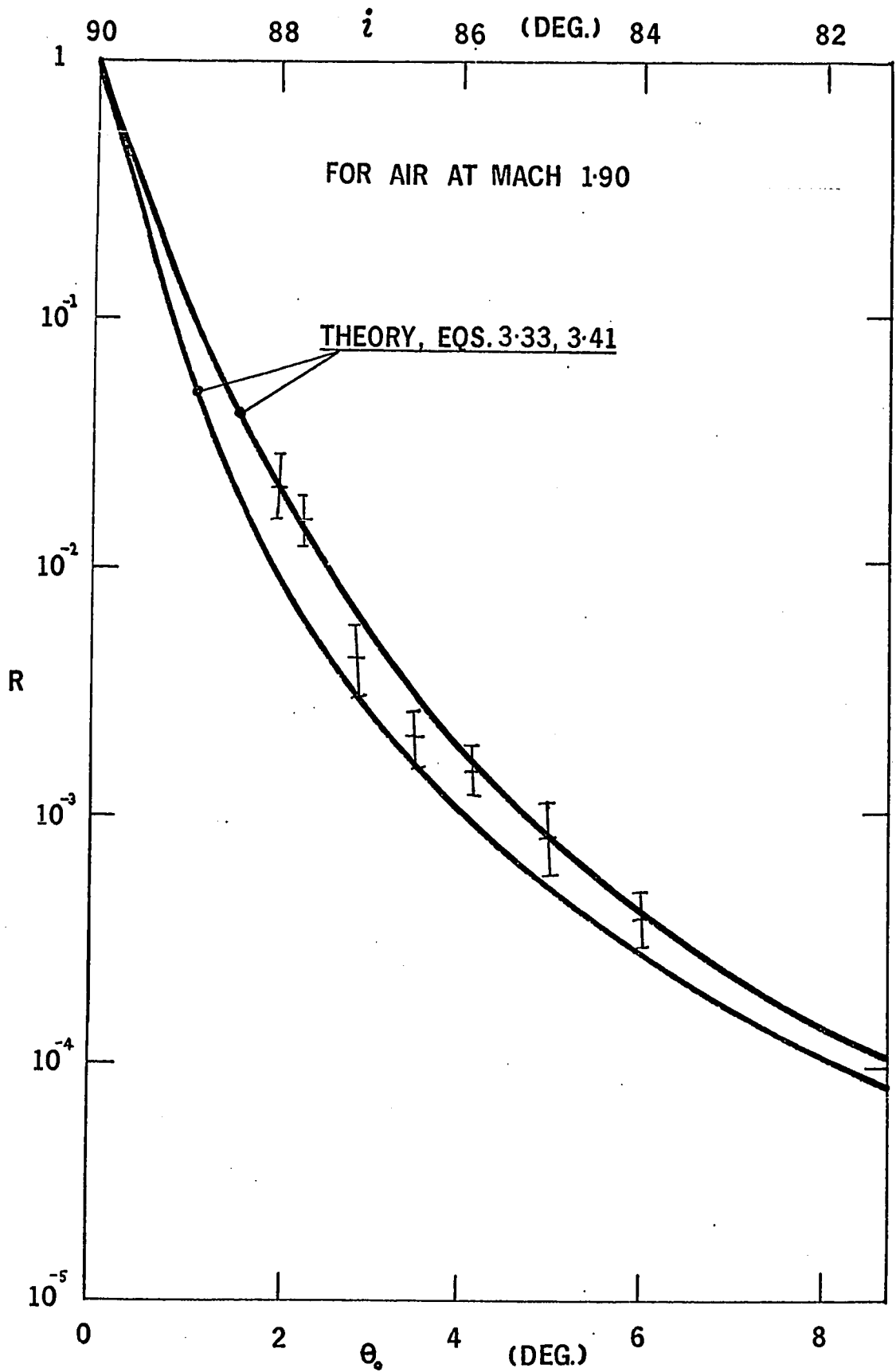
FOR AIR AT MACH NUMBERS LESS THAN 3



the theoretical dependence of R on p_0 predicted by Duff & Young⁽²²⁾ and a representative value taken from the results of Linzer & Hornig⁽¹¹⁾. Mazzella & de Boer⁽²³⁾ working in Argon have obtained similar results at 1 atm but with considerably less accuracy. Their results differ by a factor of 5 or so from those reported here at pressures less than 1 atm. It is possible that these discrepancies between theory and experiment are due to the surface roughness of the inside of the shock tube⁽¹¹⁾ which was machine finished to $\sim 3 \times 10^{-2}$ mm, for the results plotted in fig 5.6.

Fig 5.7 shows the experimental variation of (coherent) intensity reflection coefficient with angle, together with the theoretical dependence predicted by eqs. 3.33 and 3.41. Good agreement is obtained, over the full range of angles used (2° to 6° grazing incidence). The experimental points were obtained with a Mach 1.90 shock wave, using an inter-beam angle δi (or $\delta \theta$) of 0.5° . Each point on the graph represents 5 or more measurements, so that the effect of random variation in shock tilt which might be expected to produce a 40% error in R is reduced, giving an error of 10-20% for each point. A comparison of fig 5.7 with fig 4.5 shows immediately the improvement in agreement with theory given by the measurements taken with the differential interferometer, particularly at 5° - 6° . It is evident that there is normally a large amount of scattered light present at these angles - as much as ten times the true reflected signal, as given by the interferometer.

FIG. 5-7 REFLECTION COEFFICIENT VS. ANGLE (EXPERIMENT)



VI Alternative Measurement of Shock Curvature and Tilt

6.1 Introduction

In chapter V it was shown how the curvature and reflectivity of a shock front could be measured to accuracies of 20% and 40% respectively, the errors being due to the possibilities of tilt in the shock front. In this chapter an alternative method of determining curvature and reflectivity, which also detects shock tilt will be described. This experiment also is capable of detecting the presence of long-wavelength (i.e. \sim shock tube diameter) perturbations in the shock front of which shock front curvature is merely a special (1st order) case.

6.2 Experimental Arrangement

The arrangement of the optical system for these measurements is shown in Fig 6.1. The incident laser beam is focused down at a single interaction point on the shock tube axis, and light reflected from this point by a plane shock wave, perpendicular to the tube axis (i.e. zero tilt) is obstructed by a 2 mm opaque strip, mounted across the photomultiplier aperture. Angles of incidence between 70° and 88° are used, as before.

As a plane shock front passes through the test section, a square-pulse is observed at the photomultiplier output, with a dip to zero near the pulse center, corresponding to the obstructed axial reflection. The (constant) pulse height gives the reflection

coefficient of the shock front, as in the preliminary experiments (chapter IV) and the position of the zero-dip indicates whether the shock front is tilted, relative to the shock tube axis since the dip is only exactly central for reflection from the mid-point of an untilted shock front.

Any variation in pulse height during the reflection process is then due to the reflection occurring at different angles of incidence as the shock front sweeps through the interaction region - i.e. curvature of the shock front - giving a steady increase or decrease in reflected intensity across the pulse for concave and convex shocks respectively; or a long-wavelength perturbation of the shock front giving a more complex variation in the output pulse height.

The analysis of the output signal from a generalized shock perturbation is extremely complex, but for the most interesting and experimentally more common occurrence of a simple shock curvature, the radius of curvature can be calculated relatively easily from the ratio of the maximum to the minimum pulse heights. The possibility of shock tilt invalidating the results is eliminated here, since measurements are only taken from those output traces with a central 'dip', indicating zero shock tilt. The true reflectivity of such shock fronts is determined by extrapolating the trace into the central 'dip' region to obtain the reflected intensity for the on-axis point, for which the angle of incidence is well-known.

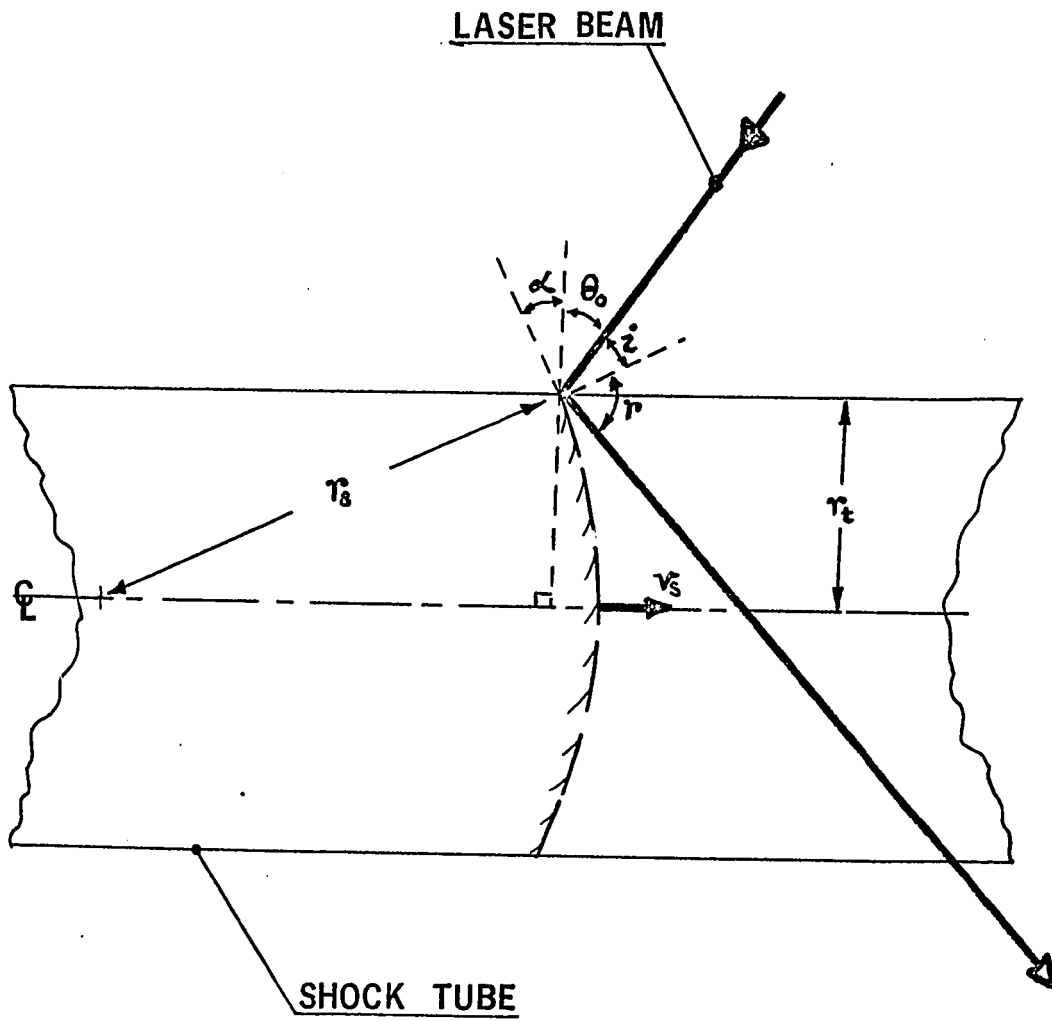
6.3 Determination of Curvature

Consider a shock front having a radius of curvature, r_s , propagating down a shock tube of radius r_t . Then a light beam reflected off the shock front at a nominal grazing angle θ , will in fact be reflected at an angle which varies from $(\theta_0 + \alpha)$ to $(\theta_0 - \alpha)$ (fig. 6.1) where

$$\alpha \equiv \frac{r_t}{r_s} \quad (6.1)$$

The intensity reflection coefficient, R , is given by eq. (3.45) viz.

$$R = \frac{1}{4\theta_0^4} \left(\frac{\delta n}{n} \right)^2 \left[1 - \frac{1}{\theta_0^2} \left(\frac{\delta n}{n} \right) \right] \quad (6.2)$$

FIG. 6.1 CURVATURE MEASUREMENT

so the ratio of the maximum reflected intensity (occurring when

$\theta_0 = \theta - \alpha$) to the minimum ($\theta_0 = \theta + \alpha$) is:-

$$\frac{I_{\max}}{I_{\min}} = \frac{\frac{1}{4(\theta - \alpha)^4} \left(\frac{\delta n}{n}\right)^2 \left[1 - \frac{1}{(\theta - \alpha)^2} \left(\frac{\delta n}{n}\right)\right]}{\frac{1}{4(\theta + \alpha)^4} \left(\frac{\delta n}{n}\right)^2 \left[1 - \frac{1}{(\theta + \alpha)^2} \left(\frac{\delta n}{n}\right)\right]} \quad (6.3)$$

$$= \left(\frac{\theta + \alpha}{\theta - \alpha}\right)^4 \left[\frac{1 - \frac{1}{(\theta - \alpha)^2} \left(\frac{\delta n}{n}\right)}{1 - \frac{1}{(\theta + \alpha)^2} \left(\frac{\delta n}{n}\right)} \right] \quad (6.4)$$

or $\frac{I_{\max}}{I_{\min}} \approx \left(\frac{\theta + \alpha}{\theta - \alpha}\right)^4$ to the first order (6.5)

so that

$$\alpha = \theta \left(\frac{\sqrt[4]{\frac{I_{\max}}{I_{\min}}} - 1}{\sqrt[4]{\frac{I_{\max}}{I_{\min}}} + 1} \right) \quad (6.6)$$

$$= \frac{r_t}{r_s} \quad (6.1)$$

giving

$$r_s = \frac{r_t}{\theta} \left(\frac{\sqrt[4]{\frac{I_{\max}}{I_{\min}}} + 1}{\sqrt[4]{\frac{I_{\max}}{I_{\min}}} - 1} \right) \quad (6.7)$$

The above derivation ignores the effects of the finite size of the

light beam, and the exact beam profile. These effects have been dealt with in a more exact analysis by Pert & Smy⁽²⁰⁾, who derive an expression which reduces to eq.(6.7) provided that the effective light beam width, d , is small:-

$$d \ll r_s \theta^2 - r_t \theta \quad (6.8)$$

For the parameters used in these experiments this yields the condition that

$$r_s \gg 500 \text{ mm} \quad (6.9)$$

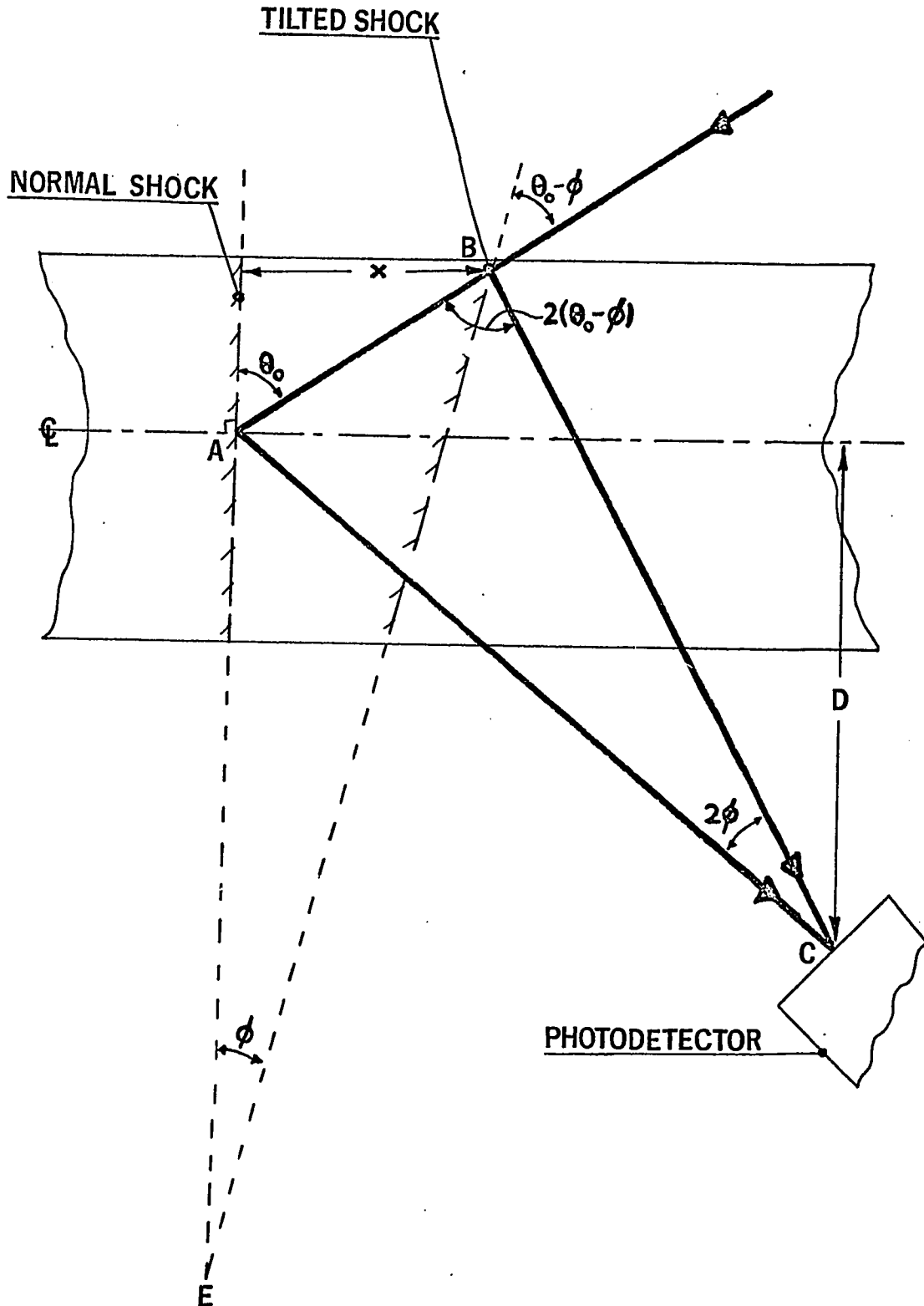
a condition which is found to be satisfied in practice.

6.4 Determination of Shock Tilt

If the shock front is tilted through an angle, ϕ , the dip in the trace due to the small obstruction at the detector will not occur at the mid-point of the reflected pulse, as set up in the initial alignment procedure, but will be earlier or later, according to the direction of the tilt.

The geometry of the system is shown in fig 6.2. The dip in the signal occurs when the shock is at BE, rather than at AE i.e. when the shock is an additional distance, X , downstream of the centre (alignment) position.

FIG. 6-2 TILT MEASUREMENT



$$\text{clearly, } x = v_s \delta t \quad (6.10)$$

where δt is the time difference between the centre of the reflected pulse, and the observed dip in the signal

$$\text{also } AB = \frac{x}{\sin \theta} \quad (6.11)$$

$$AC = \frac{D}{\cos \theta} \quad (6.12)$$

so in ΔBAC

$$\frac{x}{\sin \theta \sin 2\phi} = \frac{D}{\cos \theta \sin 2(\theta - \phi)} \quad (6.13)$$

$$\text{or } x = D \tan \theta \frac{\sin 2\phi}{\sin 2(\theta - \phi)} \quad (6.14)$$

so for small angles $\theta: \phi$,

$$x \approx D\theta \left(\frac{\phi}{\theta - \phi} \right) \quad (6.15)$$

$$\text{or } \phi = \frac{x\theta}{D\theta + x} \quad (6.16)$$

where x is given by eq (6.10):-

$$\text{and so } \phi = \frac{v_s \theta \delta t}{D\theta + v_s \delta t} \quad (6.17)$$

The maximum value of x for which reflection can still occur is limited by the shock tube radius, and the angle θ , to

$$x_{\max} = \theta r_t \quad (= v_s \delta t_{\max}) \quad (6.18)$$

so we have

$$\phi_{\max} = \frac{\theta \cdot r_t}{D + r_t} \quad (6.19)$$

and normally $D \gg r_t$ (6.20)

so. $\phi_{\max} = \theta \frac{r_t}{D}$ (6.21)

giving an upper limit to the measurable tilt of about 5 m.rad ($\frac{1}{4}^\circ$) in these experiments. In fact the observed shock tilt was always very much less than this, typical values being ± 0.5 m.rad.

Under these conditions (6.17) and (6.20) can be used to derive the more convenient approximation:-

$$\phi = \frac{v_s}{D} \delta t \quad (6.22)$$

which is sufficiently accurate for most of the experimental situations encountered here.

VII The High Intensity Shock System

7.1 Purpose

In chapter 3 it was shown that the practical upper limit to the Mach number produced in a conventional pressure-driven shock tube is about 3.5, and in fact it is inconvenient to work much above mach 2. A shock tube was therefore required which would produce the much higher Mach numbers - in the region of Mach 10⁽²⁴⁾ - which are more often encountered in plasma - dynamic situations.

7.2 Production of Strong Shocks at High Pressures

Wright⁽¹⁵⁾ has reviewed the methods by which strong shocks can be produced. With the exception of explosively driven shocks, however, it has only been possible to produce strong shock waves in gases at low pressures (i.e. a few Torr), the most common form of apparatus being the electro-magnetically driven shock tube⁽²⁵⁾, or the combustion shock tube⁽²⁶⁾. More recently, electrically-driven shock tubes have been designed which combine the ease of operation of the electromagnetic type, with the absence of circulating currents in the plasma created behind the shock front⁽¹⁸⁾⁽³⁰⁾.

In this type of shock tube, a high energy capacitor bank is discharged through the gas in the driver section of a diaphragm-type shock tube, thereby producing intense heating of the driver gas,

giving rise to an extremely high sound speed, and a very high pressure ratio across the diaphragm - both conditions being essential to the production of strong shock waves (section 3.1.7). Phillips⁽¹⁹⁾ has shown that the high Mach numbers produced in this type of shock tube are due only to the intense heating produced by the discharge, the electromagnetic forces involved in the production of the shock wave being negligible. The term "electro-thermal" is therefore used to describe this type of shock tube. Its use has so far been restricted to producing shock waves in low-pressure gases. There is no reason, however, why extremely strong shocks should not be produced in gases at high pressures (a few atmospheres) by an electrothermal shock tube which is designed to operate at the extremely high temperatures and pressures which are required, thus extending the range of previous work^(19,30).

7.3 Theory of the Electrothermal Shock Tube

From Chapter 3, (eq.3.25) the diaphragm pressure ratio can be numerically related to the shock strength, y , for a Helium-Air shock tube by:

$$\frac{P_3}{P_0} = \frac{y}{\left[1 - 0.629 \frac{C_0}{C_3} \frac{y-1}{\sqrt{6y+1}} \right]^5} \quad (7.1)$$

where C_p and C_3 are the sound speeds in the shocked and driver gases.

The Mach number is given by (eq. 3.17):-

$$M = \sqrt{\frac{6y + 1}{7}} \quad (7.2)$$

from Eq. 7.1 it is apparent that even with an infinite diaphragm pressure ratio we still have a finite shock strength, given by:-

$$0.629 \frac{C_0}{C_3} \frac{y - 1}{\sqrt{6y + 1}} = 1 \quad (7.3)$$

$$\text{or } y \approx 15.2 \left(\frac{C_0}{C_3} \right)^2 \quad \text{if } y \gg 1 \quad (7.4)$$

$$\text{giving } y_{\max} = 129$$

$$\text{and } M_{\max} = 5.8$$

for Helium-Air at 293°K.

If we assume ideal gas behaviour, then if the driver gas temperature, T_3 , is raised from room temperature T_{30} , we have

$$C_3 = \sqrt{\gamma_3 r_3 T_3} \quad (7.5)$$

$$\text{or } \frac{C_3}{C_{30}} = \sqrt{\frac{T_3}{T_{30}}} \quad (7.6)$$

$$\text{and } \frac{p_3}{p_{30}} = \frac{T_3}{T_0} \quad (7.7)$$

where C_{30} ; p_{30} are the room temperature sound speed and pressure of the driver gas, and r_3 is the gas constant for unit mass of the driver

gas.

Equation 7.1 then gives:-

$$\frac{p_{30}}{p_0} \times \frac{T_3}{T_0} = \frac{y}{\left[1 - 0.215 \sqrt{\frac{T_0}{T_3}} \frac{y-1}{\sqrt{6y+1}} \right]^5} \quad (7.8)$$

for Helium-Air.

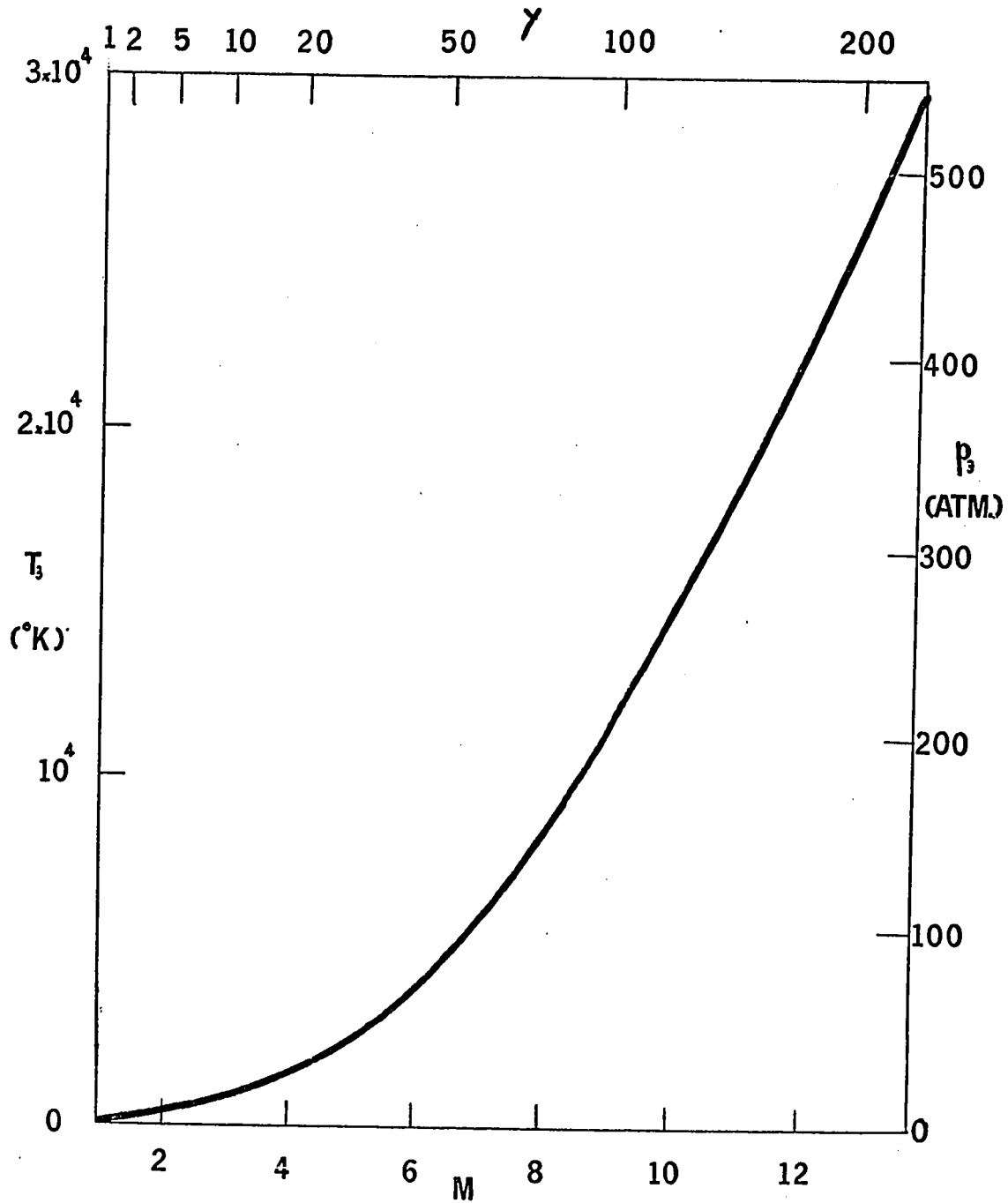
Fig. 7.1 shows this dependence of driver gas temperature (and pressure - eq. 7.7) on shock strength and mach number for a system with an initial filling pressure p_{30} of 5 atm. (Helium) and air at one atmosphere in the downstream section of the shock tube, the entire system being at 293°K , initially.

From fig 7.1 it is apparent that although the gas temperatures required to obtain Mach 10 shocks are extremely high, they are within the range which can be produced by intense discharges. The pressures involved are also considerable but are well within manageable limits. It should be realised that eq. 7.8 and fig. 7.1 represent an upper limit to the Mach numbers and shock strengths which can be obtained, since no allowance has been made for the variation of γ_3 with temperature (as the driver gas becomes ionized) or for any departures from ideal gas behaviour at high pressures.

FIG. 7.1 DRIVING CHAMBER TEMPERATURE AND PRESSURE VS.

MACH NUMBER AND SHOCK STRENGTH

FOR He-AIR, INITIALLY AT 5 ATM., 1 ATM.



The actual Mach number can be predicted for any given shock tube if the enthalpy of the driver gas is known. If we assume that the entire energy input W (stored in the capacitor bank) is transformed into thermal energy of the driver gas we have:-

$$p_3 = \frac{W}{V_3} \quad (7.9)$$

where V_3 is the volume of the driver chamber.

In fact there may be considerable energy losses in heating the walls of the chamber, and in vaporizing material from the electrodes and diaphragm - more exactly

$$p_3 = \epsilon \frac{W}{V_3} \quad (7.10)$$

where ϵ is defined as the "thermal efficiency" of the shock tube.

Phillips⁽¹⁹⁾ found values of ϵ of about 0.45, in his shock tube. Assuming a generally similar configuration we are now in a position to determine the energy input per unit volume of driver chamber required to produce a Mach 10 shock wave, as about 100 Joules for every cubic centimetre or energies of around 10 KJ for a volume of 100 cc at 5 atm. These figures are quite easily obtained in the laboratory, and the construction of a high-intensity shock system to operate at 1 atm, downstream is thus quite feasible.

7.4 Design of the Shock System

An existing capacitor bank was used to provide the required

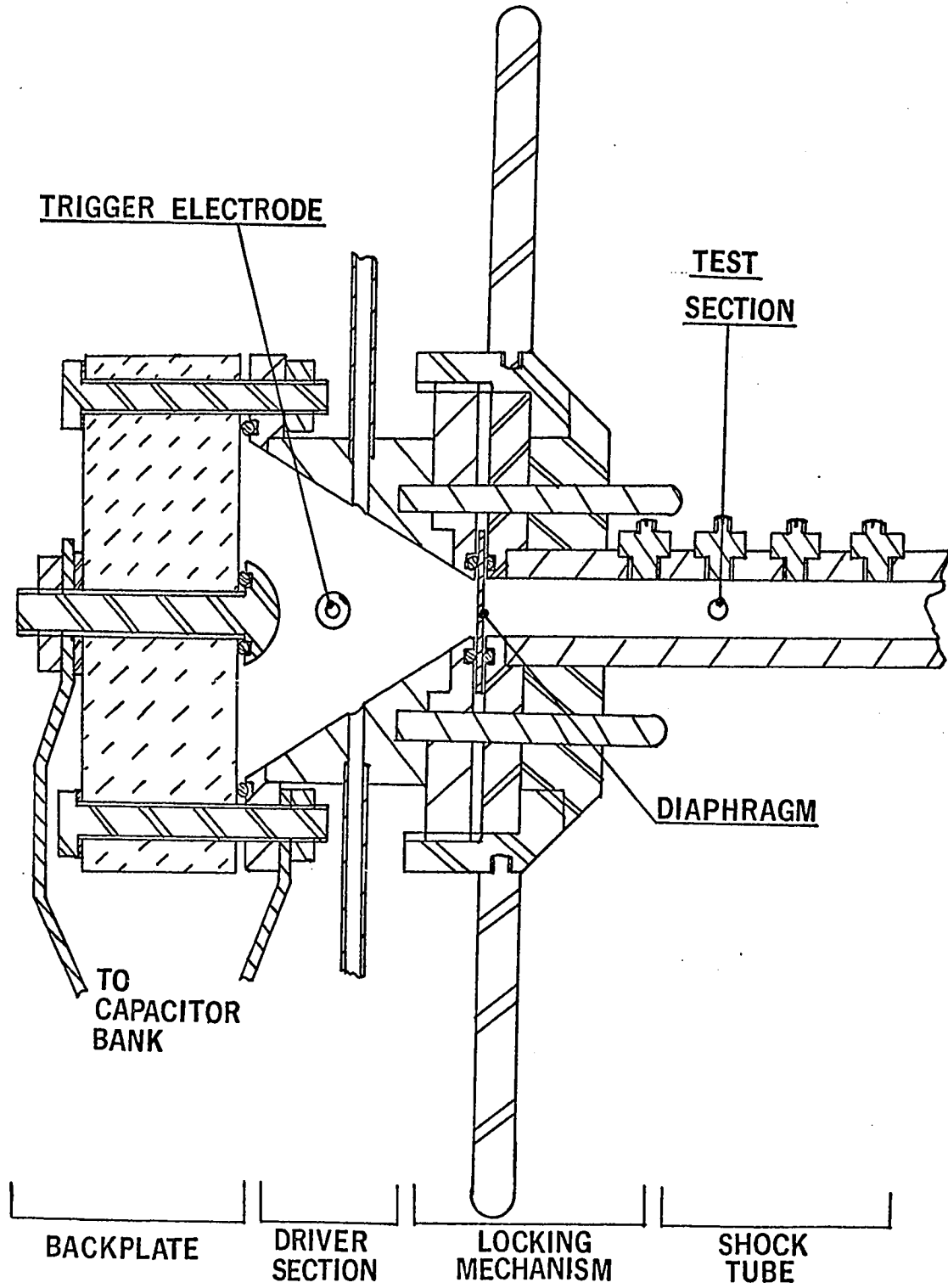
energy. This bank had a capacitance of 43 μ F at 20 kV, giving a stored energy of 8.7 KJ. The volume of the driver section was fixed at 250 cc, giving a maximum driver pressure at 100% thermal efficiency of 340 Atmospheres, and a maximum mach number of 11.4. The driver section was designed to withstand a maximum internal pressure of 680 Atm. (10,000 p.s.i), and to give an additional safety margin over the normal pressure-vessel design figure.

The downstream part of the shock tube must be capable of withstanding the shock overpressure, given by the shock strength y , of 150 Atm. This is well within the limits of normal high-pressure Steel tubing, but in order to accomodate wall-mounted piezo-electric pressure probes and ionization probes, a much heavier section steel tube was used - 32 mm o.d. by 15 mm i.d. This gives sufficient length to a standard fine-pitch threaded plug to withstand 150 atm.

A longitudinal section of the shock tube is shown in fig. 7.2, stainless steel being used throughout the system, with the exception of the insulating backplate, which was made of "teflon". The driver section was made conical in form to obtain the maximum flow velocity of the gas from the driver, after the diaphragm had opened. This has been shown to give a 10% increase in Mach number⁽¹⁶⁾ and also assists in maintaining the shock for as long a time as possible. The driver chamber length of 100 mm was sufficient to give a reasonable (170 mm) useable length of shock tube. For distances greater than about 1.7 driver chamber lengths (under the

FIG. 7-2 HIGH INTENSITY SHOCK TUBE

APPROXIMATELY HALF SIZE



conditions present after the discharge) down the shock tube the rarefaction wave reflected off the back of the driver section 'catches up' and interferes with the shock wave⁽¹⁵⁾.

The diaphragm is retained between two 25 mm diameter O-ring seals by means of a quarter-turn single start interrupted screw thread, so that diaphragms can be changed quickly and conveniently. A number of different diaphragm materials were tried. The most important properties required are that no fragments of the ruptured diaphragm should be driven down the shock tube to perturb the shock wave and damage the instrumentation, and that the diaphragm should not rupture immediately the discharge is initiated, but after most of the capacitor bank energy has been transferred to the driver gas. Two materials were found which satisfied both requirements - 0.025 mm thick "mylar" film, which was vaporized by the discharge in a time comparable to the total duration of the (underdamped) discharge, and 0.25 mm thick steel shim stock, with two 25 mm long slots 0.24 mm deep milled across it in the form of a cross, so that the diaphragm folded back against the shock tube inlet, after completion of the capacitor bank discharge. Because of the greater convenience, "mylar" film was used for most of the experiments, although the velocities obtained were less predictable than with the steel diaphragms.

The vacuum, purging and backfilling systems for the shock tube and driver sections were equipped with electromagnetic valves, so that the operation of the shock system could be made largely

automatic. The whole system could be cycled from shot to shot in less than a minute. The discharge was initiated by an additional trigger electrode, in the driver chamber, thus eliminating the energy losses (up to 50%)⁽¹⁹⁾ inherent in using an external spark-gap switch.

7.5 Operation and Performance of the Shock Tube

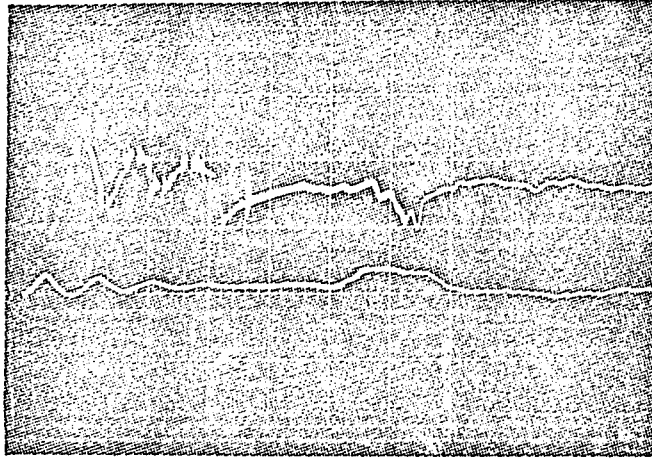
In a conventional shock tube, the finite opening time of the diaphragm, with rupture first occurring on the shock tube axis, results in an initial radial velocity and axial acceleration of the shock front, the maximum axial speed and optimum stability normally being attained at a distance of 10 to 20 shock tube diameters downstream of the diaphragm. For the shock tube described here, using "mylar" diaphragms which were vaporized completely by the driving discharge, this effect was considerably reduced, and it was found possible to work within a few diameters of the diaphragm. Most of the measurements were taken at points from 8 to 10 diameters downstream, however.

Piezo-electric pressure transducers mounted in the shock tube wall were used initially to measure the shock velocity, but the ceramic piezo-electric crystals were rapidly destroyed, apparently by the sudden reduction in overpressure as the rarefaction wave followed the shock wave down the tube⁽¹⁵⁾. Sufficient results were obtained, however, to compare with velocities obtained with ionization

probes, to check that the ionization front immediately behind (and caused by) the shock wave had the same velocity as the shock front. Modified chassis-mount B.N.C sockets were used as ionization probes, screwed directly into the shock tube wall, so that the probe was flush with the inner surface of the tube. Three probes were used at 25 mm centres. Voltages were applied between the upstream probe and each of the downstream probes, so that current pulses were generated as the shock (or ionization) front passed the second and third probes. A typical oscilloscope trace of the voltages generated across suitable load resistors is shown in fig. 7.3. The traces are initiated by the capacitor bank trigger pulse, and show the discharge current in the form of "pickup". By extrapolation of the shock velocity it can be seen that the diaphragm opens when about 90% of the capacitor bank energy has been transferred to the driver gas.

Fig. 7.4 shows the measured Mach numbers produced by the shock tube as a function of capacitor bank voltage, with the theoretical lines, for a number of different values of ϵ (eq.7.10). It was found that ϵ decreased after a number of shots and this effect was traced to the gradual contamination of the insulator surface by evaporated metal and diaphragm material, resulting in 'tracking' and giving rise to a less efficient form of discharge. The minimum value of ϵ was 0.3 which is reasonable, and values very close to one were obtained immediately after cleaning the insulator. A large number of different

FIG. 73 VELOCITY MEASUREMENT WITH IONIZATION PROBES



20 μ sec./div.

UPPER TRACE: REFLECTED LIGHT SIGNAL - NEGATIVE DEFLECTION

1 W/div.

LOWER TRACE: IONIZATION PROBE SIGNALS (NO.1—NO.2)

1 V/div.

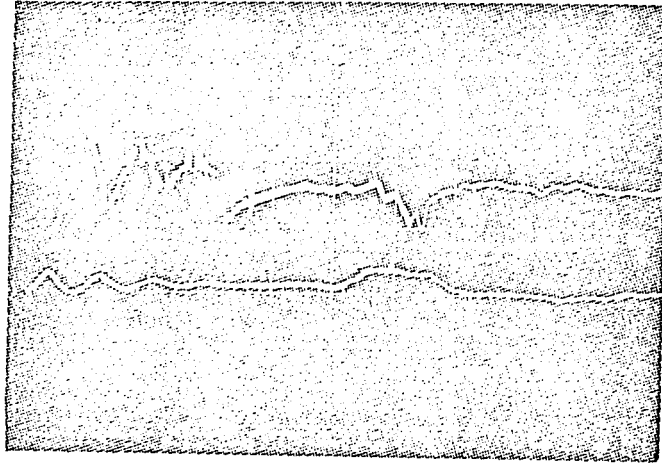
GRAZING ANGLE OF INCIDENCE = 8 DEG.

SHOCK MACH NUMBER = 3.2

SHOCK REFLECTION COEFFICIENT = 60×10^{-4}

SHOCK FRONT RADIUS = 1200 mm.

FIG. 73 VELOCITY MEASUREMENT WITH IONIZATION PROBES



→
20 μ sec./div.

UPPER TRACE: REFLECTED LIGHT SIGNAL - NEGATIVE DEFLECTION

1 W/div.

LOWER TRACE: IONIZATION PROBE SIGNALS (NO.1-NO.2)

1 V/div.

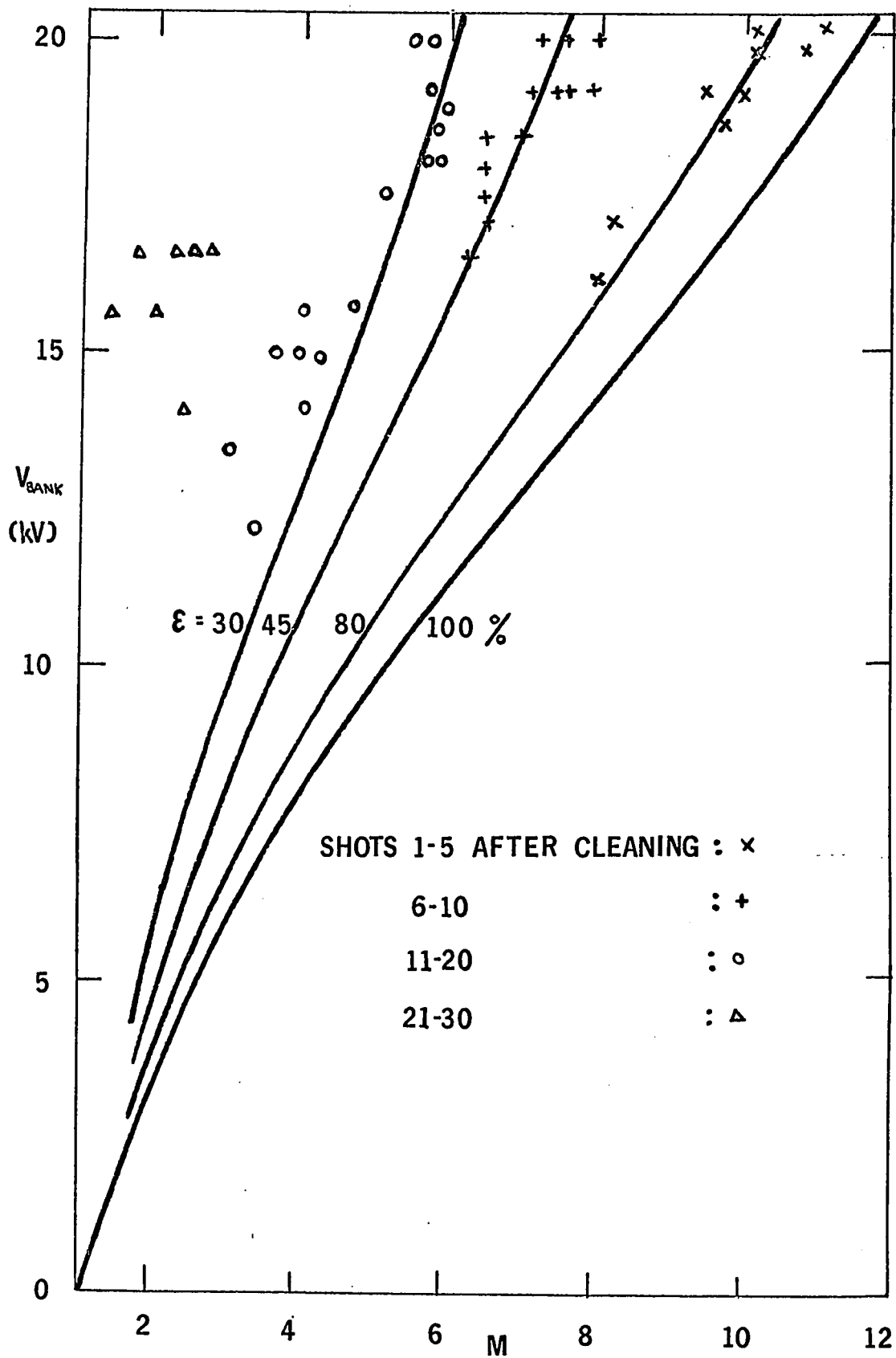
GRAZING ANGLE OF INCIDENCE = 8 DEG.

SHOCK MACH NUMBER = 32

SHOCK REFLECTION COEFFICIENT = $60 \cdot 10^{-4}$

SHOCK FRONT RADIUS = 1200 mm.

FIG. 7.4 CAPACITOR BANK VOLTAGE VS. MACH NUMBER



insulator materials were tried, but no other material was found which had such a good tracking resistance as "teflon" coupled with the required mechanical strength.

The performance of the shock tube was generally similar to that of the much larger system of Camm & Rose⁽³⁰⁾, which was operated with downstream pressures of 0.1 to 0.3 Torr, and somewhat better than that of Phillips⁽¹⁹⁾.

VIII Measurement of Reflectivity and Curvature of Hypersonic Shocks

8.1 Reflection Coefficient

8.1.1 Choice of Method of Measurement

A number of additional experimental difficulties are introduced in the measurement of reflection coefficients of shock waves having very high Mach numbers. At Mach numbers greater than about 4, the gas behind the shock front is heated sufficiently by the passage of the shock wave to cause the gas molecules to become excited⁽¹⁵⁾ and to emit light in the visible region of the spectrum. Ultimately the gas becomes ionized, at very high Mach numbers. The light emitted by the shock heated gas is intense enough to mask the reflected laser beam, even at extreme grazing incidence, and the situation is considerably worse at larger grazing angles with the shock tube used here, since the photodetector system can also see the plasma produced by the driving discharge, as it propagates down the shock tube behind the shock front.

The presence of this large amount of 'stray' light immediately suggests the use of the Differential Doppler Interferometer described in chapter 5, and used successfully to measure the reflection coefficient of low Mach number shocks (section 5.7). However, the frequencies generated by shocks moving at Mach 10 or so would be in the region of 100 MHz or more, for grazing angles up to about 10 degrees, and would thus be outside the maximum bandwidth of any state-of-the-art detector system for the expected reflected intensities (chapter 2). At angles

very near to grazing incidence, the frequencies and reflected intensities produced might just be manageable, but only about 10 fringes would be observed, even in the complete absence of any curvature or tilt of the shock front, due to the extremely short interaction time (0.1 μ sec) between the shock wave and the laser beams which in turn results from the high Mach numbers involved and the small diameter (15 mm) of the shock tube. In practice, of course, a shock tilt of around 2 degrees or the equivalent curvature (400 mm shock front radius) could very easily be present, and it is unlikely that more than two or three fringes would be observed - insufficient to give a reliable reflection coefficient measurement.

It was therefore decided to use the simple method of measuring reflection coefficient described in chapter 4 (section 4.3.1). As much stray light as possible was excluded from the detector system by carefully screening the entire optical system and interaction region from the room lights, and by using an interference filter centered at 632.8 nm wavelength, to exclude as much as possible of the light produced in the shock tube. Filters with bandwidths of 20 and 2 nm were used, and it was found that there was little to be gained from using the narrower bandwidth since this filter also attenuated the laser beam considerably (x0.3), and thus only slightly increased the "signal to noise ratio" of the detector system. The normal Doppler shift of the reflected laser beam is of the order of 10^{-3} nm so there is no possibility of the wavelength of the reflected beam falling outside the

bandwidth of the filter.

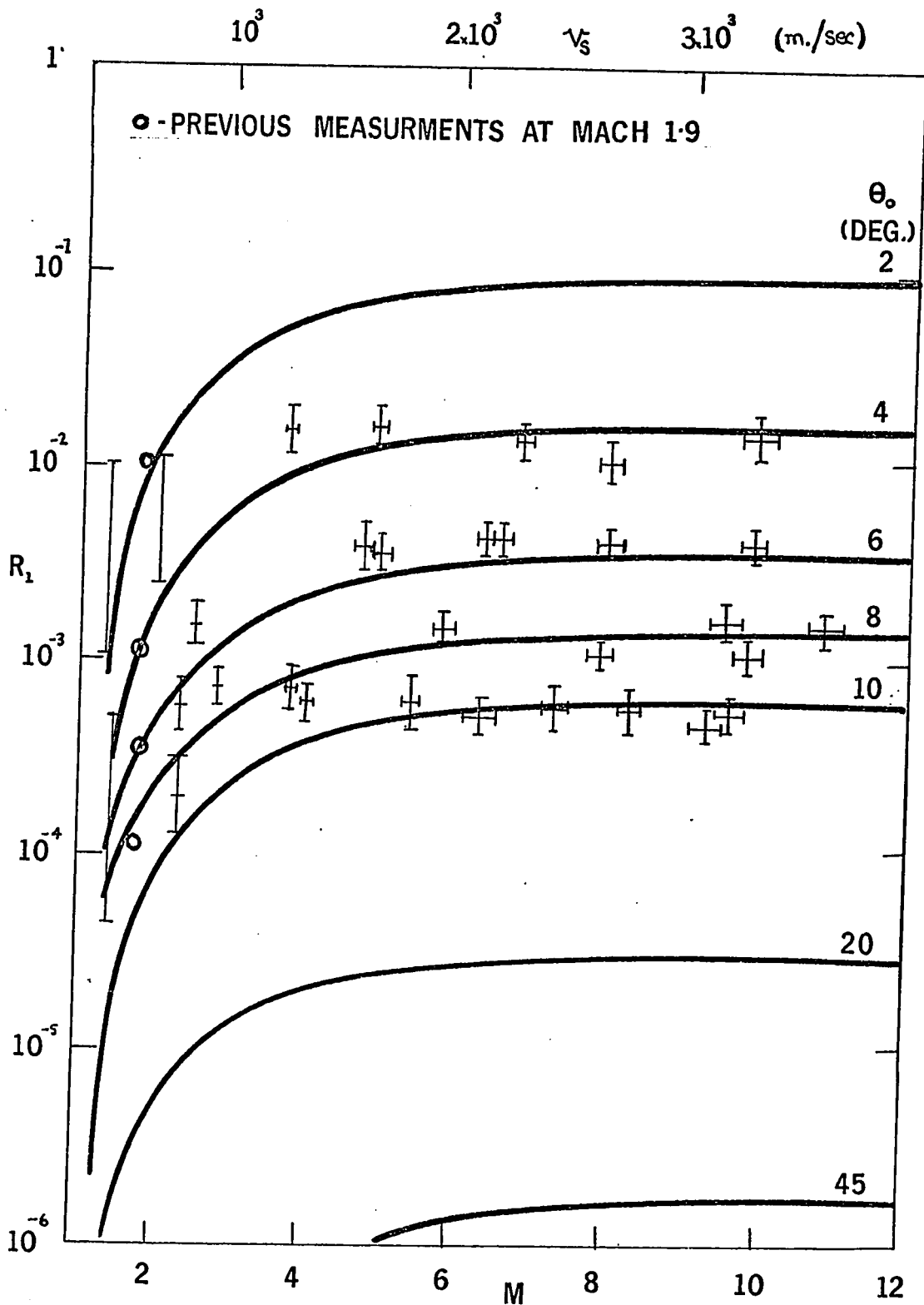
8.1.2 Experimental Results

The measurements were made as described in chapter 4, at points 75 to 150 mm downstream of the shock tube diaphragm. The photomultiplier was operated with a 50 Ω load resistance to give sufficient system risetime to accurately observe the reflected pulse whilst retaining adequate output voltage, at the grazing angles of incidence between 4 and 10 degrees which were used. Angles less than 4 degrees were not used since the laser beam had to be stopped down to an impracticably low diameter, to avoid reflection of only a part of the beam occurring. Above 10 degrees, the background light intensity became too high and the reflection coefficient too low to observe any meaningful reflected pulse, even with a 2 nm notch filter at the photodetector. Fig. 7.3 shows a typical measurement, the upper trace being the reflected light intensity, and the lower trace the ionization-probe signal for velocity measurement. Fig 7.3 is for a mach 3.2 shock, giving a reflection coefficient of 6.2×10^{-4} .

Fig 8.1 summarizes the results obtained at a number of different angles over the full range of Mach numbers available. The results obtained at velocities below mach 2 or so are somewhat unreliable, due to the low reflected light levels observed, comparison with figs. 4.5 and 5.7 showing that the results obtained in this region are as much as a factor of 3 different from the earlier results. The

FIG. 8-1 REFLECTION COEFFICIENT VS. MACH NUMBER

FOR AIR AT 1 ATM.



discrepancies are random however, and the general trend of the results is in reasonable agreement with those obtained earlier, and with theory. Fig. 8.1 also shows the theoretical variation of Reflection Coefficient, R_1 with Mach number at a number of different angles of incidence, appropriate to the experimental points, the curves being calculated from eqs. 3.33, 3.55 and 3.56. It will be seen that the experimental values of reflection coefficient are in good agreement with theory ($R_1 \approx R_2$ at these angles) over the entire range of angles and Mach numbers, with a possible trend to higher than theoretical values, at the lower Mach numbers (2-4), at all angles. It would therefore seem reasonable to assume that the shock reflection coefficient follows the theoretical variation with angle and Mach number up to the values associated with, for example, laser-produced plasmas ($M \sim 30$, $\theta \sim 45^\circ$).

8.2 Measurement of Shock Curvature

The curvature of the shock fronts produced by the high-intensity shock system were measured by the method described in chapter 6 (section 6.3), except that the central obstructing strip used to detect shock front tilt was not used, because of the short length of the reflected pulse. In view of the large but consistent curvatures (measured at various angles of incidence) it is apparent that any tilt in the shock front is randomly oriented, and of under 1 degree.

The values of the radius of curvature of the shock front were determined from the same traces as the reflection coefficients, and are

FIG. 8-2 SHOCK RADIUS OF CURVATURE VS. MACH NUMBER
FOR AIR AT 1 ATM., 150mm. DOWNSTREAM

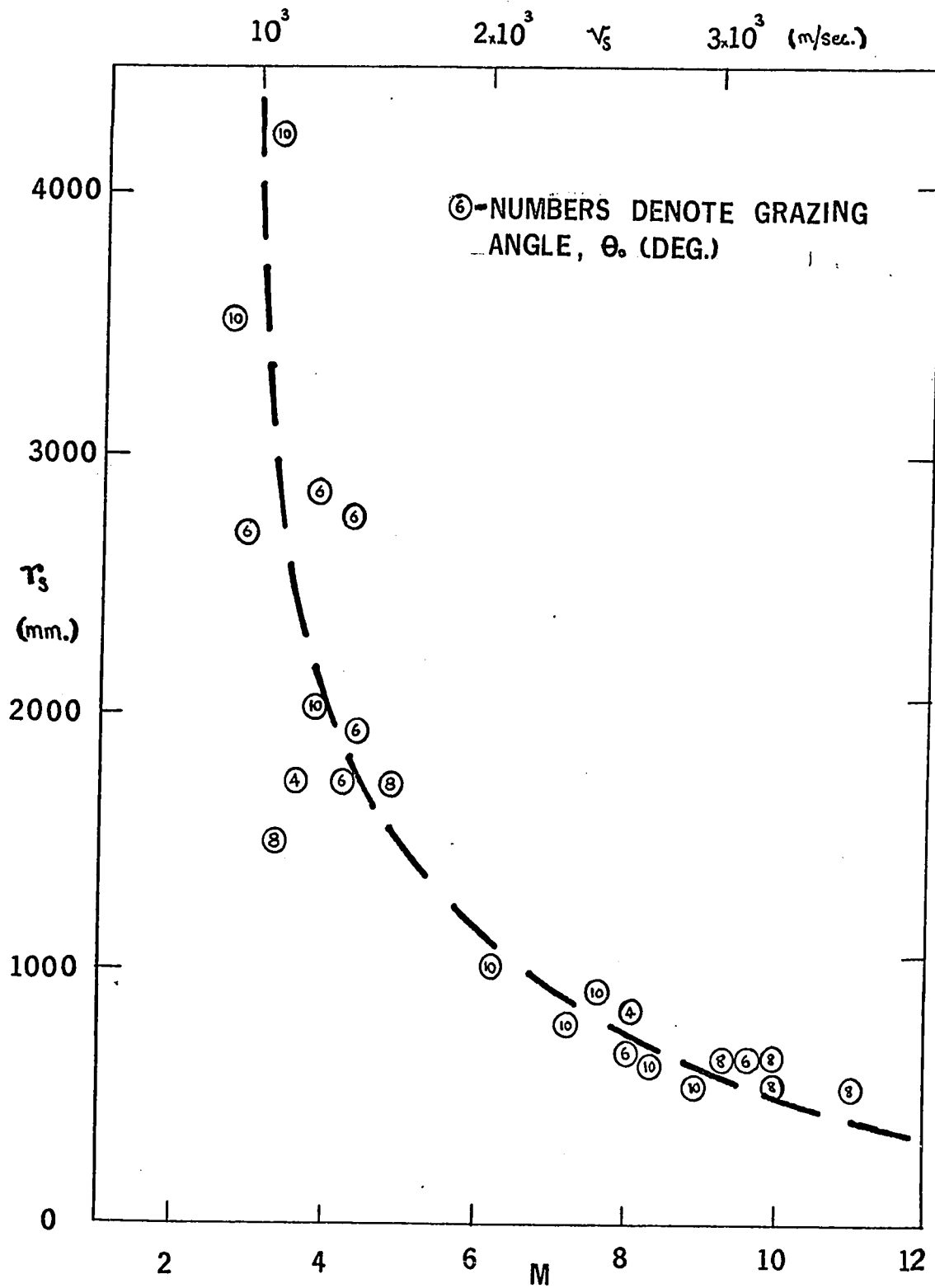
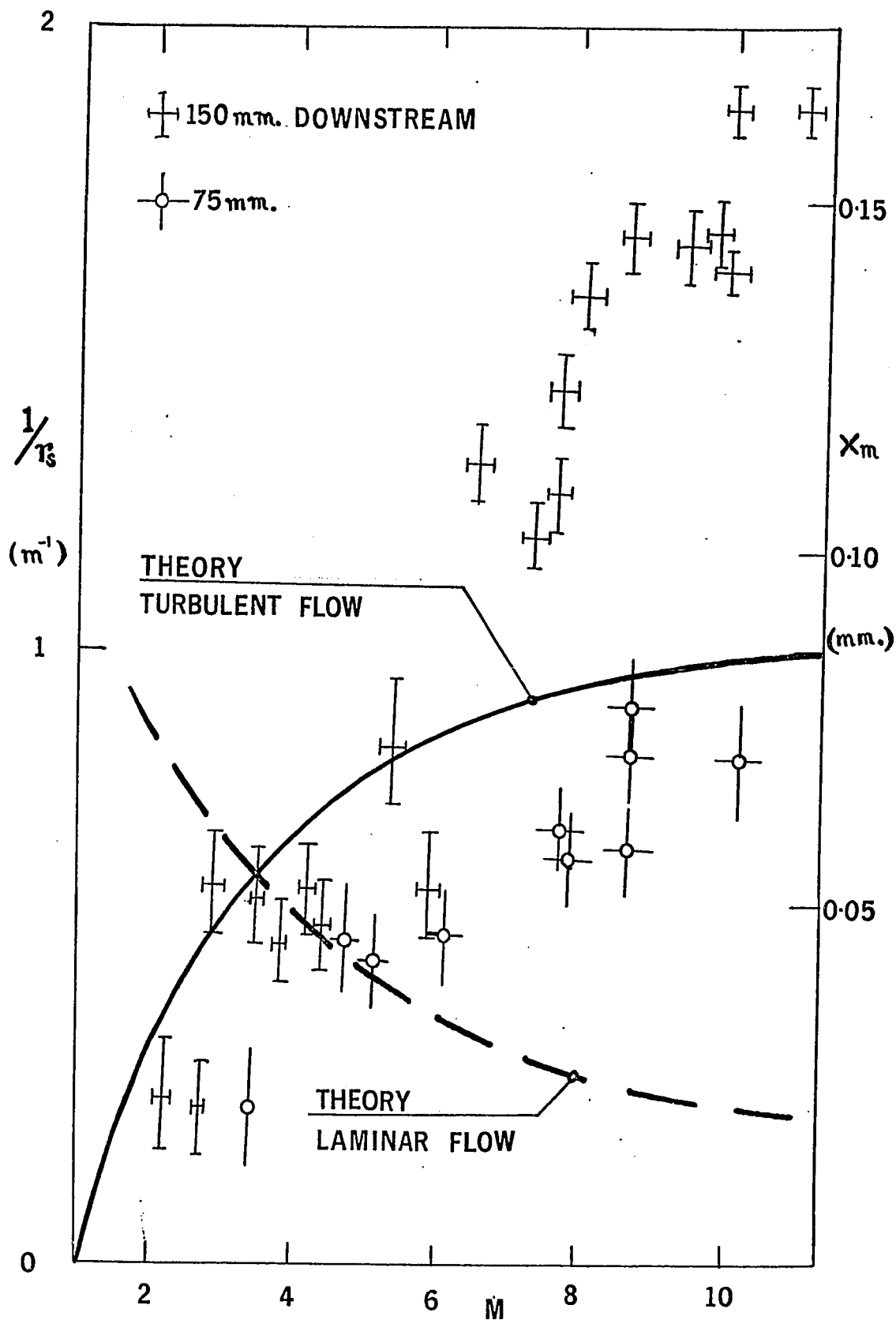


FIG. 8-3 SHOCK CURVATURE VS. MACH NUMBER



shown as a function of Mach number in fig. 8.2. It is apparent that there is no correlation between the shock radius and the grazing angle of incidence, as expected, and the results are replotted without distinguishing the angles of incidence in fig. 8.3, which indicates that the shock curvature ($\equiv \frac{1}{r_s}$) is directly proportional to the Mach number, or shock velocity. It is noteworthy that there is considerable 'scatter' and in the results at low Mach numbers (≤ 5) where all the previous work on shock waves at atmospheric pressure has been carried out, so that the linear increase of curvature with Mach number can only be detected using the High Intensity Shock System.

Fig. 8.3 also shows some curvature measurements taken at a different point along the length of the shock tube, indicating an approximately linear increase of shock front curvature with distance of propagation down the tube. This behaviour is consistent with the growth of a boundary-layer at the shock tube walls, as the shock wave progresses, the boundary layer in turn causing disturbances which distort the shock front, to a theoretically parabolic profile, with the vertex of the parabola touching the shock tube wall⁽²⁷⁾. In practice, the measurements described here are too approximate to determine the exact profile of the shock front, and it is more useful to invoke the concept of the maximum extent, or maximum protrusion, x_m of the shock from a plane surface. For a spherical shock front, it is easily shown that for small values of x_m

$$x_m = \frac{r_t^2}{2r_s} \quad (8.1)$$

where r_s is the shock front radius
and r_t is the radius of the shock tube

x_m is thus an alternative measure of the shock curvature
($1/r_s$) and is plotted as such in figure 8.3.

De Boer, in an involved but still approximate analysis⁽²⁸⁾
has determined the theoretical variation of x_m with Mach numbers for
both laminar and turbulent boundary layers, in a shock tube of
circular cross-section, the turbulent boundary layer being appropriate
to downstream pressures greater than 100 Torr. These theoretical
curves are shown in fig 8.3, which shows quite clearly that the trend
indicated by the curve for the turbulent boundary layer is followed
by the experimental results, as expected, although curvatures
considerably greater (i.e. smaller shock front radii) than predicted
were observed. Indeed, the experimentally observed curvature appears
to be still increasing, even 150 mm downstream of the shock tube
diaphragm, and it appears unlikely that the boundary-layer (and hence
shock curvature) ever grows to its equilibrium value (which seems
to be at least a factor of three greater than that predicted
theoretically), since the shock rarefaction catches up with the shock
wave some 170 to 200 mm downstream of the diaphragm.

It is possible that the enhanced curvature observed 150 mm
downstream is due to the proximity of the rarefaction wave affecting
the boundary layer behind the shock front, but since the contact surface
is observed by laser reflection at some angles of incidence, to be

about 20 mm behind the shock at this point, it would seem unlikely. It is more probable that the theory becomes very approximate for such a small-diameter shock tube, and a full investigation of shock curvature effects at high pressures must await the construction of a larger diameter shock tube, capable of operating in the same régime. It may also be remarked that the turbulent boundary layer did not produce any marked shock attenuation - the shock velocity remaining appreciably constant (to within 10%) over the first 150 mm of the tube, under any given set of conditions.

The limitation due to finite laser-beam width, given by eq. 6.8 (p. 75) yields for this shock tube (radius = 7.5 mm) the condition:-

$$r_s \gg 80 \text{ mm}$$

which is easily satisfied for all the results obtained (minimum value of $r_s \approx 500 \text{ mm}$).

IX Conclusion and Suggestions for Further Work

9.1 Conclusion

The reflection of a light beam by a shock wave has been investigated both theoretically and experimentally, and it has been shown that the results observed can be adequately explained by the exact application of the laws of optics. Experimental confirmation of the validity of the theory has been obtained at Mach numbers and ambient pressures which have hitherto been unattainable.

It has also been shown that the presence of light reflected by shock waves is likely to predominate over the required signal in a number of plasma-dynamic experiments in which light-scattering by the plasma is used as a diagnostic tool, and a method by which such scattered and reflected components may be distinguished and separated at the light detector has been demonstrated. The advantages and limitations of this technique have been investigated in some detail.

Finally, a shock tube has been developed which is capable of producing hypersonic ($>Mach\ 10$) shock waves in air at one atmosphere, and some new information on the curvature of such shocks, resulting from a turbulent boundary layer at the shock tube wall, has been obtained, thereby extending the results of previous workers.

9.2 Suggestions for Further Work

The Differential Doppler Interferometer (chapter 5) lends itself to a variety of Plasma Physics Experiments, possibly the most interesting of which would be the light reflection and scattering occurring at the plasma produced by a focused high-power (200 MW) laser beam, where very small 'scattering' coefficients have been reported, in the presence of extremely strong, (and therefore relatively highly reflecting) shock waves.

The investigation of these extremely strong shock waves at high pressures (one or more atmospheres) would also prove very interesting in its own right, if the measurements could be extended to grazing angles of 20 to 30 degrees - by the use of a higher power laser as a light source - since at these angles the values of the reflection coefficient obtained can be used to calculate the gas density profile through the shock wave, and information on the gas relaxation rates behind the shock front can be obtained.

The construction of a large-diameter High Intensity Electrothermal Shock Tube along the lines of that described in chapter 7 would enable more reliable information on the structure (and curvature) of high pressure hypersonic shocks to be obtained, by the use of a differential interferometer, and would give some further information on the effect of tube diameter on shock front curvature.

The present High-Intensity Shock System could fairly easily

be adapted to operate with reduced pressures downstream, and with gases other than air in the downstream section of the tube, giving still higher Mach numbers in a variety of gases, and thus forming a convenient source of dense highly-ionized plasma⁽³⁰⁾. It has also been suggested⁽²⁹⁾ that a further increase in shock Mach number could be obtained by discharging a second energy storage capacitor bank into the shock tube, behind the shock front, using the ionization produced by the present shock to initiate the discharge.

References

1. Malyshev, G.M: "Plasma Diagnostics by Light Scattering on Electrons", Sov. Phys. Tech. Phys., 10, 12, 1633-1643, (1966).
2. Fünfer, E., Kronast, B., and Kunze, H.J: "Experimental Results on Light Scattering by a θ -Pinch Plasma using a Ruby Laser", Phys. Lett., 5, 2, 125-127, (1963).
3. Davies, W.E.R., and Ramsden, S.A: "Scattering of Light from the Electrons in a Plasma", Phys. Lett., 8, 3, 179-180, (1964).
4. Ramsden, S.A., and Savic, P: "A Radiative Detonation Model for the Development of a Laser-Induced Spark in Air", Nature, 203, 4951, 1217-1219, (1964).
5. Ramsden, S.A., and Davies, W.E.R: "Radiation Scattered from the Plasma Produced by a Focused Ruby Laser Beam", Phys. Rev. Lett., 13, 227, (1964).
6. Askaryan, G.A., Savchenko, M.M., and Stepanov, V.K: "Investigation of Light Spark and of Other Optical Effects in Focusing of Light by a Lens with a Channel on the Axis", JETP Lett., 10, 4, 101, (1969).
7. Hey, J.S., Pinson, J.T., and Smith, P.G: "A Radio Method of Determining the Velocity of a Shock Wave", Nature, 179, 4671, 1184-1185, (1957).
8. Cowan, G.R., and Hornig D.F: "The Experimental Determination of the Thickness of a Shock Front in a Gas", J. Chem. Phys. 18, 8, 1008-1018, (1950).
9. Greene, E.F., Cowan, G.R., and Hornig, D.F: "The Thickness of Shock Fronts in Argon and Nitrogen Heat Capacity Lags", J. Chem. Phys. 19, 4, 427-434, (1951).
10. Greene, E.F., and Hornig, D.F: "The Shape and Thickness of Shock Fronts in Argon, Hydrogen, Nitrogen and Oxygen", J. Chem. Phys. 21, 4, 617-624, (1953).
11. Linzer, M., and Hornig, D.F: "Structure of Shock Fronts in Argon and Nitrogen", Phys. Fluids, 6, 12, 1661-1668, (1963).
12. Court, I.N., and Mallory, W.R: "Anomalous Reflectivity of Shock Waves", Nature, 211, 5049, 625, (1966).

13. Lucovsky, G., Lasser, M.E., and Emmons, R.B: "Coherent Light Detection in Solid State Photodiodes", Proc. I.E.E.E., 51, 1, 166-172, (1963).
14. Siegman, A.E., Harris, S.E., and McMurty, B.J: "Optical Heterodyning and Optical Demodulation at Microwave Frequencies", Proc. Symp. Optical Masers, New York 1963 (Polytechnic Press, New York, 1963), pp 511-527.
15. Wright, J.K: "Shock Tubes", (Methuen & Co., London, 1961).
16. Alpher, R.A., and White, D.R: "Flow in Shock Tubes with Area Change at the Diaphragm Section", J. Fluid Mech., 3, 5, 457-460, (1958).
17. Resler, E.L., Lin, S.C., and Kantrowitz, A: "The Production of High Temperature Gases in Shock Tubes", J. Appl. Phys., 23, 12, 1390-1394, (1952).
18. Smy, P.R: "Design and Performance of a Low-Attenuation Electromagnetic Shock Tube", Rev. Sci. Inst., 36, 1334-1339, (1965).
19. Phillips, M.G.R: "The Production of Hypersonic Shock Waves in an Electrothermal Diaphragm Shock Tube", Ph.D. Thesis, University of British Columbia, (1969).
20. Pert, G.J., and Smy, P.R: "Optical Reflection from a Shock Front at Grazing Incidence", Canad. J. Phys., 48, 13, 1521-1527, (1970).
21. Born, M., and Wolf, E: "Principles of Optics", 3rd Ed. (Pergamon Press, Oxford, 1965), pp 38-40.
22. Duff, R.E., and Young, J.L: "Shock Wave Curvature at Low Initial Pressure", Phys. Fluids, 4, 7, 812-812, (1961).
23. Mazzella, A.T., and De Boer, P.C.T: "Shock Front Curvature at Initial Pressures up to 700 mmHg", Phys. Fluids, 9, 5, 892-895, (1966).
24. Panarella, E., and Savic, P: "Blast Waves from a Laser-Induced Spark in Air", Canad. J. Phys., 46, 183-192, (1968).
25. Kolb, A.C: "Production of High Energy Plasmas by Magnetically Driven Shock Waves", Phys. Rev., 107, 2, 345-353, (1957).
26. Pain, H.J., and Smy, P.R: "The Electrical Conductivity of Shock-Ionized Argon", J. Fluid. Mech., 9, 3, 390-400, (1960).

27. Hartunian, R.A: "Shock Curvature due to Boundary-Layer Effects in a Shock Tube", Phys. Fluids, 4, 9, 1059-1063, (1961).
28. De Boer, P.C.T: "Curvature of Shock Fronts in Shock Tubes", Phys. Fluids, 6, 7, 962-971, (1963).
29. Davies, C: Private Communication, (1970).
30. Camm, J.C., and Rose, P.H: "Electric Arc-Driven Shock Tube", Phys. Fluids, 6, 5, 663-678, (1963).

BIBLIOGRAPHY

The following papers (based on material contained in this thesis, as indicated) have been published in the technical press:-

- D. Simpson & P.R. Smy, "Optical Mixing of Laser Radiation Reflected from a Shock Wave", J. Appl. Physics, 40, 12, pp 4928-4932, Nov. 1969, (Chapter 5).
- G.J. Pert, G.M. Seeds, D. Simpson & P.R. Smy, "Optical Reflection at Grazing Incidence to a Shock Front", J. Appl. Physics, (Chapter 6).
- C. Davies & D. Simpson, "Production of Hypersonic Shock Waves at Atmospheric Pressure", Submitted for publication in J. Sci. Inst. (Chapter 7).

Appendix

Theory of Reflection from a Beam Splitter

Consider a plane parallel splitter having a front-surface intensity reflection coefficient R_F ; and a back surface reflection coefficient of one.

Then a beam of intensity W_1 (watt) will be reflected from the front surface at intensity

$$W_A = R_F W_1 \quad (A1)$$

and a beam of intensity W_2 will be refracted at the front surface with intensity

$$(1 - R_F) W_2$$

and will emerge again, after reflection at the back surface with an intensity

$$W_B = (1 - R_F)^2 W_2 \quad (A2)$$

Then if the initial beams are of equal intensity,

$$\text{i.e. } W_1 = W_2 = W \quad \dots \quad (A3)$$

the two main reflected beams will have equal equal intensities

(as desirable in the differential Doppler interferometer) if:-

$$R_F = (1 - R_F)^2 \quad (A4)$$

$$\text{or } R_F^2 - 3R_F + 1 = 0$$

$$\text{giving } R_F = 0.38 \quad (A5)$$

as the only root less than one.

For unequal reflected intensities, W_A , W_B , the maximum total intensity occurs when the two beams are in phase, i.e.

$$W_{\max} = (\sqrt{W_A} + \sqrt{W_B})^2 \quad (A6)$$

and the minimum intensity occurs when

$$W_{\min} = (\sqrt{W_A} - \sqrt{W_B})^2 \quad (\text{A7})$$

so the modulation, m , is given by

$$m = \frac{W_{\min}}{W_{\max}} = \frac{W_A + W_B - 2\sqrt{W_A W_B}}{W_A + W_B + 2\sqrt{W_A W_B}} \quad (\text{A8})$$

which gives

$$\sqrt{W_A} = \sqrt{W_B} \left[\frac{(1+m)}{(1-m)} \pm \sqrt{\left(\frac{1+m}{1-m}\right)^2 - 1} \right] \quad (\text{A9})$$

and for any observed modulation depth, m_1 the relative values of W_A and W_B can be calculated, and hence R_F can be determined from equations A1, A2 and A3. It is a relatively easy matter to extend the theory to cover the case of multiple reflections in the splitter; and for the use of two splitters in succession, as in the Differential Doppler Interferometer. In this general case it can be shown that if $m = 0.85$ we have $R_F = 0.36$ or 0.41 at each splitter.